Applied Energy 416 (2026) 127951

Contents lists available at ScienceDirect

Applied Energy

journal homepage: www.elsevier.com/locate/apen

Advancing wind turbines through control co-design: An integrative review

Saeid Bayat [a,*], Chad Peterson [b], Yong Hoon Lee [c,*], Jenna Iori [d], James T. Allison [b]

[a] Department of Naval Architecture and Marine Engineering, University of Michigan, 1085 South University Avenue, Ann Arbor, Michigan 48109, USA
[b] Department of Industrial and Enterprise Systems Engineering, University of Illinois Urbana-Champaign, 104 South Mathews Avenue, Urbana, Illinois 61801, USA
[c] Department of Mechanical Engineering, The University of Memphis, 312 Engineering Science Building, Memphis, Tennessee 38152, USA
[d] Faculty of Aerospace Engineering, Delft University of Technology, Kluyverweg 1, 2629 HS, Delft, Netherlands

HIGHLIGHTS

- Presents an integrative review of wind turbine control co-design (CCD).
- Analyzes multidisciplinary couplings in rotor, tower, platform, and control design.
- Discusses the impact of CCD on reducing LCOE and improving system performance.
- Proposes modeling and optimization frameworks for CCD in wind systems.
- Identifies current research gaps and proposes a roadmap for future CCD advancements.

GRAPHICAL ABSTRACT

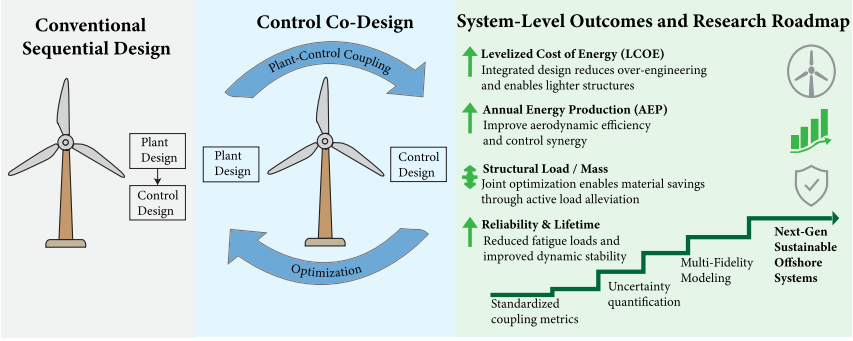

ARTICLE INFO

Keywords:
Wind turbine
Control co-design
Floating offshore wind turbine
Multi-fidelity optimization
Optimization methods

ABSTRACT

Control co-design (CCD) represents an integrated approach to simultaneously optimize the physical design and control strategies of wind turbines, aiming to improve efficiency and reduce costs. This review explores the current state of CCD, addressing advancements in methodologies, challenges in defining and quantifying couplings, and limitations in existing applications. While CCD has demonstrated potential in improving wind turbine design, gaps remain in standardizing coupling metrics and expanding its applicability to broader design problems. By establishing robust methodologies and addressing current challenges, CCD can become a transformative approach in advancing sustainable and cost-effective wind energy systems.

1. Introduction

The global demand for energy is accelerating, with 2024 marking the largest absolute increase ever recorded [1]. Renewable sources, including wind energy, are playing an increasingly central role in meeting this demand, now supplying roughly one-third of global electricity [1,2]. Nevertheless, designing the next generation of multi-megawatt wind turbines and configuring them within multi-gigawatt wind farms to keep pace with demand remains a significant challenge.

The challenges are inherently multifaceted, demanding not only incremental improvements, e.g., higher turbine efficiency, lower cost, greater scalability, improved manufacturability, and enhanced controllability, but also fundamentally novel concepts for domains that conventional wind energy research and development have yet to explore. Consider the coastlines of the United States, where some of the nation's most densely populated urban areas generate exceptionally high electricity demand. Nearly two-thirds of its offshore wind resources exist in water depths that exceed the limits of existing fixed-bottom turbine

* Corresponding authors.
Email addresses: saeidb@umich.edu (S. Bayat), yhlee@memphis.edu (Y.H. Lee).

https://doi.org/10.1016/j.apenergy.2026.127951
Received 19 February 2026; Received in revised form 7 April 2026; Accepted 19 April 2026
Available online 30 April 2026

foundation technology [3]. An emerging solution is to replace those foundations with moored floating platforms. However, this change introduces an entirely new dimension of complexity to system-dynamics modeling, as well as additional techno-economic challenges. Conventional optimization techniques often neglect the tightly coupled nature of designing these complex systems, leading to sub-optimal design solutions and configurations that deliver limited performance and inflated cost. In response to these challenges, recent review studies have provided comprehensive assessments of offshore wind turbine structural and tower design optimization, including the growing role of artificial intelligence (AI)-driven methods and system-level considerations; however, these efforts have largely focused on component- or structure-centric design perspectives rather than integrated dynamic control-structure interactions [4].

Control co-design (CCD) has emerged as an integrative alternative to conventional sequential design approaches by unifying and synergizing plant and control design within a single framework. CCD enables designers to optimize wind turbines more holistically, considering the dynamic interactions between components to achieve better overall performance. This integration allows for innovations such as lighter and more flexible components, improved load management, and ultimately, reduced levelized cost of energy (LCOE).

Despite its potential, applying CCD to wind turbine design presents substantial challenges. Because CCD integrates domains of knowledge that have conventionally been treated separately, the interfaces between them are especially susceptible to inefficiencies and errors. Moreover, researchers must contend with modeling the complex interactions among system elements and disciplines, handling the high computational burden of optimization, and establishing standardized methodologies.

This article bridges these gaps with an integrative review of the current state of CCD in wind turbine engineering. It surveys the methodologies, tools, and strategies employed in CCD, identifies the key challenges that must be addressed, and highlights promising opportunities for future research. By fostering broad adoption of CCD, the work seeks to advance the development of more efficient, reliable, and sustainable wind energy systems, thereby supporting the global transition toward a cleaner energy future.

The remainder of this paper is organized as follows. Section 2 introduces a design framework for actively controlled engineering systems, illustrating why CCD principles supersede traditional design approaches and reviewing the available CCD tool sets. Section 3 provides a narrative-driven exploration of CCD applied to wind turbines, emphasizing the diverse considerations, trade-offs, and common pitfalls. Section 4 discusses current research gaps and proposes a roadmap for the future of wind turbine CCD. Finally, Section 5 summarizes the key findings and provides concluding remarks.

2. Formulating control co-design

John Betts' seminal book, *Practical Methods for Optimal Control and Estimation Using Nonlinear Programming* [5], reminds us that a proper formulation is the most important aspect for solving an optimization problem successfully, yet many domain experts still treat the optimization step as an "afterthought." In the context of CCD, this means that the proper formulation must explicitly incorporate the coordination between the physical (plant) and control disciplines (i.e., co-design), rather than treating each design problem in isolation and combining them at a later stage.

Fig. 1 provides an overview and visual roadmap for this section. It organizes the material into two complementary themes: the *formulation stage* (top box with dotted line), which defines the essential elements of a control co-design problem (design variables, system dynamics, objectives, and constraints) and the *solution stage* (bottom box with dashed line), which introduces the approaches and computational tools required to solve it, including co-design architectures, optimization

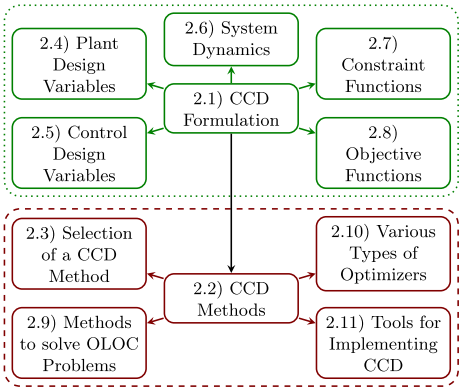

Fig. 1. Overview of the control co-design (CCD) framework. The figure illustrates the CCD framework in two sub-groups: formulation (top box with dotted line) and solution strategies (bottom box with dashed line). The formulation stage defines design variables, system dynamics, objectives, and constraints, while the solution stage introduces methods, optimizers, and tools for implementing the formulated problem.

methods, optimizers, and implementation tool sets. Together, these components outline the logical progression of Section 2, guiding the reader from fundamental formulation principles to the practical implementation of CCD in wind turbine design. In Section 2.1, we introduce a numerical model that incorporates both plant and control variables, establishing the foundation for the subsequent CCD discussions. Section 2.2 then presents methods for conducting co-design studies, both directly and indirectly, and discusses their respective trade-offs. Subsequently, Sections 2.4 through 2.8 examine specific considerations for individual elements of CCD formulation. Finally, Sections 2.9–2.11 address methods and tool sets available for implementing and solving CCD.

Wind turbine controls can be broadly categorized into dynamic control and operational control [6]. Dynamic control refers to fast, feedback- and trajectory-driven control action that regulates subsystems and component behavior of the wind turbine to achieve performance and load objectives on short time scales, e.g., blade pitch and generator torque control. In contrast, operational or supervisory control refers to higher-level operating strategies that make control actions on longer time scales and explicitly account for real operating conditions, such as farm-level coordination, wind turbine-electric grid coordination, and curtailment and derating policies. These supervisory controls can further be classified into wind farm-level and individual wind turbine-level operational controls [7,8].

This paper primarily focuses on dynamic control within the wind turbine CCD. However, design considerations in dynamic and operational controls are not fully separable. Incorporating operational control considerations early in the design stage can further unlock additional performance potential by expanding the feasible design space. For example, dynamic wake steering control enables optimized power extraction from a wind farm under transient flow conditions [9]. In addition, there is no clear boundary between these two control categories, as operational control logic often activates changes in dynamic control, influencing dynamics of the wind turbine up to component-wise level, while dynamic capabilities can also determine which operational strategies are viable. For these reasons, we treat operational control as an important layer that interacts with the dynamic CCD formulation, although our focus remains on CCD with dynamic control design.

2.1. A common model for plant and control design disciplines

The first step in a CCD study is to construct a numerical model that captures both plant- and control-disciplinary design parameters, and relates them to common performance objectives and constraints. A compact, generalizable optimization formulation for this coupled problem

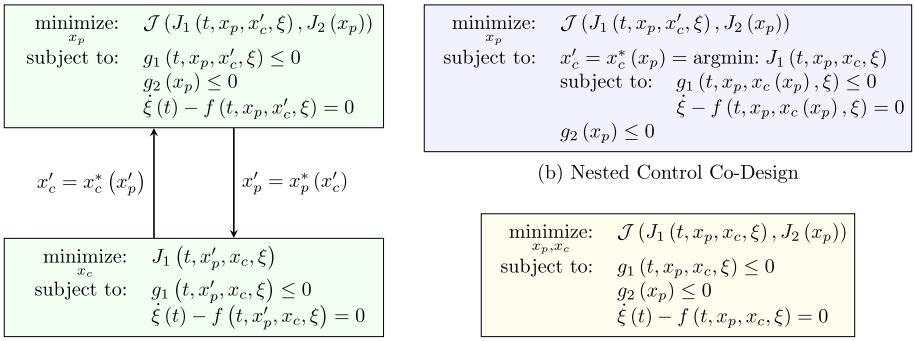

Fig. 2. Three approaches to coordinating plant- and control-design disciplines.

can be written as:

$$\underset{x_p,x_c}{\text{minimize:}} \quad \mathcal{J}\left(J_1\left(t,x_p,x_c,\xi\right),J_2\left(x_p\right)\right) \tag{1a}$$

$$\text{subject to:} \quad g_1\left(t,x_p,x_c,\xi\right)\le 0 \tag{1b}$$

$$g_2\left(x_p\right)\le 0 \tag{1c}$$

$$\dot\xi(t)-f\left(t,x_p,x_c,\xi\right)=0, \tag{1d}$$

where $x_p\in\mathbb{R}^{n_p}$ denotes the vector of plant design variables (e.g., geometric dimensions), $x_c\in\mathbb{R}^{n_c}$ denotes the vector of control design variables (e.g., controller gains or control signal trajectories), $\mathcal{J}$ is the objective function, g_i is the inequality constraint function, $\xi(t)$ is the state of the system, and f is the system model function that provides the time derivative of the state. The state value at any instant can be obtained by integrating the dynamics over time up to the desired point.

Linear or nonlinear inequality constraints g_i may represent limit loads, stresses, actuator limits, and many other plant- or control-related restrictions. For convenience, we partition the objective and constraint functions into a time-dependent part (J_1 and g_1) and a time-independent part (J_2 and g_2). This decomposition is utilized and discussed in more detail later.

The equality constraint given in Eq. (1d) enforces dynamic feasibility. The state derivative $\dot\xi(t)$ must match the model prediction $f\left(t,x_p,x_c,\xi\right)$, given explicitly as:

$$\dot\xi(t)=f(t,x_p,x_c,\xi), \tag{2}$$

or equivalently in a negative null form, given as:

$$\dot\xi(t)-f(t,x_p,x_c,\xi)=0, \tag{3}$$

which is precisely the dynamic feasibility constraint referenced in Eq. (1d).

2.2. Control co-design approaches

Three general families of approaches that coordinate plant and control design, i.e., (a) iterative sequential design, (b) nested CCD, and (c) simultaneous CCD, are illustrated in Fig. 2. However, before examining these three coupled strategies, it is useful to define the baseline single-pass (non-iterative) sequential design approach. In this scheme, the plant is first optimized under an assumed control law. Once a plant optimum has been obtained, the design is frozen, and a separate optimization is performed on the control design variables, yielding an optimal control design. Because the plant was optimized for the original, pre-optimized control design, its performance is no longer guaranteed to be optimal under the newly derived control design. Thus, this approach is not considered a form of CCD.

In iterative sequential design, given in Fig. 2(a), the plant and control design problems are treated as independent sub-problems that are solved one after the other. At each iteration, one discipline is optimized while the other is held fixed; the roles are then reversed subsequently before the next iteration. This approach is conceptually straightforward and mirrors how design organizations partition problems and tasks by specialty. Although alternating between disciplines introduces a minimal form of coordination, each sub-problem optimizes greedily, improving its own disciplinary design without accounting for its impact on the counterpart. As a result, the intermediate design solutions "zig-zag" through the design space, approaching (but rarely reaching) a synergistic optimum. In limited cases, if the incremental improvement per iteration is sufficiently small and the number of iterations is sufficiently large, the process can converge to the same solution that a fully coupled CCD would provide. In practice, however, cross-disciplinary synergies remain largely untapped, leading to designs that are either sub-optimal or fail to converge.

Both the single-pass sequential and the iterative sequential approaches rely on an exchange of the plant and control design variables (x_p and x_c, respectively). Here, this exchange is denoted by $x_p'=x_p^*\left(x_c'\right)$ and $x_c'=x_c^*\left(x_p'\right)$, where a prime ($'$) marks the variable that is held fixed during an optimization, and an asterisk ($*$) indicates the optimal value returned by that sub-problem.

A typical process of sequential or iterative sequential design starts with plant design optimization from feasible initial guesses $x_{p,0}$ and $x_{c,0}$. Keeping the control design fixed at $x_c'=x_{c,0}$, solve the plant optimization sub-problem to obtain the optimal plant design, $x_p^*=x_p^*\left(x_c'\right)$. Subsequently, control design optimization follows using the newly obtained plant design variables, i.e., set $x_p'=x_p^*$. Starting from an initial control design guess (often the previous value $x_{c,0}$), solve the control design sub-problem to obtain $x_c^*=x_c^*\left(x_p'\right)$. Iterative sequential design then feeds updated control design variables back into the next plant design optimization sub-problem by setting $x_c'=x_c^*$, and repeat the whole procedure until the solutions (x_p^* and x_c^*) converge.

The second coordination strategy, illustrated in Fig. 2(b), is the nested CCD architecture. It comprises two hierarchical optimization levels: an outer-loop that governs one discipline and an inner-loop that solves the other. For every iteration of the outer-loop optimizer, a full inner-loop optimization is performed to convergence before the other decision variables are updated. In practice, the plant design problem is most often placed in the outer loop, while the control design problem resides in the inner loop. Consequently, each outer-loop evaluation requires solving the entire control design optimization sub-problem for the current plant configuration, thereby capturing the strong interdependence between the two disciplines within a single coordination framework.

The important distinction between iterative sequential and nested CCD approaches lies in the treatment of the two disciplinary designs during the optimization process. In the iterative sequential approach, the plant and control designs are solved alternately as two independent optimization problems. Each sub-problem seeks a complete optimum before any information is exchanged. On the other hand, the nested CCD approach obtains optimal control decisions while solving the plant design problem, and vice versa. For each tentative plant design supplied by the outer-loop, the inner-loop control design optimization solves the control problem to convergence with respect to the intermediate plant design candidate ($x_c^*(x_p^\dagger)$), where dagger (†) denotes the current design candidate that the optimizer supplies. This cycle continues until both plant and control designs reach convergence together.

It is worth noting that, in both iterative sequential and nested CCD approaches, the control (inner) discipline optimizes a different objective function denoted J_1 rather than the overall system objective function $\mathcal{J}$. This distinction is clearly shown in the lower box of Fig. 2(a) and in the "argmin" term of the nested objective function in Fig. 2(b). When the plant design variables are held fixed, $\mathcal{J}$ collapses to a function that depends solely on J_1; consequently, using $\mathcal{J}$ as the control (inner) objective function yields exactly the same minimizer as J_1. Nevertheless, retaining J_1 avoids unnecessary algebraic overhead and keeps the inner-loop problem simple, while using $\mathcal{J}$ is still possible and sometimes useful for certain cases.

Suppose the system-level objective function is LCOE, defined as cost divided by annual energy production (AEP). Because cost depends only on plant variables while AEP is governed by the control strategy, a natural nesting arises: the inner-loop control discipline maximizes AEP, and the outer-loop plant discipline minimizes LCOE. The inner-loop control problem is typically smooth, so gradient-based methods can effectively maximize AEP. In contrast, the cost model may be complex, discontinuous, or noisy; consequently, a derivative-free optimizer is often preferred for the outer-loop discipline. Here, it should be noted that x_c in these formulations denotes the control design variable, which can represent open-loop optimal control (OLOC) trajectories or simply the gains of a proportional integral derivative (PID) controller.

The third coordination strategy, illustrated in Fig. 2(c), is the simultaneous CCD architecture. In this formulation, the plant- and control-design sub-problems are merged into a single optimization formulation that treats both design variables x_p and x_c concurrently. As a result, sensitivities of the objective and any constraints can be evaluated with respect to both plant and control design variables, providing cohesive bi-directional coupling between the disciplines. Consequently, simultaneous and nested CCD can identify synergistic design mechanisms, whereas pure sequential and iterative sequential approaches cannot.

2.3. Selection of co-design approaches

Choosing an appropriate co-design strategy depends on several problem-specific characteristics: model fidelity, the strength of coupling between plant and control disciplines, dimensionality of the design space, and available computational resources. In general, CCD methods with more cohesive coordination approaches, such as nested or simultaneous architectures, outperform sequential approaches because they exploit the inherent synergies between plant and control disciplines to find holistic solutions. While both nested and simultaneous approaches can yield optimal solutions, practical considerations often dictate which is more suitable.

The dimensionality of the control design variables is a key factor in determining whether to adopt a nested CCD architecture. When the control design variable x_c contains many degrees of freedom (e.g., an OLOC trajectory), a gradient-based optimizer becomes an attractive choice for solving this high-dimensional control design problem within the nested inner-loop sub-problem. The simultaneous CCD often produces a highly multimodal landscape with respect to plant design variables. Consequently, purely gradient-based algorithms typically converge to a local minimum near the initial guess. In contrast, nested CCD allows a derivative-free algorithm to drive the outer-loop plant design discipline, providing more global search, while the inner-loop control design discipline can efficiently exploit the control design solution. Conversely, if x_c is low-dimensional (e.g., PID controller gains), simultaneous architecture may be more efficient [10,11].

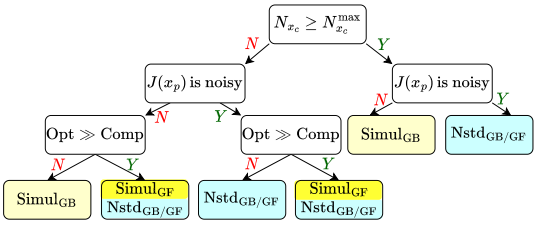

Fig. 3. High-level decision flowchart for selecting a suitable CCD method based on the number of control design variables (N_{x_c}), noise level in the plant objective function $J(x_p)$, and relative importance of optimality versus computational time (*Opt* ≫ *Comp*).

Computational effort is another factor in determining the architecture. Because simultaneous CCD solves one large-scale problem, it often requires fewer overall model evaluations and thus lower wall-clock time, provided that gradients are available and the problem size is moderate. Nested CCD, on the other hand, incurs additional cost due to repeated inner-loop optimizations. However, this extra effort can be justified when the plant objective function exhibits many local minima or when global exploration is needed. Detailed discussions in comparing nested and simultaneous CCD are given in [12].

Fig. 3 presents a simplified high-level flowchart for selecting a suitable CCD method based on three key criteria: (1) whether the number of control design variables, N_{x_c}, is large (i.e., greater than a problem-dependent threshold $N_{x_c}^{\max}$), (2) whether the objective function is noisy with respect to the plant design variables, $J(x_p)$, and (3) whether achieving a solution close to the global optimum is prioritized over computational time (*Opt* ≫ *Comp*). The terminal nodes of the tree indicate which CCD method to adopt: Simultaneous CCD with a gradient-based optimizer (Simul_{GB}), Simultaneous CCD with a gradient-free optimizer (Simul_{GF}), or a Nested CCD architecture using a gradient-based inner loop and a gradient-free outer loop ($\text{Nstd}_{\text{GB/GF}}$).

Each branch connecting the nodes indicates whether the condition inside the preceding decision box is satisfied (*Y*) or not (*N*). Thus, given these three high-level conditions, one can identify both the appropriate CCD architecture and the corresponding optimizer type. It should be noted that this flowchart represents only a simplified, general selection guideline; in practice, the choice of CCD method can depend on additional parameters and problem-specific characteristics.

2.4. Plant design variables

In wind turbine design, plant design variables, such as tower height, tower thickness, blade twist, and chord length, are time-invariant, and the total number of these variables (i.e., number of scalars) is usually modest. This provides two principal advantages for optimization. First, because they do not vary with time, they can be treated as fixed parameters in transient analyses, eliminating the need to update them at each time step. Second, this time-independent nature means that the dimensionality of the plant design space is far smaller than that of the control design space, which frequently contains many time-varying quantities, particularly for trajectory-based optimal control problems (see Section 2.5).

However, not all plant design variables can be represented compactly. For example, the chord length and twist distribution of a blade are continuous functions of the spanwise coordinate, and the internal

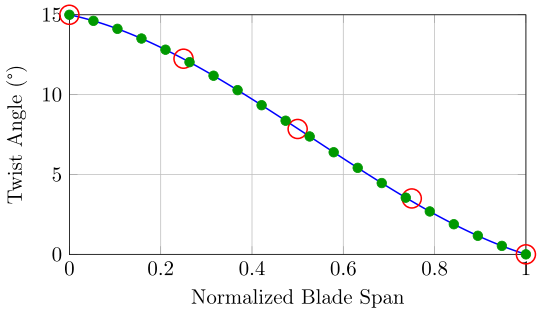

Fig. 4. Bézier curve approximation for blade twist: The plot shows the rough mesh points (hollow circles) defining the blade twist, the Bézier curve (smooth line) providing a smooth approximation, and the fine mesh points (circular filled dots) used for evaluating the Bézier curve along the blade span. This approach demonstrates how a coarse set of design variables can be refined into a continuous representation for optimization or analysis purposes.

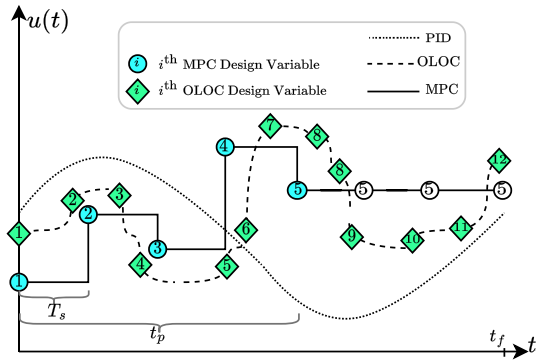

Fig. 5. Time-varying control signals. A comparison of how closed-loop control, model predictive control, and open-loop control are parameterized.

structure of a turbine blade often exhibits complex geometry and configuration with various composite materials that cannot be adequately captured with only a few parameters. A typical remedy is to replace the high-resolution design representations with a lower-dimensional parametric model, e.g., a Bézier curve employed in [11]. By fitting such a smooth function to a coarse set of control points and evaluating it at any desired location, it is possible to achieve a substantial reduction in design space dimensionality while preserving design fidelity.

Fig. 4 illustrates this concept using a Bézier curve to approximate the blade twist distribution along the span of a wind turbine blade. The coarse discretization is represented as hollow circles, which define an initial low-resolution set of twist values. A Bézier curve (smooth line) is then fitted through these points, yielding a smooth representation of the twist profile. Circular filled markers denote the finer discretized points obtained by evaluating the fitted curve at a dense set of spanwise locations. This approach drastically reduces the number of plant design variables while preserving sufficient geometric detail for optimization and analyses.

2.5. Control design variables

In an actively controlled engineering system, a controller generates control signals that regulate the system states. Three broader classes of controllers are typically considered: closed-loop control (CLC), model predictive control (MPC), and OLOC. The nature of the design variables x_c differs across these families, as illustrated in Fig. 5. The horizontal axis denotes time, while the vertical axis shows the corresponding control signal $u(t)$.

CLC adopts a fixed feedback structure (e.g., a PID controller) that merely reacts to a feedback signal. The control design variables x_c consist solely of its tunable gains in proportional, integral, and derivative elements that parameterize this structure. Thus, x_c is low-dimensional and time-invariant; therefore it does not appear as nodes in Fig. 5. Once the gains have been selected, the controller computes the instantaneous command $u(t)$ by applying a predefined control law with the measured feedback inputs. The dimensionality of x_c remains constant regardless of the horizon.

By contrast, OLOC imposes no predetermined control structure. The control design variables are the entire control signal trajectories over the full simulation horizon, which vary with time. Because no a priori control structure is imposed, the optimization must represent $u(t)$ on discretized time points that span the whole horizon and are not limited to any shorter prediction time horizon. Consequently, this yields a much higher dimensionality than in CLC.

In practice, a relatively large number of nodes is required to capture the temporal richness of the optimal control signal. The control value at an arbitrary time instance is obtained by interpolating values at discretized time points. The placement of these time discretization nodes and the choice of interpolation (or quadrature) scheme, such as Legendre-Gauss-Radau (LGR) or Legendre-Gauss-Lobatto (LGL) collocation, are important decisions in formulating OLOC problems and have a significant impact on solution accuracy and computational cost [13].

MPC bridges these two extremes, adopting a trajectory-based formulation of OLOC, but restricts the optimization to a smaller prediction horizon t_p. At each sampling instant $t_n = nT_s$ (n can be any non-negative integer), the controller solves a finite-horizon optimal control problem over a prediction horizon t_p, producing a sequence of candidate control actions. Only the first element of this sequence is applied with zero-order hold, after which the horizon recedes and the optimization is repeated. In this receding-horizon loop, the controller continuously updates its predicted trajectory using the latest feedback, in a manner analogous to how CLC reacts to feedback [14]. Consequently, x_c at a given sampling instant consists of a limited number of control values associated with the current prediction horizon (the shaded circles in Fig. 5, numbered $i = 1, \ldots, 5$). As with CLC, the dimensionality of x_c is independent of the total simulation length, but it does grow with the length of the prediction horizon. A distinctive advantage of MPC over CLC is its ability to incorporate explicit state, input, and rate constraints directly into the optimal control problem. Because MPC can be viewed as an advanced form of CLC, it can be implemented in real-world applications with higher complexity and cost compared to simpler CLCs such as PID; however, doing so necessitates hardware capable of solving these more demanding calculations in real time.

The three control approaches trade off realistic implementation, computational cost, and attainable performance. First, CLC offers low-dimensional design parameters with a fixed feedback law. The reduced dimensionality typically leads to faster convergence of the CCD optimization, and importantly, the controller can be deployed directly on the physical system, guaranteeing consistency between the optimization and real-world implementation [15]. The downside of CLC, however, is the rigidity of the chosen control structure that limits the achievable system performance. If CLC is adopted early in the design process, the system's full potential would never be explored.

Extending this perspective, OLOC offers a complementary advantage by enabling exploration of the full control trajectory without imposing a predefined structure. This flexibility can reveal system-level performance limits and uncover design opportunities that may not be accessible through lower-dimensional control formulations. However, these benefits are accompanied by important practical considerations. The high dimensionality of OLOC enlarges the optimization search space, which can increase computational cost, particularly in CCD problems where plant and control variables are optimized simultaneously. In addition, because the control trajectory is defined over the entire time horizon of interest, OLOC relies on model accuracy, and its performance

may be influenced by modeling uncertainties, global truncation errors, or time-varying conditions [16]. Furthermore, unlike feedback-based controllers, OLOC is typically implemented in an offline setting and is therefore less directly suited for real-time control. Despite these considerations, OLOC remains a powerful tool for identifying performance bounds and informing the design of more practical controllers such as CLC and MPC.

2.6. System dynamics

Designing actively controlled engineering systems requires evaluating system responses to various inputs, including disturbances and control signals, in time or frequency domains. The resulting trajectory of the dynamic state vector $\xi(t)$ influences the objective function, constraint functions, and any other system output responses. Consequently, an accurate representation of the system dynamics is essential in formulating and solving CCD problems.

In its most general form, the dynamics of a system can be written as:

$$\dot{\xi} = f\left(t, x_c, x_p, d\right), \tag{4}$$

where t denotes time, x_p and x_c are plant and control design variables, and d denotes disturbances or other external inputs. In some cases, such as when f is highly nonlinear, geometry is complex, dynamics occur across multiple time scales, etc., the cost of a single simulation and/or the number of simulations required throughout optimization may become computationally prohibitive. When this occurs, simplification methods, such as linearization with respect to an operating point, reduced order modeling with state reduction, or data-driven dynamic system modeling, can be employed. These methods aim to retain the dominant dynamics while discarding higher-order modes that do not largely impact overall dynamic responses to reduce computational expenses.

Explicit access to system dynamics, given in Eq. (4), is particularly important in OLOC and MPC optimization. Advanced OLOC solvers based on pseudospectral collocation, for example, transcribe the continuous dynamics into a set of algebraic equations and form a set of equality constraints that must be satisfied at the collocation points [13]. Unfortunately, many wind turbine simulation packages, such as OpenFAST [17], Bladed [18], and QBlade [19], are provided as black-box models, which preclude direct extraction or modification of the state vector at each time step. Moreover, these tools often combine discrete events with continuous dynamics, so their behavior cannot be captured solely by the form in Eq. (4). Consequently, the governing model must be inferred from simulation data for these cases.

Several strategies have been proposed to obtain a tractable representation of function f in Eq. (4) when it is found to be computationally prohibitive, including (1) low-order analytical modeling, (2) linear parameter-varying approximations, and (3) data-driven surrogate modeling techniques.

The first approach constructs a low-order analytical model by applying first-principles analysis to the dominant dynamic modes and simplifying the governing equations into a compact form, e.g., Bayat et al. [11] and [20]. This yields a computationally efficient model that permits OLOC or MPC solvers to directly extract or modify the state vector at each time step. The second approach leverages the linearization capabilities that many mid- or high-fidelity simulation tools have, and builds a linear parameter-varying (LPV) model using the obtained linear models to capture underlying nonlinear system dynamics, e.g., Sundarrajan et al. [21]. Although LPV models can represent operating-point dependence, they can expand to support the full operating envelope by leveraging extensive datasets with varied operating points, particularly when complex disturbances, such as harsh wind and wave loads, are present.

The third approach builds on this idea by fitting a function $\hat{f}$ (a surrogate of function f in Eq. (4)) to a large simulation dataset. This approach is often referred to as derivative function surrogate modeling (DFSM), first introduced in [22] and further developed in subsequent studies, such as [23] and [24]. DFSM can accommodate broader operating ranges and greater design flexibilities, but it demands larger training datasets, which may become computationally expensive. Moreover, because $\hat{f}$ is an approximation, integration errors accumulate over time steps. A small discrepancy at time t_i propagates to t_{i+1} and beyond, potentially compounding throughout the time horizon. Consequently, careful construction and validation of the surrogate function $\hat{f}$ are essential to avoid compounding inaccuracies in the system dynamics.

2.7. Constraint functions

In general optimization problems, constraint functions $g(x)$ represent the limitations, restrictions, or conditions that any solution must satisfy. They delineate the feasible region, shape the exploration space, and enforce the rules of the underlying physics or other disciplines for engineering systems. Such constraints can appear in several forms: equality constraints, inequality constraints, simple variable bounds, and more complex logical or combinatorial conditions.

Equality constraints, in the form of $g(x) = 0$, enforce strict relationships among variables, such as conservation laws, that must hold exactly. This type of constraint reduces dimensionality in design exploration space. Inequality constraints, in the form of $g(x) \leq 0$, specify limits that the function value cannot exceed, e.g., safety margins or stress limits. They define the bounds of the feasible region. Variable bounds, in the form of $x_{\text{lb}} \leq x \leq x_{\text{ub}}$, are the simplest form of inequality constraints, limiting the allowable range of an individual design variable x to reflect physical or design limits. Logical or combinatorial constraints, which often arise in discrete or mixed-integer optimization problems, enforce relationships that can be defined with logic or selection rules among discrete alternatives.

In the CCD context, these constraints may be imposed concurrently on plant and control disciplines, or they may be defined separately for each discipline. For the control discipline, it could typically be further classified into two families: boundary constraints, which need only hold at the initial and/or final point of the time horizon, and path constraints, which must be satisfied continuously throughout the entire prediction interval. Because path constraints have to be satisfied continuously, they make the optimization problem considerably more demanding than boundary constraints alone.

CCD problems address the concurrent design of plant and control systems by modeling the dynamic behavior of the system through its states, their derivatives, and control inputs over a specified range in time or frequency. In time-domain formulations, these relationships are enforced as equality constraints, often referred to as dynamic or defect constraints in direct collocation or transcription-based optimal control methods. Such constraints ensure that the discretized states evolve consistently with the underlying governing dynamic equations throughout the time horizon.

Boundary constraints, expressed either in equality or inequality form, may be imposed on both states and time-dependent outputs to enforce state or time-dependent output trajectories at the initial time ($t = t_0$, initial condition) and final time ($t = t_f$, terminal condition). When a periodic time horizon is imposed (e.g., in the control of cyclic behaviors, such as a vertical-axis wind turbine rotor), the initial and final time values of state trajectories and their derivatives may be constrained to be equal, while their specific values remain undetermined within the optimization formulation. Since boundary constraints enforce states and time-dependent outputs only at initial and final times, the dimensionality of these constraints is relatively low.

Path constraints represent restrictions that must be satisfied over the entire time domain, rather than only at boundaries (i.e., initial and final time). Therefore, unlike boundary constraints, the dimensionality of such constraints is relatively high. In the context of CCD or general optimal control problems, path constraints often enforce operational, physical, and safety limitations that the system must satisfy at every time

instant along state, control input, and system output trajectories. For example, path constraints can enforce maximum displacement ($-\xi_{\max} \leq \xi(t) \leq \xi_{\max}$), velocity or acceleration limits ($-\dot{\xi}_{\max} \leq \dot{\xi}(t) \leq \dot{\xi}_{\max}$), actuator physical limits on control inputs ($u_{\text{lb}} \leq u(t) \leq u_{\text{ub}}$), real-time stress limits ($\sigma(\xi(t)) \leq \sigma_{\max}$), among others.

Constraints, regardless of their specific forms, define the feasible region within the design space and thereby restrict the set of attainable design solutions. As tighter constraints are imposed, the achievable performance of the optimal design solution is inevitably limited. Consequently, during the early stages of the design process, it is advisable to adopt broader variable bounds, relax non-critical constraints, and permit wider operational conditions to facilitate thorough exploration of the design potential. Constraints can be progressively tightened in later stages as system understanding improves and design priorities become clear. This approach helps identify which constraints exert the most significant influence on performance, enabling informed trade-offs among competing decisions, such as energy production, efficiency, production capability, reliability, and cost. Furthermore, it is beneficial to analyze constraint activity, determining which constraints are active (binding) at the optimal solution. Inactive constraints indicate design margins that are not limiting performance and may represent opportunities for simplification or removal of unnecessary limitations. Conversely, persistently active or nearly active constraints identify critical design drivers that require closer attention or redesign of related sub-systems.

When multiple competing objective functions are of interest, constraints can serve as an alternative to direct multiobjective optimization techniques. This approach, known as the ϵ-constraint method, is a scalarization strategy for solving multiobjective optimization problems [25]. In this method, one objective is designated as the primary objective function, while the remaining objectives are reformulated as inequality constraints with specified upper or lower bounds. By systematically varying these bounds across successive optimization runs, a family of Pareto-optimal solutions can be generated, effectively representing the trade-offs among the competing objective functions.

2.8. Objective functions

The objective function $\mathcal{J}$ for a CCD problem that includes time-domain optimal control can be written in general form, given as:

$$\mathcal{J} = \int_{t_0}^{t_f} \mathcal{L}\left(t, \xi(t), u(t), x_p\right)\, dt + \Phi\left(\xi\left(t_0\right), t_0, \xi\left(t_f\right), t_f, x_p\right), \tag{5}$$

where t_0 and t_f denote initial and final time, $\mathcal{L}$ is the Lagrange (running cost) term, Φ is the Mayer (terminal cost) term, and $u(t)$ denotes the control input trajectory.

In a direct collocation formulation, the discretized values of both state $\xi(t)$ and control input trajectories $u(t)$ are decision variables; consequently, they belong to the control design variable x_c. By contrast, in simpler CLC methods, x_c contains only a few controller parameters, for example, the proportional K_p, integral K_i, and derivative K_d gains of a PID controller. In CLCs, the feedback law computes the instantaneous control input u from the current state, and the system dynamics then computes the state at the next time step. Thus, changing x_c modifies the resulting trajectories of ξ and u, but these trajectories are not explicit components of x_c.

The Lagrange term integrates a running cost over the entire time horizon, while the Mayer term accounts for the cost only at the initial and final states. The two terms are interchangeable. Introducing an auxiliary state that accumulates $\mathcal{L}$ converts a Lagrange term into a Mayer-only formulation, while embedding a Dirac delta at t_0 or t_f allows a Mayer term to be expressed as a part of the integral in a Lagrange-only formulation. This flexibility allows the objective function to be shaped to match specific modeling preferences or computational restrictions.

When a cost component depends solely on plant design variables x_p, it is natural to place it in the Mayer term. For example, the capital cost of a wind turbine, determined only by its plant design parameters (e.g., geometry, structural architecture, materials), belongs in Φ, whereas the AEP accumulates over time and therefore appears in the Lagrange term.

2.9. Solving open-loop optimal control problems

OLOC problems can be solved with either direct or indirect methods. Direct optimal control methods, often described as “discretize-then-optimize,” first discretize the continuous problem (typically the control trajectories, and additionally state trajectories depending on specific numerical algorithms) and then solve the resulting finite-dimensional nonlinear programming (NLP) problem with a general-purpose optimizer [5].

Within the direct optimal control family of methods, two classes of formulations are distinguished: shooting and direct transcription (DT) approaches. The shooting approach discretizes only the control variables. The state trajectories are obtained by forward integration of the dynamics for each candidate control. This yields either single shooting, in which the entire horizon is treated as a single simulation interval, or multiple shooting, where the horizon is partitioned into sub-intervals and continuity between them is enforced through defect constraints. Single shooting computes the states starting from the known initial condition, whereas in multiple shooting, the time window is divided into smaller sections, with continuity between sections ensured through defect constraints.

The DT approach, also referred to as the simultaneous approach, discretizes both control and state trajectories, and imposes the dynamics as algebraic equality (defect) constraints in the NLP problem [13,26,27]. Methods in this class of approach include single-step collocation, a transcription method based on function approximations, typically using Runge-Kutta schemes, and global collocation, a transcription method that uses a single, high-order orthogonal polynomial in representing the entire trajectory, also referred to as pseudospectral methods.

Indirect optimal control methods, also described as “optimize then discretize,” derive the optimality conditions, such as those from Pontryagin’s Maximum Principle or Calculus of Variations. These optimality conditions then lead to boundary value problems, which are solved numerically. Indirect methods are typically less efficient than direct methods and are sensitive to initial guesses for the solution [13].

2.10. Selection of optimization algorithms

A wide variety of optimization algorithms can be used to solve the design formulation given in Eq. (1), and in practice, they broadly fall into three categories: gradient-free, gradient-based, and hybrid methods. There is no single class of methods that dominates all others in solving CCD problems [28]. Choosing an appropriate optimization algorithm requires a holistic assessment of problem characteristics and available computing resources, such as objective-function smoothness, problem dimensionality, availability of derivative information, required solution accuracy, the scale of available parallel computing hardware, and allowable solution time. For a detailed taxonomy of optimization problem attributes, see Fig. 1.15 and the accompanying chapter in [29].

Gradient-free algorithms require only function evaluations, and they do not need access to the model’s internal states or gradient information. Consequently, these algorithms are straightforward to apply *out of the box* with black-box simulation models. Many of them have superior performance in escaping from local optima regardless of whether they are local optimizers, such as constrained optimization by linear approximation (COBYLA) [30], or global optimizers, such as covariance matrix adaptation evolution strategy (CMA-ES) [31]. This is an advantageous characteristic for problems with noisy objective functions, such as capital and operational expenses of wind turbines. Moreover, since they do not rely on gradient information, they tend to converge more robustly than gradient-based methods.

The main drawback of gradient-free algorithms is their poor scalability. First, the number of required function evaluations at each iteration scales combinatorially with the number of design variables. Particularly

for OLOC and MPC problems, these methods may not be suitable due to high dimensionality in control design variables. In addition, achieving fine convergence (after initial rough convergence) can require orders of magnitude more function evaluations than gradient-based algorithms because small perturbations of the design variable yield only small deviations in the performance metric, providing a negligible impact on driving the optimization algorithm for further improvement. Therefore, while gradient-free methods might efficiently identify the ballpark of a good design, they can easily become inefficient when an accurate solution is demanded or a fine convergence criterion is set.

Gradient-based algorithms, on the other hand, exploit the gradients of objective and constraint functions with respect to the design variables. These gradients can be supplied in various ways. Characteristically, they can be analytically derived—either manually or symbolically [32]. Gradients can also be obtained numerically using finite differencing, the complex step method, or algorithmic differentiation (AD), also referred to as automatic differentiation [29].

The primary advantage of gradient-based methods is that they typically require fewer function evaluations than gradient-free methods, making them more efficient. However, they often converge to a local optimum near the initial guess, and this limitation becomes critical when the objective and constraint function responses are multimodal or noisy, gradients are unreliable, or when the problem is poorly scaled. For problems involving ODE solvers, errors that accumulate during numerical time integration can introduce noise into the objective function. Because numerical integration errors accumulate, even a tiny perturbation in a design variable can produce overly large fluctuations in the computed objective function value that stem from error propagation rather than from the underlying physical behavior.

Optimization performance can be improved by pairing gradient-free and gradient-based methods to tackle different aspects within a system. A common hybrid strategy employs a gradient-free algorithm for the plant design sub-problem, and a gradient-based algorithm for the control design sub-problem. Embedding this hybrid approach in a nested CCD framework, where an outer-loop optimizes the plant design and an inner-loop solves the control sub-problem, further exploits the strengths of each method. However, in contrast, a monolithic simulation-based approach treats all variables as a single optimization problem, eliminating any opportunity of assigning each discipline to its most suitable optimization algorithm.

2.11. Software tools for wind turbine control co-design

There are generally two main approaches to CCD: nested and simultaneous, as discussed earlier in Fig. 2. In the simultaneous approach, both the plant and control design variables are optimized within a single, unified optimization loop, requiring one solver to handle all design variables and constraints concurrently. This formulation fully captures plant-controller design interactions, but often leads to larger, more complex optimization problems. In contrast, the nested approach decomposes the problem into two hierarchical optimization loops: an outer loop (typically for plant design) and an inner loop (for control design). This separation enables the use of different optimizers or solution strategies for each loop, which can be advantageous in certain cases, and will be discussed in later sections. Importantly, the choices of architecture and optimizer vary based on the specific problem.

Fig. 6 illustrates a wide range of computational toolsets available to support CCD workflows. These tools can be grouped into several categories, reflecting methodologies required for modeling, optimization, and control of complex wind turbine systems. Fig. 6 and software tools introduced in this section list only a representative subset of the available tools. It is not an exhaustive catalog, and numerous other useful tools exist that lie beyond the scope of this review.

To solve the OLOC problem, several dedicated OLOC (or trajectory) solvers are available, including Dymos [33], ICLOCS2 [34], GPOPS-II [27], PSOPT [35], ACADO [36], and DIDO [37]. These tools transcribe the continuous-time optimal control problem into a finite-dimensional NLP problem using direct collocation or pseudospectral methods, which can then be handled by generic numerical optimizers.

For CCD with CLCs, simple feedback controllers and more advanced MPC frameworks can be employed. Notable examples of MPC solvers include MATLAB MPC toolbox [38], SS-MPC [39], LGR-MPC [40], do-mpc [41], and ModelPredictiveControl.jl [42]. These tools allow dynamic systems to be optimally controlled at runtime by repeatedly solving a finite-horizon OLOC problem. By contrast, more conventional wind turbine CLCs, such as National Laboratory of the Rockies' (NLR) ROSCO [43], DTUWEC [44], DRC_Fortran [45], and TUBCon [46], can be employed along with wind turbine simulation tools. These CLCs provide simple, industry-oriented control architectures that support various control objectives within the CCD context.

Comprehensive wind turbine models that predict and simulate wind turbine dynamic responses to various load cases are essential to CCD studies. Widely utilized wind turbine time-domain simulation frameworks include OpenFAST [17], QBlade [19], HAWC2 [47], Bladed [18], and SIMA [48]. Frequency-domain simulation frameworks provide faster computation for more comprehensive design space exploration, and widely utilized tools include RAFT [49], HAWCStab2 [50], and QuLAF [51].

Component and discipline-specific analysis tools also provide essential model responses to CCD studies. Farm-level aerodynamic wakes and associated control design can be modeled with tools, such as FAST.Farm [52], pyWake [53], and FLORIS [54], or higher-fidelity simulation tools, such as SOWFA [55]. Structural analysis on composite materials used in wind turbine rotor blades can be provided by specialized structural analysis tools, such as pyNuMAD [56] and VABS [57]. Hydrodynamic loadings and responses on the floating structures can be provided by potential flow hydrodynamic solvers, such as WAMIT [58], HAMS [59], Capytaine [60], and NEMOH [61]. The dynamic response of mooring lines to floating platform motions, hydrodynamic forces, and ocean current loadings can be simulated using MoorDyn [62].

The NLPs generated by optimal control solvers and wind turbine CCD formulations are typically solved using generic optimization frameworks and packages. Widely employed tools include optimizers, such as COIN-OR [63] project's interior-point optimization package: IPOPT [64] and sparse sequential quadratic programming package: SNOPT [65]; collections of optimizers and their wrappers, such as pyOptSparse [66], Pyomo [67], SciPy.optimize [68], and Matlab fmincon [69]; and multidisciplinary design analysis and optimization (MDAO) frameworks, such as OpenMDAO [70] and Dakota [71].

Optimization algorithms employed in these numerical optimization packages can be categorized into gradient-based and derivative-free optimizers. Optimization algorithm selection within these frameworks depends on several factors, including the mathematical properties of the response surface, dimensionality and modality of the design space, and the computational cost associated with function evaluations.

For nested CCD architectures, especially where the outer design loop involves non-smooth or computationally expensive evaluations, derivative-free optimizers, such as COBYLA [30], CMA-ES [31], genetic algorithm (GA) [72], particle swarm optimization (PSO) [73], and simulated annealing [74], are often employed. On the other hand, when derivative information is available, gradient-based optimizers, such as interior-point method [64], sequential quadratic programming (SQP) [65], sequential least squares programming (SLSQP) [75], augmented Lagrangian [76], and barrier method [77], offer faster convergence and higher computational efficiency for smooth design spaces.

In some cases, providing derivative information to the optimizer could be enabled via AD (or autodiff, in short). This approach applies the chain rule to each elementary operation in a computer program to

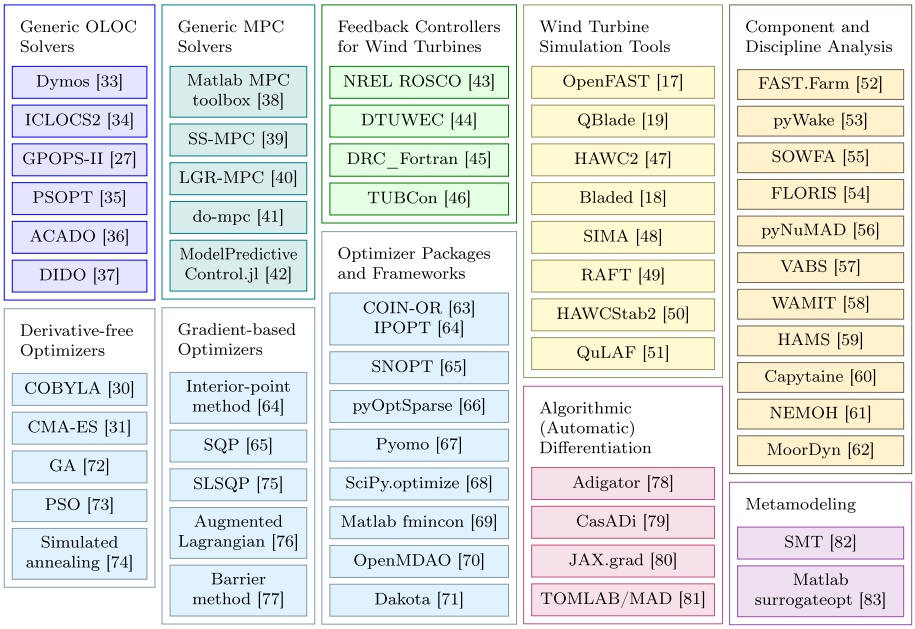

Fig. 6. Toolsets commonly used in control co-design problems. Categories include generic OLOC and MPC solvers along with specialized CLC for wind turbines, wind turbine simulation tools, wind turbine component and discipline analysis tools, optimizers and optimization packages, AD tools, and metamodeling tools.

compute exact derivatives of its outputs with respect to its inputs. Widely utilized AD tools include Adigator [78], CasADi [79], JAX.grad [80], and TOMLAB /MAD [81].

Finally, when analytical or physics-based models are unavailable or too expensive to evaluate at each optimization iteration, metamodeling (or surrogate modeling) frameworks are employed to approximate system responses. Widely utilized tools include the Surrogate Modeling Toolbox (SMT) [82] and MATLAB surrogateopt [83]. These tools provide various surrogate representations, such as Kriging and radial basis functions (RBF), and frameworks to represent uncertainties, e.g., via Gaussian processes.

3. Design considerations and trade-offs

In this section, we present discussions on the CCD of wind turbines, focusing on the key design considerations and associated trade-offs. Wind turbines comprise various sub-systems and components, such as the tower, rotor, generator, actuators, and foundation/platform, and span multiple physical and non-physical disciplines, including aerodynamics, structural dynamics, hydrodynamics (for floating offshore wind turbines, FOWTs), and controls. Therefore, we partition the discussions into dedicated sub-sections. Each sub-section details the relevant design variables, constraints of major importance, and other relevant factors that impact the formulation and solution of wind turbine CCD problems. In this regard, Sections 3.1–3.6 respectively cover the following components: control, tower, rotor, and floating platform. Section 3.7 discusses the farm-level design of wind turbines, Section 3.8 discusses the model complexity, Section 3.9 highlights the common objective functions used in the literature, and finally Section 3.10 synthesizes overall CCD performance trends and trade-offs in wind turbine design.

3.1. Wind turbine controls

Control design influences wind turbine performance in two primary ways: (1) improving power production and operational efficiency, and (2) alleviating mechanical loads to ensure safety and prevent damage. In the first case, an advanced control design extracts more energy; in the second case, it enables the use of less expensive structures and materials while extending the wind turbine's operational life [84].

A simple dynamic model of a rotor can be written as:

$$I\dot{\omega} = T_{\text{aero}}(\beta, \lambda) - T_g \tag{6}$$

where $\lambda = \dfrac{r\omega}{v_{\text{rel}}}$.

Here, I is the moment of inertia of the rotor, ω is the angular speed of the rotor, T_{aero} is the aerodynamic torque, T_g is the generator torque, β is the blade pitch angle, λ is the tip speed ratio (TSR), r is the rotor radius, and v_{rel} is the relative wind speed experienced by the rotor. Based on Eq. (6), two torques can be varied to directly affect rotor speed: the aerodynamic torque T_{aero} and the generator torque T_g.

The aerodynamic torque depends on the blade pitch angle and TSR. It can be regulated directly by adjusting blade pitch β. The blade pitch can be controlled either collectively or individually for each blade of the rotor [85–91]. In collective pitch control, β parameter is shared for all blades, whereas in individual blade pitch control, β value is controlled for each blade according to its azimuth angle and blade load. Larger wind turbines especially benefit from individual blade pitch control, as each blade experiences significantly different aerodynamic conditions throughout its rotation.

Flap control and active flow control directly modify T_{aero} by altering the blade aerodynamics over all or part of the blade span [84,88,92]. Instead of rotating the entire blade via a pitch control, these approaches adjust local wind flow or loads using actuators placed spanwise along the blade.

The TSR is a derived quantity that depends on wind speed, system dynamics, and rotor speed, making it an indirect parameter for regulating rotor speed. The yaw control mechanism, which aligns the rotor with the wind direction, adjusts the relative wind speed v_{rel}. Yawing introduces an additional dimension of aerodynamic complexity that steers wake, and this effect becomes valuable when downstream turbines are present in a wind farm [93]. Farm-level control with wake steering is discussed further in Section 3.7.

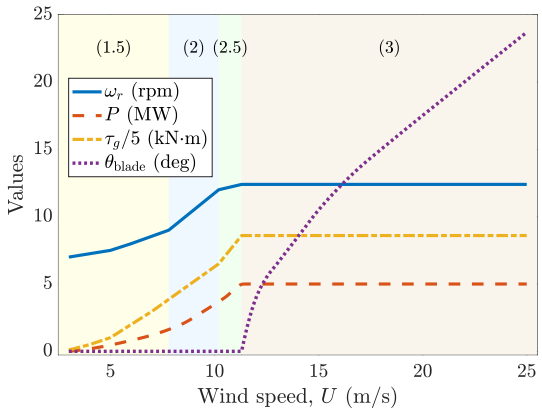

Fig. 7. Operating regions for the wind turbine and the corresponding trends of rotor speed ω_r (rpm), generator power P (MW), generator torque τ_g (kN·m; plotted as $\tau_g/5$ to share a common axis), and blade pitch θ_{blade} (deg). Background colors denote Regions 1.5 (yellow), 2 (blue), 2.5 (green), and 3 (light brown).

The generator torque T_g is regulated through dq-axis vector control that changes electromagnetic characteristics of the generator's currents and voltages, enabling simultaneous control of active and reactive power [94]. Specifically, the q-axis component of the stator current governs electromagnetic torque, which is used to regulate the rotor speed, while the d-axis component regulates reactive power.

Vibration control strategies mitigate structural fatigue in wind turbine components while modestly improving energy capture by reducing dynamic losses [95]. Various control devices and mechanisms have been studied, such as actuated struts within rotor blades for mitigating resonance vibration [96] and actively-controlled virtual tuned mass damper (TMD) for vibration suppression [97]. Although their direct influence on aerodynamic torque T_{aero} is relatively smaller than that of other power regulation controls, it primarily aims to suppress unwanted motions of the tower, foundation/platform, and rotor blades which improves overall LCOE of the wind turbine system.

Emerging research on TMD demonstrates significant value for FOWT systems where platform-tower coupling amplifies low-frequency motions that accelerate structural fatigue. Passive and semi-active configurations substantially reduce nacelle displacement and acceleration under combined stochastic wind-wave excitation scenarios [98]. In addition, inerter-enhanced variants further achieve comparable or improved vibration suppression with significantly lower physical damper mass, thereby avoiding adverse impacts on global stability associated with added tower-top weight [98,99]. By stabilizing tower dynamics, these vibration suppression mechanisms indirectly enhance both structural longevity and energy yield, particularly for FOWTs where excessive platform motion would otherwise hinder power capture and thereby raise LCOE [100].

Fig. 7 shows the schematic power curve for a 5 MW wind turbine across varied wind speed regions. Region 1 (not depicted in the figure) corresponds to winds that are too low for operation, because turbine losses exceed the captured energy. Region 1.5 represents the onset of operation. Rotor speed and generator torque increase gradually along with wind speed. Region 2 is dedicated to maximum power extraction, with generator torque as the primary control input while blade pitch remains nearly constant at a small angle. Region 2.5 corresponds to the transition to rated operation, where both generator torque and blade pitch are varied to regulate output power. Region 3 occurs at wind speeds higher than the rated wind speed, where the focus shifts to load reduction. Blade pitch (and any other control that influences T_{aero}) becomes the dominant control variable. The rotor speed is held near its rated value, and depending on the design, either generator torque or output power is fixed. Since $P_{\text{out}} = T_g\omega$, fixing T_g allows P_{out} to vary slightly with ω, whereas fixing P_{out} permits T_g to vary slightly. Finally, region 4 (not depicted in the figure) represents excessively high wind speeds at which the turbine is shut down to prevent damage.

Santoni et al. [91] demonstrated that individual pitch control can reduce the damage equivalent load (DEL) in Regions 2 and 3 by 3% and 40%, respectively, while having no impact on power production. The study also presents that the individual pitch control reduces high-frequency oscillations of wind turbine loads, thereby reducing fatigue and increasing the turbine's lifetime. Despite these benefits, individual blade pitch introduces drawbacks. Jelavić et al. [89] reported a concern about wear in individual pitch mechanisms due to the increased actuation cycles.

Implementation of actively-controlled mechanisms, such as individual pitch, yaw, or active flow, requires additional, more sophisticated sensors, actuators, and controllers that can increase cost. Because some of these technologies are not yet mature, further research is required before commercial deployment. Nonetheless, these studies demonstrate strong potential for coupling plant and control design disciplines. Advanced control strategies and actuators can reduce turbine loading, enabling the use of cost-effective materials and lighter structures, thereby lowering cost. These advanced methods can also increase power production, consequently reducing the LCOE.

When OLOC or MPC are employed for these controllers, the control design variables correspond directly to the control actions. Consequently, upper and lower bounds can be defined straightforwardly based on mechanical limits, such as the allowable blade pitch range, or component specifications, such as generator torque limits. In contrast, conventional CLC uses control gains rather than the actual control signals as design variables. As a result, physical limits must be enforced through path constraints. Path constraints are more complex for optimization algorithms than simple bound constraints, and the fixed structure of a CLC further diminishes its ability to satisfy them effectively. Therefore, ensuring compliance with these limits is inherently more challenging for CLCs than for OLOCs or MPCs.

3.2. Tower design

A primary design constraint for wind turbine towers is their natural frequency [101], which has been widely recognized as a dominant driver of tower mass, cost, and dynamic performance in offshore wind turbine design and optimization studies [4]. While the tower must provide adequate structural support for the rotor-nacelle assembly and resist wind and dynamic loads, resonance induced by certain excitation frequencies poses a significant design challenge. To avoid resonant excitation caused by thrust fluctuations at the blade passing frequency (3P, three times 1P) and, to a lesser extent, at the rotor rotational frequency (1P), it is essential that the tower's lowest natural frequencies do not coincide with these excitation frequencies [102].

The first natural frequency determines the tower classification: a "soft-soft" tower has its natural frequency below the rotor speed; a "soft-stiff" tower falls between the rotor speed and the blade passing frequency; and a "stiff-stiff" tower exceeds the blade passing frequency [103]. These categories indicate the tower's susceptibility to resonance and guide design for performance and structural integrity [104,105]. As tower height increases, achieving high stiffness becomes increasingly difficult because stiffness scales unfavorably with the height-to-diameter ratio. Consequently, soft towers have become the preferred solution [102,106].

The frequency constraint often becomes the binding constraint that limits the viable design space, especially in the soft-stiff configurations. As tower height grows while maintaining a fixed diameter and thickness profile, the natural frequency drops and the required mass rises drastically to keep natural frequency within an acceptable range [102, 106]. Conventional tower designs predominantly select soft-stiff configurations that can conveniently avoid resonance-induced loads. Recent advances in wind turbine control now enable effective load management

even under resonance conditions. This capability opens the door to soft-soft towers with very low natural frequencies, which can be realized using less stiff, thinner structures and reduced diameters [106].

In contrast, FOWT towers are typically engineered to be significantly heavier and stiffer than those installed on fixed-bottom structures. The FOWT towers need to withstand increased inertial and gravity loads from platform motion, and the natural frequencies need to be kept outside the range affected by wave motions [107,108].

The design of towers for FOWTs must carefully account for the 1P and 3P frequencies, particularly because these turbines operate over a wide range of rotor speeds under varying wind conditions. Consequently, the allowable design window (often soft-stiff design regime) is significantly narrower than that for fixed foundation wind turbines, and can dangerously approach resonance frequencies [108].

FOWTs also experience dynamic loads induced by ocean waves, which are stochastic and span frequencies from 0.05 to 0.20 Hz, corresponding to wave periods from 5 to 20 s. A soft-stiff tower design, where the natural frequency lies between 1P and 3P frequencies, is generally suitable for fixed foundation wind turbines. However, on floating platforms with large-scale turbines (e.g., ≥15 MW), this frequency window overlaps with the wave excitation band, making the traditional approach impractical.

For example, the NLR's 15 MW reference wind turbine supported by the University of Maine's VolturnUS-S semi-submersible floating platform employs a heavily reinforced tower with a first natural frequency of 0.496 Hz, which lies above the 3P frequency [107,109]. Raising the natural frequency to this level (a stiff-stiff tower design) increases the tower mass by 47% relative to an equivalent turbine with the monopile (fixed foundation) configuration. The additional mass reduces the platform's pitch and roll stiffness, thereby influencing its stability and other dynamic responses. Moreover, soft-stiff tower designs for FOWTs often exhibit excessive long-term fatigue damage, making a stiff-stiff configuration (first natural frequency above 3P) the more viable solution. This stiff-stiff tower design is typically implemented by thickening its wall while maintaining diameter and height. Offshore towers, however, are typically kept shorter to exploit reduced wind shear, but a minimum blade-tip clearance of a certain distance above the water surface (e.g., 25 m) is required for ship passage. As rotor diameter increases, taller towers become necessary [110].

Fig. 8 summarizes these frequency considerations by comparing tower natural frequencies with the excitation ranges of 1P, 3P, and ocean waves [109]. Wind turbine towers on fixed foundation structures have traditionally targeted soft-stiff designs, placing the tower frequency between 1P and 3P to avoid resonance. For larger FOWTs, on the other hand, this window overlaps substantially with the wave excitation band, making the soft-stiff configuration impractical. The figure also highlights recent FOWT designs, e.g., VolturnUS-S [107], that adopt a stiff-stiff approach to avoid both rotor and wave excitations at the expense of increased tower mass.

Control designs, such as generator torque, blade pitch, and active flow controls, significantly affect turbine rotor loads and thus, the tower's dynamic responses. Vibration control can further dampen these dynamic responses and reduce fatigue loading, extending tower life without requiring additional mass (e.g., thicker walls or larger diameters). Consequently, within the CCD context, advanced control designs may potentially enable lightweight soft-soft towers while limiting fatigue damage. Some important constraints to consider in tower design include (1) maximum stress at the base and top of the tower, (2) maximum tower tip deflection, (3) tower buckling, (4) fatigue loading, (5) diameter-to-thickness ratio (for welding during turbine assembly), (6) tower heights taller than the rotor radius plus ground clearance, (7) shell buckling with maximum thrust and survival load conditions (with appropriate safety factors), and (8) simple variable bounds for manufacturability [105,111].

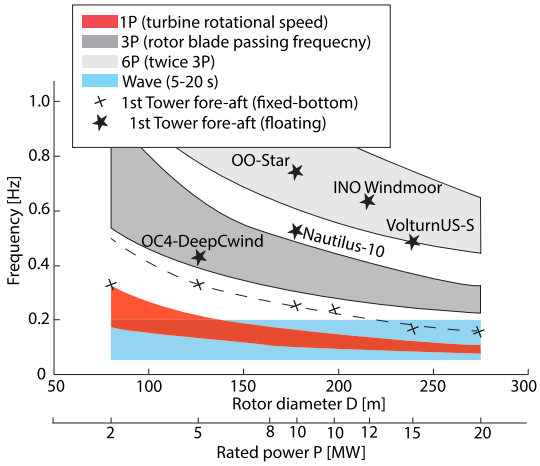

Fig. 8. Tower natural frequencies relative to turbine excitation frequencies and wave frequencies. The shaded regions indicate the ranges of 1P (rotational speed), 3P (blade-passing frequency), 6P (twice 3P), and ocean waves (5–20 s). Black crosses mark the first tower fore-aft natural frequency for fixed-bottom turbines, while blue stars indicate floating turbine designs, including OC4-DeepCwind, NAUTILUS-10, OO-Star, INO WINDMOOR, and VolturnUS-S. Reproduced from Sergiienko et al. [109], © Elsevier (2022), used with permission.

3.3. Rotor design

The wind turbine rotor is connected to the main shaft of the drivetrain, and comprises several components, including blades, rotor hub, pitch system, and nose cone. Among these components, the blades along with pitch system control dominate power capture and overall efficiency. Blade design is split into two tightly coupled sub-problems: (1) aerodynamic design and (2) structural design. Along the blade span, each region serves a distinct role. The root is the thickest part that carries the highest load [112]. Structural constraints dominate in designing this region. The mid-span design is dominated by aerodynamic performance and lift-to-drag (C_L/C_D) ratio is maximized by employing an optimal airfoil cross-section shape that is permissible from a structural standpoint [113,114]. The tip is aerodynamically critical, and often specialized geometry is employed to enhance performance and reduce noise and losses [113]. A comprehensive review on the evolution of wind turbine rotor and blades is given in Refs. [115,116].

Fig. 9 presents these aerodynamic and structural elements in a section of a generic rotor blade, highlighting the leading and trailing edges, spar caps, and shear webs.

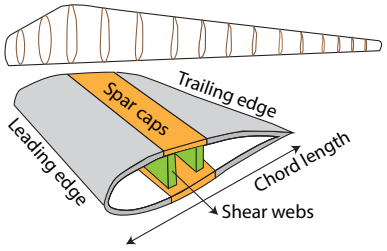

Fig. 9. Wind turbine blade schematic highlighting aerodynamic and structural elements. Aerodynamic performance is governed by chord, twist, and airfoil shape, while structural integrity is provided by spar caps and shear webs. The inboard section is structurally dominant, whereas the outboard section is more critical for aerodynamic efficiency [113,114].

In the aerodynamic design sub-problem, the design variables are typically associated with the spanwise distributions of chord length, twist angle, and airfoil cross-sectional profile. Particularly, the airfoil profile distribution is obtained by selecting discrete cross-sectional profiles at several stations along the blade and smoothly blending them to produce a continuous geometry [117]. Common objective functions in the aerodynamic design sub-problem focus on (1) power extraction within certain range of TSR by maximizing power coefficient (C_p) [118], (2) aerodynamic efficiency by maximizing lift-to-drag ratio (C_L/C_D) [119], (3) thrust load management by minimizing thrust coefficient (C_t) [120], (4) acoustic noise by minimizing sound power level (L_{WA}) [121], and (5) finding optimal TSR that achieves optimal power generation while balancing structural loading due to centrifugal and aerodynamic forces, costly reinforcing materials used, and acoustic noise level [122].

The structural design sub-problem is typically associated with the chord-wise location of shear webs, their thicknesses, chord extension, spar-cap thickness, and composite material layers [90,113,122]. Widely employed objective functions in the structural design sub-problem are (1) minimizing blade mass [113,122–124], (2) minimizing peak stress, strain, compliance, or DEL on various blade components, including root, spar caps, and shear webs [90,125,126], (3) minimizing blade tip flap-wise and edge-wise deflection [122,127,128], and (4) maximizing frequency separation margin from 1P and 3P frequencies [128,129].

From a system design perspective, these component sub-problem objective functions are typically recast as inequality constraint functions that impose minimum or maximum allowable values. The overall system design problem therefore focuses on maximizing system performance metric (e.g., AEP), while the sub-problem targets may be relaxed within their feasible bounds to improve the global objective. Regardless of whether system-level design or component sub-problem is formulated, CCD enables simultaneous optimization of rotor structure, aerodynamics, and control, ensuring that all loading constraints are satisfied, power output is maximized, and blade mass is not necessarily increased [11].

Wind turbine blades must withstand cyclic loading caused by gravity and wind shear at 1P frequency [90]. Prior to finalizing the design, the blade geometry has to be mapped to the capabilities of the available manufacturing processes. Even small geometric variations can largely affect aerodynamic efficiency as well as production difficulty, and hence cost. For example, reducing the twist angle or linearizing the chord distribution simplifies lay-up and material handling, but it also diminishes the wind turbine's power capture. Consequently, trade-offs in manufacturing against performance should be considered to achieve the optimal net benefit [122].

Although alternative numbers of blades (e.g., two-bladed turbines) and downwind configurations are occasionally examined for niche applications (e.g., SUMR 50 MW [130]), the upwind three-blade layout is generally regarded as optimal for large-scale wind turbines [115,116]. Three blades achieve aerodynamic efficiency close to the Betz limit, while additional blades yield diminishing returns. The three-blade configuration also provides inherent dynamic balance and smoother rotation, thereby reducing gyroscopic stresses compared to two-blade designs. Moreover, a two-blade turbine must operate at a higher TSR, which increases mechanical loading on the blade structure and significantly increases acoustic noise levels.

3.4. Foundation design for land-based wind

The foundations provide structural support for the wind turbines to be securely anchored to the ground, seabed, or other locations of installation [131–134]. The foundation design directly affects wind turbine dynamics, structural integrity, and performance, thereby largely influencing cost and service life [133,135]. The foundations are largely categorized into land-based foundations, offshore fixed foundations, and offshore floating platforms. Each category requires unique design considerations to balance performance and cost effectiveness.

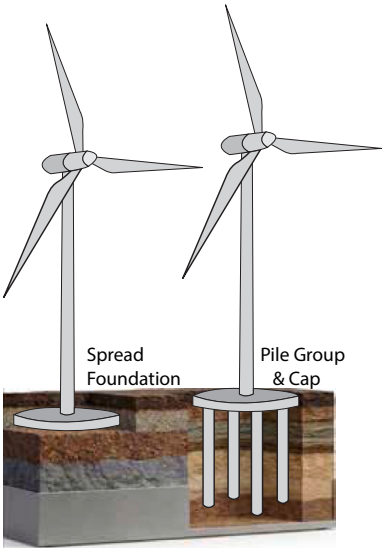

Fig. 10. Representative land-based wind turbine foundations. (a) A shallow spread-footing foundation transfers overturning loads primarily through its own mass and bearing pressure distribution. (b) A deep pile group foundation transfers loads to deeper, stiffer soil layers, providing higher lateral stiffness and moment capacity in weak or compressible soils.

Land-based wind turbines are supported either by shallow or deep foundations. Most existing land-based wind turbines are mounted on a spread-footing foundation (see Fig. 10(a)), which is a shallow foundation, made from cast-in-place reinforced concrete slab [136]. This type of foundation requires a relatively large area, but the amount of required excavation and refilling is minimal [136,137]. It supports wind turbine structure by using its own mass to withstand the overturning moment produced by wind thrust [138]. Because the resisting mechanism is purely gravitational, the slab must rest on an extensive base area so that the pressure applied to the ground does not cause excessive soil deformation [136].

As wind turbine size increases, the required area of foundation's footprint and volume of reinforced concrete grow drastically [136]. Beyond a certain scale, the practical and economic constraints of enlarging the shallow foundation become prohibitive, demanding the adoption of alternative foundations to meet the structural requirements. While a similar area of footprint is still required, a few types of shallow foundations, including ribbed and braced structures, significantly reduce the required amount of volume-filling materials [138,139].

Deep foundations are often employed for very large turbines because they convey the substantial overturning moment to deeper soil or to bedrock, allowing a much smaller surface footprint. They can also be used when soil conditions are poor [140]. By anchoring the structure in deep soil layers or bedrock, the foundation can achieve the necessary stiffness and load bearing capability (see Fig. 10(b)). Typical deep foundations utilize solid piles, bored caissons, or anchors to reach deep inside soil or tie down to a reliable bedrock layer [139].

Many of the design considerations for land-based foundations fall within the area of geotechnical engineering. Nonetheless, the dynamic behavior of the foundation strongly affects the design of other components of wind turbines. Rocking, translational, and torsional impedances of the foundation-soil (or -bedrock) system dictate how vibrations propagate through the entire wind turbine system. Consequently, the foundation system must be concurrently designed along with other parts of the wind turbine system. The foundation's dynamic model must explicitly incorporate the total overturning moment transmitted by the wind turbine to support the system [140]. The natural frequencies of soil-structure interaction (SSI) must be positioned away from both the

operational frequency range and prevailing seismic excitation to prevent resonance [141].

3.5. Fixed foundation design for offshore wind

Fixed foundations are commonly used as the primary support structures for wind turbines installed in shallow to moderate water depths, depending on their types, typically up to 60 m [142]. The aim of these foundations is to support the offshore wind turbines (OWTs) by anchoring rigidly to the seabed, thereby providing stability through structural stiffness and lateral resistance using the SSI [132]. Unlike land-based foundations, offshore fixed foundations must resist not only aerodynamic and gravitational loads but also hydrodynamic forces produced by waves, ocean currents, and in some cases, floating sea ice [133,134,143]. As shown in Fig. 11, the most prevalent types include monopile, gravity-based, suction bucket, tripod, and jacket structures [142,144]. Each type is selected based on site-specific conditions, such as water depth, wind, wave, and water current loadings, and seabed soil conditions [142].

Monopile foundation is the most widely adopted foundation type for OWT projects in shallow waters. Although monopiles can be installed in depths of up to 35 m, they are most commonly used at sites shallower than 25 m [146,147]. It consists of a single cylindrical steel pile driven into the seabed, which provides lateral stiffness and moment resistance through the SSI [132]. The monopile diameter and embedment depth are key design parameters determined along with the wind turbine system and soil characteristics.

Monopile diameter and its embedment depth are the primary plant design variables, determined along with the wind turbine system design, design load cases (DLCs), and the site-specific geotechnical conditions [147,148]. A CCD approach that incorporates SSI tightens the dynamic response envelope of the wind turbine system under DLCs, improving cost-effectiveness across manufacturing, installation, and operation, while mitigating fatigue damage [149,150]. As with any foundation type, monopile systems' natural frequencies, accounting for soil, hydrostatic, and hydrodynamic effects, must be kept separate from rotor and wave excitation frequencies [151].

Monopile foundations dominate OWT deployments because of their simplicity and cost-effectiveness in design, manufacturing, and installation [133,148]. However, for turbines larger than 15 MW or water depths beyond 35 m, monopile foundations become less viable due to reduced structural and dynamic performance, stronger hydrodynamic interactions, fatigue from pile driving, and difficulty achieving the required lateral stiffness [133,144,152]. In such large, deep-water, or high-stiffness scenarios, jacket or tripod foundations are often adopted [133,153].

Jacket foundations are lattice-type frames where the loads are distributed through multiple slender tubular members fixed to the seabed with small-diameter piles [153]. By distributing forces among many members, they achieve high stiffness while using far less steel than a large-diameter monopile [154]. This makes jacket foundations suitable for water depths up to 60 m and for large wind turbines that require strong lateral support [153]. Although jacket foundations overcome the limitations of monopiles in deep water or for very large wind turbines, their complex geometry and the need for multiple small piles demand more sophisticated manufacturing and installation. Consequently, they are presently designed using sequential procedures [155]. Here, a CCD approach can further improve the cost-effectiveness of these foundations by leveraging tightened dynamic response envelope achieved through plant-control synergies.

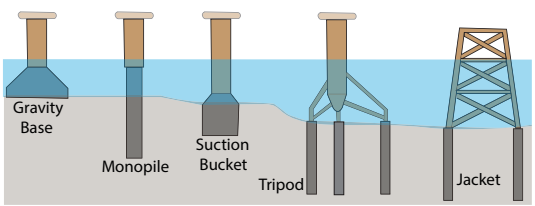

Fig. 11. Common fixed-bottom foundation types for offshore wind turbines: gravity-based, monopile, suction bucket, tripod, and jacket. Selection depends on water depth, soil conditions, and required lateral stiffness. Reproduced from Nikitas et al. [145], © Elsevier (2020), used with permission.

Dynamic interaction between the foundation, sub-structure, and soil significantly influences the global response of OWTs. The design of fixed foundations must address the combined effects of geotechnical and structural influences on the wind turbine system, including bearing capacity, lateral stiffness, fatigue resistance, and installation techniques. The foundation design also has to meet the system-level dynamic requirements, such as ensuring the natural frequency is kept away from 1P and 3P excitation frequencies and wave-induced resonance frequencies [141,151]. Therefore, foundation design for OWTs is intrinsically coupled with the dynamics of the wind turbine, demanding CCD optimization to further improve system performance and the life of the wind turbines.

3.6. Floating platform design for offshore wind

While fixed foundations remain viable for shallow to moderate depths, typically within 60 m, as established in Section 3.5, they become physically impractical beyond this threshold, where stronger and consistent offshore wind resources are concentrated, necessitating floating platform deployment [156]. FOWTs inherently exhibit greater motion under aerodynamic and hydrodynamic loads compared to OWTs with fixed foundations or land-based turbines due to their reduced system stiffness. Moreover, the system must maintain stability under both operational and extreme metocean conditions. Consequently, the design of floating platforms significantly governs the dynamic response, lifetime cost, and overall viability of the entire FOWT system.

FOWTs are typically classified based on the physical principle that provides their stability into three categories: ballast-stabilized, buoyancy-stabilized (e.g., semi-submersible), and mooring-stabilized (e.g., tension-leg) platforms [157,158]. Ballast-stabilized platforms achieve their stability by a low center of gravity relative to the center of buoyancy. Typical ballast-stabilized platforms include spar-buoys, where a long vertical hull provides a large hydrostatic restoring moment. The key plant design variables are draft height, diameter distribution, and ballast mass distribution along the hull [11].

Buoyancy-stabilized platforms, such as semi-submersibles, rely on hydrostatic stability generated through a large waterplane area rather than buoyant force generated by displacement alone. These platforms achieve restoring moments by strategically distributing buoyant forces across widely spaced columns and connecting pontoons, which increases the moment of inertia of the waterplane geometry. This configuration establishes a positive metacentric height and the center of buoyancy shifts laterally during inclination to produce a restoring moment [157]. The key plant design variables can include various geometric parameters, such as column spacing, column diameters, draft height, and pontoon shape and volume [21,24,159]. There is a clear link between the diameter of the wind turbine rotor and the combined value of the distance between offset columns and their diameters [109].

Mooring-stabilized platforms, such as tension-leg platforms (TLPs), fundamentally differ by operating in a hydrostatically unstable configuration, where stability is entirely dependent on vertical tether tension. The platform achieves near-constant immersion depth through high pretension forces that keep tethers taut during normal operation, while pitch and roll stiffness are dominated by the axial stiffness of these tethers [160,161]. Key design variables include material, thickness, axial stiffness of tether, pretension force that balances with buoyancy and system mass, tether count and layout, and attachment geometry, in addition to the floating platform geometry that generates buoyant force [157,162,163]. Important characteristics distinguishing TLPs

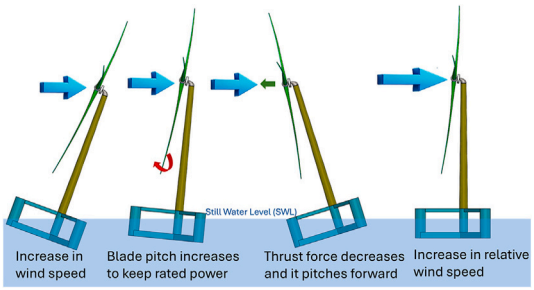

Fig. 12. Illustration of the negative damping dynamic cycle in FOWT. The cycle begins with an increase in wind speed, prompting the turbine controller to increase the blade pitch angle to maintain rated power. This adjustment causes a reduction in thrust force, leading the floating platform to pitch forward. As the platform pitches, the rotor experiences an increase in effective wind speed, perpetuating the cycle. This phenomenon, known as negative damping, highlights the coupling between blade pitch control and platform motion, which can destabilize the system under certain conditions.

include their minimal waterplane area which reduces wave excitation loads [164]. However, this minimal waterplane area increases risk of slackening tethers during extreme heave motions [165].

Because the floating platform of FOWT systems can pitch and heave in response to wave-induced forces, the inflow wind seen by the wind turbine rotor varies with platform motion. Therefore, floating platform dynamics affect the wind turbine control design. This coupling raises concern in the well-known *negative aerodynamic damping* phenomenon for FOWT systems, which may lead to increased platform motion and wind turbine loads as the floating platform pitches [166]. Fig. 12 illustrates the sequence of negative aerodynamic damping phenomenon. When the turbine operates in Region 3 (full-load region), the blade pitch control reduces thrust to keep power at its rated value. The resulting drop in thrust allows the platform to pitch forward, which in turn increases the effective wind speed on the rotor and triggers an additional increase in blade pitch angle. The loop can become unstable if the hydrodynamic damping of the platform is insufficient to counteract the negative aerodynamic damping [167]. Several studies have demonstrated that augmenting the control scheme with direct feedback of measured platform pitch angle can provide an effective stabilization [168].

With the CCD framework, this insight opens the possibilities to exploit the couplings between turbine control and floating platform dynamics, which could be adjusted by optimizing physical configurations, such as draft height, column diameters, and stiffness of the tethers. Designing plant and control systems simultaneously helps stabilize the FOWT systems without significantly increasing the platform mass, which would otherwise increase the total project cost significantly.

When designing a floating platform for a FOWT, several constraints must be considered. First, the stability of the FOWT system is the key constraint for the floating platform design under both normal operating and extreme survival conditions. This constraint is typically expressed as limits on maximum pitch and roll inclinations or their accelerations [169]. Next, a minimum freeboard height needs to be kept to maintain the floating platform's stability under large wave motions [169]. As with any other wind turbine foundation, the natural frequencies of the floating platform (also accounting for the wind turbine system) must lie outside any potential excitation frequencies, including wave period band (typically 5–25 s) and 1P and 3P frequencies [169]. In addition, the floating platform must provide sufficient buoyancy to support the entire wind turbine system. The upward buoyant force must balance all downward loads, including the weight of the wind turbine system and ballast, the mass of the mooring lines, and the tension in these lines, while providing an adequate draft and displaced volume [159].

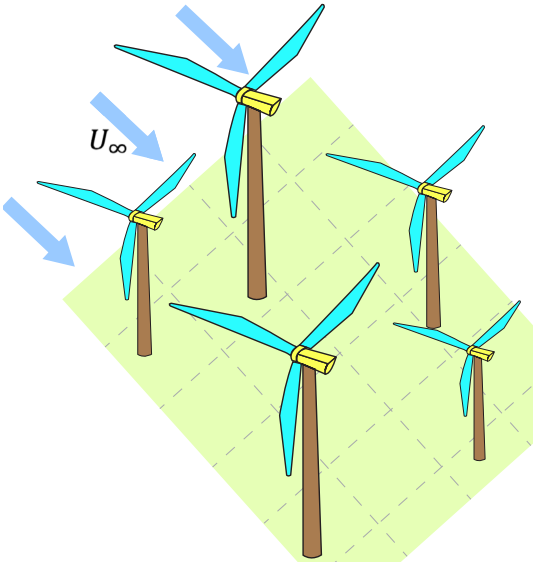

Fig. 13. Illustration of a wind farm layout with turbines of different hub heights positioned at various locations to reduce wake interference and maximize overall energy production.

3.7. Farm-level design

While most CCD studies for FOWTs address the coupling between plant and control design within a single wind turbine system, extending the scope to farm-level control opens additional opportunities to harness performance gains via synergistic design among interacting turbines across the entire wind farm [111,170,171]. In these wind farm design studies, the design problem extends beyond a single turbine's plant and control systems. It also encompasses turbine locations, array layout, heterogeneous hub-height and rotor diameter selection, and collective control coordination strategies so that all turbines within the farm maximize the total energy production, as illustrated in Fig. 13. Particularly, such heterogeneous farm layouts can reduce wake-induced losses and lower the overall LCOE [111]. These added degrees of freedom substantially enlarge the optimization space and can be effectively solved within CCD framework.

In addition to combined wind turbine and farm-level plant design problems, wake steering has emerged as a key strategy that significantly enhances farm-level performance [93,172–175]. Wake steering has also been investigated in the context of CCD [176]. The basic idea is to yaw an upstream wind turbine deliberately away from the wind direction, so that its wake is deflected away from downstream wind turbines. This technique increases the inflow velocity and consequently increases the power of downstream wind turbines. Although the steering turbine suffers a slight loss in its own power output, the net farm power output can increase, as demonstrated in various analytical, numerical, and experimental models and field measurement studies [177,178].

Recent full-scale field experiments and coordinated wind farm campaigns have further validated the practical feasibility of wake steering under real operating conditions, demonstrating consistent farm-level energy gains across different sites and atmospheric regimes [179–182]. These studies confirm that wake steering can be deployed in commercial wind farms without major hardware modifications, strengthening its relevance for industrial applications.

However, these results also highlight important challenges associated with real-world implementation. The effectiveness of wake steering is highly sensitive to wind direction variability, turbulence intensity, and atmospheric stability, which introduce uncertainty into optimal yaw misalignment strategies [173,183]. In particular, increasing the

yaw update frequency does not necessarily improve performance; overly frequent updates can lead to overreaction to turbulent fluctuations, reducing net energy gains while increasing yaw actuator duty and fatigue [184].

From a modeling and control perspective, most wake steering approaches rely on steady-state or reduced-order wake models to determine optimal yaw offsets [185]. While these models enable tractable optimization and real-time implementation, they introduce inaccuracies due to simplified physics and limited representation of transient wake dynamics. Moreover, scaling wake steering to large wind farms introduces additional complexity, as turbine interactions become highly coupled and sensitive to spatial and temporal variability. Recent studies have identified key barriers to widespread deployment, including uncertainty in inflow conditions, model mismatch, actuator limitations, and trade-offs between energy gains and increased structural loading [186]. These challenges motivate the need for more robust, adaptive, and system-level control strategies, reinforcing the importance of integrating wake steering within the broader CCD framework.

Building on these practical insights and identified challenges, wake steering has progressed further from a static yaw-offset concept to a dynamic, time-varying control problem [9]. Since wind direction fluctuations occur on time scales comparable to wind turbine yaw actuation, an optimal steering control strategy must balance the steering effectiveness and yaw alignment uncertainties. Probabilistic wake models that explicitly account for wind direction variability have been shown to recover substantially more power from wake losses than fixed-offset approaches [173]. Consequently, yaw-based real-time wake steering control, together with other farm-level design variables, constitutes a natural candidate for inclusion in the CCD framework.

Active wake mixing (AWM) has recently emerged as an effective approach for mitigating wake effects on downstream turbines by leveraging interaction with the atmospheric boundary layer [187]. Practical implementations of AWM employ deliberate blade pitch modulation to generate controlled unsteady disturbances, such as pulsed or helical structures, into the wake [188,189]. These disturbances enhance turbulent mixing between the low-energy wake flow and the surrounding high-energy ambient wind, accelerating wake recovery and increasing downstream wind velocity.

Building on these developments, wind farm control must also account for multi-turbine dynamic coupling, where turbines interact through complex aerodynamic wakes and, in offshore settings, additional structural and platform-induced dynamics [190,191]. These interactions, already evidenced in recent field-scale wake steering studies, highlight that optimal farm performance cannot be achieved by treating turbines independently. Instead, both plant and control decisions must be coordinated across the farm to manage coupled dynamics, uncertainty, and real-time variability.

3.8. Model complexity

Numerical models can range from simple first principle equations that govern low order physical response of a system to complex fluid dynamics simulations. The former models can be solved manually via simple algebraic manipulations, while the latter models require high-performance computing (HPC) equipment with a massive number of cores and other hardware resources. For practical purposes, the range of these models can be classified into three larger categories: low-, medium-, and high-fidelity models. Multi-fidelity models also exist, which blend data sampled from different fidelity-level models. There are also various surrogate models or data-driven models that predict system behaviors rather than relying on underlying physics, an approach that has been increasingly adopted in offshore wind turbine structural and tower optimization to reduce computational cost while enabling large-scale design exploration [4].

Typically, low-fidelity models are used during the initial stage of wind turbine design for sizing analysis and optimization. Mid-fidelity models, or engineering-level tools, are used after the initial design stage for loads analysis of wind turbines to examine operational and extreme conditions. High-fidelity models are typically used during the final design stages for detailed investigations, especially to accurately obtain stresses on the structure, as summarized in Fig. 14.

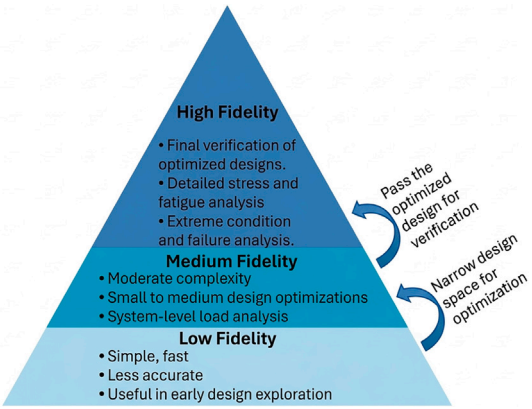

Fig. 14. Pyramid representation of model fidelity in wind turbine design. Low-fidelity models are simple, fast, and suitable for early-stage sizing and design of experiments (DOE). Mid-fidelity models balance accuracy and computational cost, making them practical for system-level loads and operational analysis. High-fidelity models provide the highest accuracy and are used for final verification and detailed stress analysis. A multi-fidelity approach can combine these levels across different design stages.

However, choosing the right model fidelity also requires consideration of the underlying physics. On one hand, if the physics is relatively simple, then a low-fidelity model may be highly accurate, and more sophisticated simulations will yield diminishing returns. On the other hand, if the underlying physics is complex, then the results of a low (or even medium) fidelity model may be unreliable. This trade-off is confounded by the fact that some systems can be difficult to accurately simulate on one size or time scale (e.g., macro vs. micro) but exhibit relatively easy-to-model patterns on the other scale; in these cases, a multi-fidelity approach may also be used where elements of each fidelity-level model are used in the different stages of design. As an example, higher fidelity tools may be used to tune lower fidelity ones, or as checks for certain high-impact design conditions [192].

Here, accuracy refers to the degree to which simulated estimation deviates from measured or real physical behavior. It is typically expressed through statistical summaries or direct comparison metrics. On the other hand, fidelity level characterizes the extent to which the numerical model simplifies or preserves the underlying physics or phenomena of interest. It reflects the level of confidence that the reported accuracy is genuinely representative of real physical behavior. Computational efficiency is often used for comparing different computational approaches. It is frequently reported as the amount of time required for a computer model to complete using specified computing equipment and conditions. However, instead of using computational efficiency with time as a metric, directly comparing the complexity of each computational approach or problem becomes more visible in the dynamical systems domain [192]. This metric is often measured through the required floating-point operations to solve problems.

Various general purpose open-source, commercial, and specialized in-house numerical software packages exist for modeling and designing wind turbines and farms across all fidelity levels. A few popular computational codes and toolsets are introduced in Section 2.11 and Fig. 6.

Within these, low-fidelity models are further categorized as either frequency-domain (e.g., RAFT [49], HAWCStab2 [50], QuLAF [51], and in-house codes [158,193]) or time-domain (e.g., SLOW [20] and specialized codes [163,194]). They are predominantly utilized during

early-stage sizing and conceptual design. These models typically achieve solution times faster than real-time, a critical advantage for digital twin implementation where real-time simulation with feedback is essential.

Mid- and high-fidelity models employ progressively detailed analyses, as illustrated in Fig. 14. Mid-fidelity models, such as OpenFAST [17], QBlade [19], HAWC2 [47], SIMA [48], and Bladed [18], provide more detailed physical response information beyond low-fidelity simplifications. These engineering-level tools integrate coupled aero-hydro-servo-elastic dynamics while maintaining tractable computational costs, making them ideal for system-level design analysis under operational and extreme conditions. Specialized mid-fidelity disciplinary solvers (e.g., OrcaFlex [195] or ANSYS AQWA [196] for hydrodynamic interactions) further enhance system response details in targeted physics domains.

High-fidelity models, while computationally intensive, provide highly detailed resolution for local phenomena validation, such as aerodynamic stall, vortex shedding, or stress concentrations at structural components. General purpose high-fidelity solvers, such as OpenFOAM [197], Star-CCM + [198], and ANSYS Fluent [199] for fluid dynamics, and ANSYS Mechanical [200] for structural analyses, enable rigorous validation of specific load scenarios at detailed scale behaviors. Some high-fidelity tools, such as SOWFA [55] for atmospheric turbulence, and VABS [57] and pyNuMAD [56] for structural analysis of laminated composite blade materials, are specifically developed for wind turbine applications.

In CCD, low- and medium-fidelity models are typically used, considering practical computational expenses. The optimized design from CCD is then further investigated with higher fidelity models in the next step to ensure the design candidate meets all guidelines. Therefore, the optimized design from CCD should not be viewed as the final design, but rather as a preliminary one requiring further study.

3.9. Objective function for wind turbines

Formulating a CCD problem requires defining an objective function (or multiple functions in multiobjective formulations) to minimize or maximize for an optimal design solution. The selection of these objective functions is driven by design-stage requirements, priorities, and practical considerations within wind turbine development projects. Some available objective functions are specific to particular disciplines, e.g., optimal TSR tracking, turbine load minimization, and platform mass minimization, while other objective functions holistically capture integrated system behaviors of wind turbine through metrics, such as power output, capital cost, and cost of energy [201,202]. In general, cost, mass, AEP, and LCOE are popular choices for system-wide CCD problems.

Mass minimization often serves as a lower fidelity proxy for cost reduction during early-stage sizing. Mass correlates strongly with material and manufacturing costs, and direct cost quantification is often infeasible at low fidelity design representation due to complexities. This simplification enables tractable exploration of design spaces. AEP is another intermediate metric that can be used as an objective function in the CCD problem, particularly when cost factors remain unchanged. It is often utilized as the objective function for inner-loop control discipline in nested CCD formulation. On the other hand, the LCOE represents the higher fidelity objective that encompasses mechanical to electrical energy conversion, capital and operational expenses, and other financial considerations over the lifetime of the system. Minimizing LCOE thus becomes the ultimate goal throughout major stages within the wind turbine design process.

Among wind turbine design objective functions, LCOE provides a comprehensive evaluation compared to alternatives [202]. Pure AEP maximization risks economically nonviable designs through excessive cost growth, while cost minimization sacrifices energy yield. Despite its advantages, the adoption of LCOE introduces drawbacks when detailed cost modeling links to wind turbine design variables. Cost functions often exhibit discontinuities and noise from discrete elements, hindering gradient-based optimizers to converge to solutions. Furthermore, LCOE functions are poorly scaled with highly flat response topography near optima, challenging convergence to optimal solutions. These limitations must be addressed in CCD formulation. As discussed in Sections 2.2 and 2.3, the nested CCD approach (Fig. 2(b)) using gradient-free optimizer for outer-loop plant design offers a practical solution to these challenges.

3.10. CCD performance trends and trade-offs

Despite the diversity of formulations in wind turbine CCD, several consistent quantitative trends emerge across the literature when comparing different architectures and modeling approaches. Foundational reviews and methodological studies emphasize that the effectiveness of CCD depends strongly on plant-control coupling strength, constraint activity, and architectural choice, particularly when transitioning from decoupled to integrated formulations [12,90]. These observations are supported by a wide range of application-specific studies across both onshore and offshore wind turbines.

Table 1 summarizes representative studies categorized by CCD architecture, turbine scale, control strategy, and reported performance metrics. Across these works, simultaneous and integrated CCD formulations generally outperform purely sequential approaches when strong coupling exists between plant and control sub-systems. This effect is especially pronounced in FOWTs, where platform motion directly influences aerodynamic loading and control response [11,21,163,204,208,210].

Several studies report explicit quantitative improvements. For example, an integrated aero-structural-control design of a 13 MW downwind rotor achieved approximately 25% reduction in LCOE, demonstrating the economic impact of tightly coupled design decisions at utility scale [206]. In floating systems, a nested CCD applied to a spar-type FOWT reported more than 11% improvement in AEP relative to baseline designs [11], while an LPV-based nested formulation achieved approximately 3.4% reduction in LCOE [21]. At larger scales, a 22 MW semisubmersible FOWT study showed that simultaneous CCD reduced structural mass by approximately 2% compared to a sequential approach, although the latter exhibited greater robustness and convergence stability [210]. Additional multidisciplinary studies further highlight the importance of integrated design; for example, floating vertical-axis wind turbine (VAWT) systems achieved up to 24% improvement in AEP under realistic constraints and up to 40% under relaxed conditions [163]. At smaller scales, techno-economic co-design of distributed wind turbines demonstrated substantial reductions in LCOE and payback period when design and control were optimized jointly [203].

In contrast, when plant-control coupling is weaker or dominated by a single sub-system, the quantitative benefits of CCD are more modest. A sensitivity-based study focusing on tower design reported approximately 0.53% reduction in cost of energy, along with structural changes such as lighter and taller tower configurations under fatigue-driven constraints [211]. This indicates that the magnitude of CCD benefits depends not only on the selected architecture but also on the relative importance of coupled dynamics within the system.

Control strategy selection plays a critical role in shaping CCD outcomes and can itself be treated as a design variable. For example, in a spar FOWT study, OLOC yielded the highest AEP, while MPC provided improved constraint satisfaction and feasibility [204]. Similarly, comparisons between collective pitch control (CPC) and individual pitch control (IPC) demonstrate that control architecture significantly influences structural loading, with IPC achieving approximately 3%-40% reduction in fatigue loads depending on operating conditions [91]. These findings indicate that controller structure directly affects both performance and the feasible design space.

Parameter sensitivity analyses further reveal that performance improvements are strongly governed by a subset of dominant variables. Across multiple studies, tower-related parameters (e.g., height and structural properties) and platform-related variables (e.g., geometry,

Table 1
Comparison of representative wind turbine CCD studies, including architecture, control strategy, performance outcomes, and key sensitivity drivers.

Ref.	System scale	Arch.	Control	Key quantitative results	Key sensitivity insights
[203]	Small-scale WT (0.6–5.8 kW)	Simul.	CL, Maximum power point tracking (torque control)	~40–45% LCOE reduction and ~50% discounted payback period (DPP) reduction	Rotor diameter, specific power (rated power/rotor area), and nominal wind speed dominate performance
[204]	5 MW Spar FOWT	Nested	OLOC, MPC	~5–7% higher AEP with OLOC compared to MPC; OLOC satisfies constraints while MPC and ROSCO exhibit violations	Tower height dominates AEP; controller choice strongly affects the feasible design space
[205]	Large WT (25 MW)	Simul.	CL, Setpoint optimization (pitch, torque)	~0.2–0.3% AEP increase compared to classical control; up to ~12% reduction in peak thrust	Optimal pitch varies with wind speed; performance is highly sensitive to TSR mismatch and control law selection
[163]	5 MW Floating VAWT	Simul. (MDO-based CCD)	OLOC, optimal torque/RPM control	Up to ~24% AEP increase (up to ~40% with relaxed constraints); CCD yields lower LCOE than sequential design	Performance is dominated by control design; control constraints strongly influence platform design and coupling
[206]	13 MW downwind rotor	Seq. (iterative CCD)	CL, load-reducing control	~35% AEP increase; ~24% LCOE reduction compared to a conventional rotor	Blade length and aerodynamic design drive AEP, while control reduces loads, enabling lighter structures
[21]	15 MW FOWT	Nested	OLOC	~3.4% LCOE reduction (89.30 → 86.27 $/MWh)	Platform geometry strongly influences cost-performance trade-offs and control coupling
[207]	Blade system (~10 MW WT)	Simul.	CL, distributed aerodynamic control	~21% tip deflection reduction, ~5% blade cost reduction, and ~1.3% LCOE reduction	Blade-control coupling via flap design and controller tuning dominates performance
[208]	15 MW FOWT (semisub.)	Simul.	ROSCO pitch, torque control	Minimization of tower DEL under constraints (platform pitch < 6°, rotor overspeed < 30%), enabling lighter structures with an AEP-load trade-off	Platform geometry and pitch control gains jointly govern AEP, loads, and stability
[209]	FOWT + TLMCD	Simul.	CL, pitch control & damping	Reduced loads and motions at fixed displacement, or reduced displacement at fixed loads (Pareto trade-off)	Damper and pitch control tuning jointly govern performance
[210]	22 MW FOWT	Seq. vs Simul.	ROSCO	~2% structural mass reduction (simultaneous CCD) with comparable performance	Trade-off between robustness (sequential) and performance/mass reduction (simultaneous)
[11]	5 MW Spar FOWT	Nested	OLOC	>11% AEP increase	Tower geometry (especially thickness) dominates AEP due to strong aero-structural-control coupling

pitch motion, and hydrodynamic characteristics) consistently emerge as primary drivers of system performance [11,21,204,205,211]. In floating systems, hydrodynamic and structural parameters governing platform motion are tightly coupled with control behavior, amplifying the importance of integrated design [21,205,208,210]. Additional elements, such as damping systems and distributed aerodynamic control devices, further increase design dimensionality and influence optimal solutions [207,209].

The choice of CCD architecture significantly affects both achievable performance and computational tractability. Sequential approaches remain practical and robust but may overlook critical coupling effects. Nested formulations provide a scalable compromise by embedding controller optimization within an outer-loop plant design, enabling improved performance with moderate computational cost [11,21]. Simultaneous CCD offers the most comprehensive treatment of coupling but can introduce substantial computational challenges and sensitivity to numerical implementation, as highlighted in both wind turbine applications and general methodological studies [12,210]. These findings confirm that no single architecture is universally optimal; rather, the appropriate choice depends on system complexity, model fidelity, and available computational resources.

For large-scale offshore and floating wind turbines (15 MW+), these trends become even more pronounced. Strong coupling between platform dynamics, aerodynamic loading, and control actions introduces nonlinear interactions that significantly influence performance and cost metrics. As turbine size increases, even modest improvements in AEP, load mitigation, or mass reduction can translate into substantial economic benefits. At the same time, the increased computational burden of high-fidelity models motivates the use of reduced-order or steady-state approximations in early-stage design, followed by higher-fidelity refinement in later stages [21,205].

Overall, the literature demonstrates that CCD provides the greatest benefit when applied to systems with strong plant-control coupling and active performance-limiting constraints. Future studies should emphasize consistent reporting of quantitative performance metrics, sensitivity analyses, and computational cost to enable more direct and rigorous comparisons across CCD architectures for next-generation offshore wind turbines.

4. Research gaps in wind turbine CCD

Literature review reveals numerous wind turbine optimization studies aiming to achieve enhanced performance under various design conditions and constraints [4]. Ashuri et al. [212] investigated wind turbine upscaling to determine whether and to what extent larger designs inherently reduce LCOE. They conducted multidisciplinary design studies on rotor and towers for three land-based wind turbines with 5, 10, and 20 MW rated power values. Their study demonstrated that while increased power ratings elevate AEP, associated cost growth outpaces energy gains, yielding higher LCOE beyond a certain size threshold. This occurs because larger turbines experience higher loading, necessitating thicker, heavier, and costlier structures and components to meet all constraints. It leads to increased overall mass and, consequently, cost. Merely scaling existing wind turbines does not necessarily lower (improve) LCOE; innovative concepts and design methods are demanded to achieve this goal. For instance, Pao et al. [206] demonstrated that a 13 MW downwind configuration incorporating the two-bladed segmented ultralight morphing rotor (SUMR) reduces blade stress through larger coning angles while resolving blade-tower clearance constraints, yielding a 25% lower LCOE relative to conventional upwind three-blade designs.

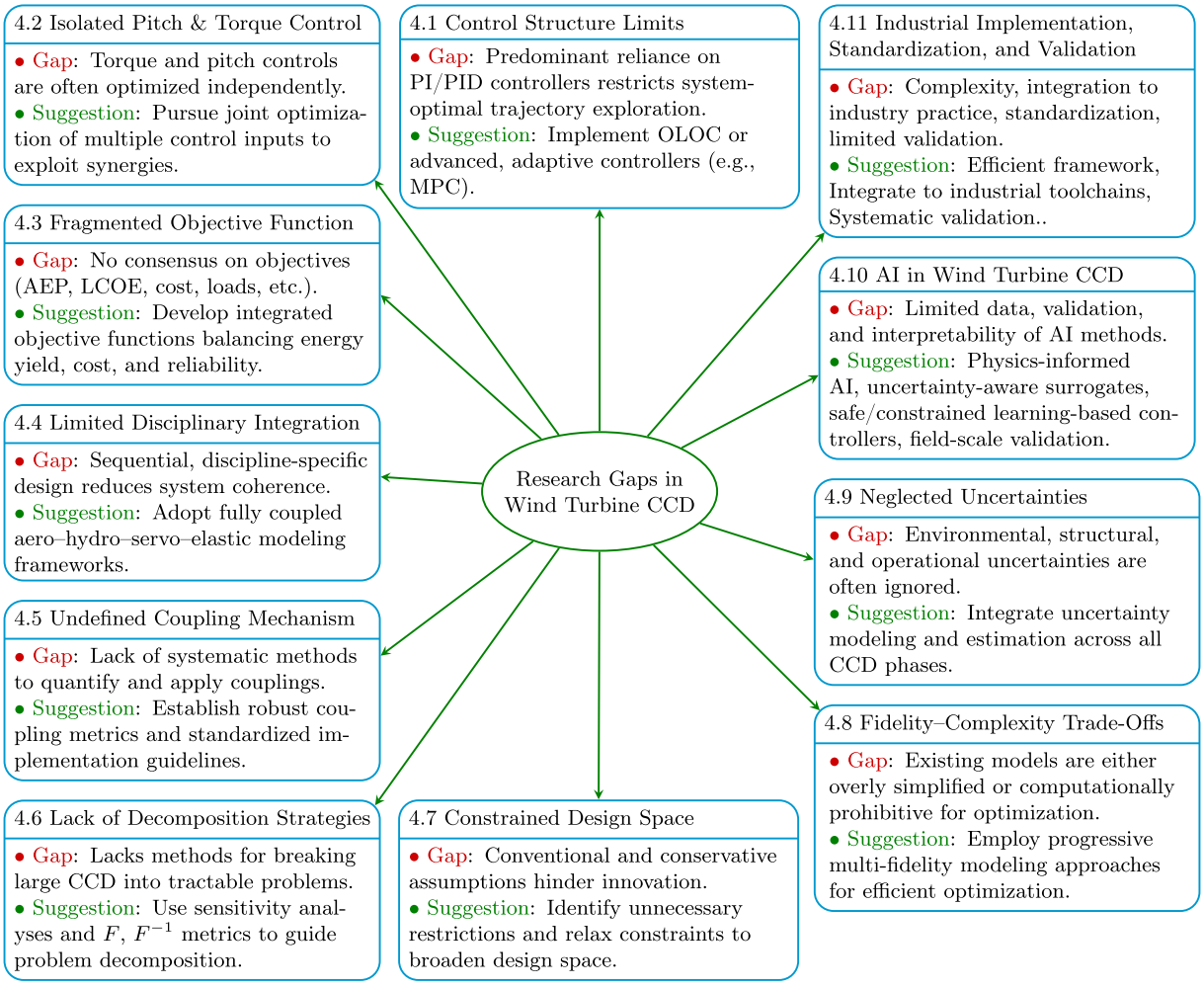

Fig. 15. Summary of key research gaps and suggested directions for advancing wind turbine CCD.

CCD unlocks significant potential in such design studies by exploiting synergistic plant-control design couplings neglected in sequential approaches. While [206] achieved a 25% LCOE reduction through their nonconventional downwind two-bladed SUMR configuration, their sequential design process inherently constrained plant-control design synergy. Adopting CCD frameworks could yield substantially greater improvements, as evidenced by recent studies such as [207]. Control design directly impacts system loads (affecting structural mass/cost) and AEP, thereby dictating LCOE, while plant design simultaneously influences both AEP and structural constraints, thereby influencing LCOE as well. Exploiting this bidirectional coupling, where plant and control disciplines mutually shape optimal system outcomes, holds significant potential for synergistic LCOE reduction beyond sequential approaches.

Despite that CCD provides profound insights into wind turbine design synergies, critical research gaps remain that limit further efficiency gains and cost reductions. These span control architecture, signal coordination, objective function selection, multidisciplinary integration, coupling frameworks, design freedom, problem decomposition strategies, model fidelity, and uncertainty treatment. As summarized in Fig. 15, opportunities for methodological advancements and potential design innovations are presented for each research gap. These suggested possibilities can enhance wind turbines' contribution to power generation.

4.1. Control structure tradeoffs and limitations

Control design constitutes a critical element within CCD, but a critical limitation arises from reliance on fixed-structure controllers. In many wind turbine CCD studies, control architectures typically remain predefined, employing optimization solely over a limited set of tuning parameters rather than full control trajectories. For instance, Hegseth et al. [213] employed collective blade pitch control design via proportional integral (PI) controller, Abbas et al. [207] employed blade flap control design via PI controller, Pao et al. [206] employed generator torque and collective blade pitch control design via NREL's reference open source controller (ROSCO), a software implementation of PI and PID controllers, Santoni et al. [91] employed generator torque, collective blade pitch, and individual pitch control design via PI controller, and López et al. [214] employed collective blade pitch control via an H_∞ controller.

While fixed-structure control designs, such as PI and PID, dominate in CCD studies, relaxed-structure approaches offer improved flexibility. OLOC significantly relaxes assumptions imposed on control structure, enabling high-dimensional design flexibility in control signal trajectories. However, despite its flexibility, the practical deployment of OLOC in real-world wind turbine systems remains challenging. Its reliance on high-fidelity models complicates validation and tuning, while the lack of an inherent feedback structure can limit robustness under realistic operating conditions. In addition, OLOC-based approaches

are less straightforward to integrate into existing industrial control architectures, which are predominantly based on PI/PID frameworks, and can incur significant computational cost. Nevertheless, OLOC remains a powerful tool within the CCD framework, particularly for exploring theoretical performance limits and informing the development of more practical control strategies.

MPC balances relaxed control structure flexibility of OLOCs with real world adaptability of CLCs, providing a viable solution for wind turbine development projects, but remains underutilized in wind turbine CCD context. [22,215], and [163] employed generator torque control design via OLOC, Deshmukh and Allison [216] employed induction factor and rotor yaw angle control design via OLOC, and [11,21], and [24] employed collective blade pitch and generator torque control design via OLOC. Although outside the CCD scope, Lao et al. [217] demonstrate generator torque control design using economic nonlinear MPC. Each control design structure with its advantages and limitations are presented in Section 2.5, along with the selection of control design variables and structures.

4.2. Concurrent use of blade pitch and generator torque controls

One control design issue in CCD arises because conventional wind turbine control rules optimize only one of the rotor-generator control methods, i.e., either generator torque or blade pitch, at a given wind speed, while the other remains fixed. This is primarily because each control method dominates distinct wind speed regions. For example, [22,215] considered region 2, thereby optimizing generator torque control, while keeping blade pitch angle constant. Hegseth et al. [213] optimized collective blade pitch control, while fixing generator torque. Abbas et al. [207] optimized flap and peak shaving, while holding generator torque and blade pitch angle constant.

This single-method control action also stems from risks in simple fixed-structure controllers. Simultaneous control of both methods may cause conflicting actions, control instability, and undesirable load oscillations. However, while one method dominates at specific wind speed regions, exploring coupled controls with advanced CCD and controller structures could unlock performance gains while mitigating the aforementioned conflicts and instabilities. Pusch et al. [205] demonstrated that optimizing blade pitch alongside generator torque in region 2 further improves performance, although common conception does not use blade pitch in this wind speed region. Therefore, simultaneous control of blade pitch and generator torque needs to be further investigated with advanced CCD methodologies and more flexible control structures.

4.3. Objective function usage consensus

Another issue in wind turbine CCD is the use of a diverse range of objective functions without a consensus on a unified one. For example, [11,215], and [216] have used AEP, while [21,24,207,212,218], and [163] have employed LCOE. On the other hand, [22,91,219], and [220] adopted various other objective functions, such as mass, cost, blade root bending moment, DEL, or combinations thereof.

Although some objective function diversity stems from various aims of studies, many studies select varied objective functions due to implementation ease, simplifications, or limitations unrelated to specific design goals. Given that wind turbine projects ultimately prioritize economic viability, LCOE or a similar metric is theoretically the most appropriate metric for CCD problems. However, practical challenges, such as discontinuous and noisy cost estimates, lack of detailed cost models, and flatness of LCOE, limit the utilization of this metric. Particularly, the flatness in LCOE is largely due to the fact that changes in the numerator (cost) and denominator (AEP) follow similar trends with respect to many parameters that define wind turbine design. This reduces its effectiveness as an optimization driver compared to more sensitive objective functions, such as AEP.

Fig. 16 shows this using LCOE, AEP, and cost data for a semi-submersible FOWT system across rotor diameter (D_{rotor}) and main column diameter ($D_{\text{Main-Clmn}}$) as design variables, obtained by frequency-domain simulations using RAFT code. Changes in D_{rotor} and $D_{\text{Main-Clmn}}$ from the baseline design are presented on the x- and y-axes, respectively, in all plots. The baseline design used in this study has D_{rotor} value of 242,000 mm (242 m) and $D_{\text{Main-Clmn}}$ value of 10,000 mm (10 m). Plots in the upper row (sub-figures a, b, and c) represent large design perturbations (4000 mm increments in D_{rotor} and 1000 mm increments in $D_{\text{Main-Clmn}}$), while plots in the lower row (sub-figures d, e, and f) represent small design perturbations (1 mm increments in both D_{rotor} and $D_{\text{Main-Clmn}}$).

Table 2
Sensitivity analysis of three objectives (levelized cost of energy (LCOE), annual energy production (AEP), and cost) with respect to two design variables (rotor diameter and main column diameter) uncovers several dynamics. For example, the main column diameter has a negligible effect on cost (and consequently the LCOE); in a nested CCD formulation, the main column diameter could be included in the inner loop whose objective is not sensitive to cost (i.e., AEP).

	$\frac{\Delta \text{LCOE}/\text{LCOE}}{\Delta x_p/x_p}$	$\frac{\Delta \text{AEP}/\text{AEP}}{\Delta x_p/x_p}$	$\frac{\Delta \text{cost}/\text{cost}}{\Delta x_p/x_p}$
D_{rotor}	−0.3018	0.3421	0.0426
$D_{\text{Main-Clmn}}$	0.0009	−0.0014	10^{-6}

Table 2 quantifies the normalized sensitivity of LCOE, AEP, and cost metrics with respect to these two design variables, D_{rotor} and $D_{\text{Main-Clmn}}$, based on the design perturbations presented in the upper row data in Fig. 16. Normalized sensitivity values of LCOE with respect to both design variables (−0.3018 and 0.0009, respectively) have relatively smaller absolute values compared to those of AEP (0.3421 and −0.0014, respectively), meaning that LCOE is flatter compared to the AEP metric. Furthermore, sensitivity is largely dependent on the perturbing variable. For instance, LCOE is significantly less dependent on $D_{\text{Main-Clmn}}$ than D_{rotor}. In this case, if $D_{\text{Main-Clmn}}$ is the only design variable, using LCOE as the objective function may cause numerical stability or non-convergence issues for optimization algorithms, and it would be beneficial to find a more suitable objective function as an alternative.

One clear difference between upper and lower rows in Fig. 16 is noisiness. Changes in all three metrics (LCOE, AEP, and cost) in the upper row with respect to design changes are consistent because increments in design perturbation are large enough to smooth local noisiness. However, sub-figures in the lower row exhibit inconsistencies in changes with respect to design perturbation. For example, as D_{rotor} increases, AEP initially increases and then decreases. This behavior results in noisy objective function values. A possible solution to address this issue in optimization is to use a larger step size or adopt gradient-free algorithms.

4.4. Developing more holistic control co-design formulations

Current CCD formulations, despite incorporating MDAO principles and various coupled disciplinary models, remain insufficiently comprehensive to capture all synergistic cross-disciplinary couplings. This gap prevents realizing the full design potential that holistic integration could unlock, as simplified CCD approaches inherently overlook critical interactions that could be revealed only through holistic system-level disciplinary interactions. Additionally, considering beyond a single wind turbine, i.e., farm-level considerations, introduces a larger range of couplings that exist in the CCD of wind turbines, which most current wind turbine CCD studies lack. For example, [11,22,215] considered CCD of control, rotor, and tower, Hegseth et al. [213] considered CCD of control, tower, and spar platform, Lee et al. [163] considered CCD of VAWT intracycle speed control and TLP, Ashuri et al. [218] performed CCD of rotor, tower, and spar platform, and [216] performed CCD of control and farm-level optimization. One of the reasons that existing studies did not formulate highly comprehensive CCD models is due to a limitation in computational time and resources to account for the massive number of models, variables, and coupling mechanisms.

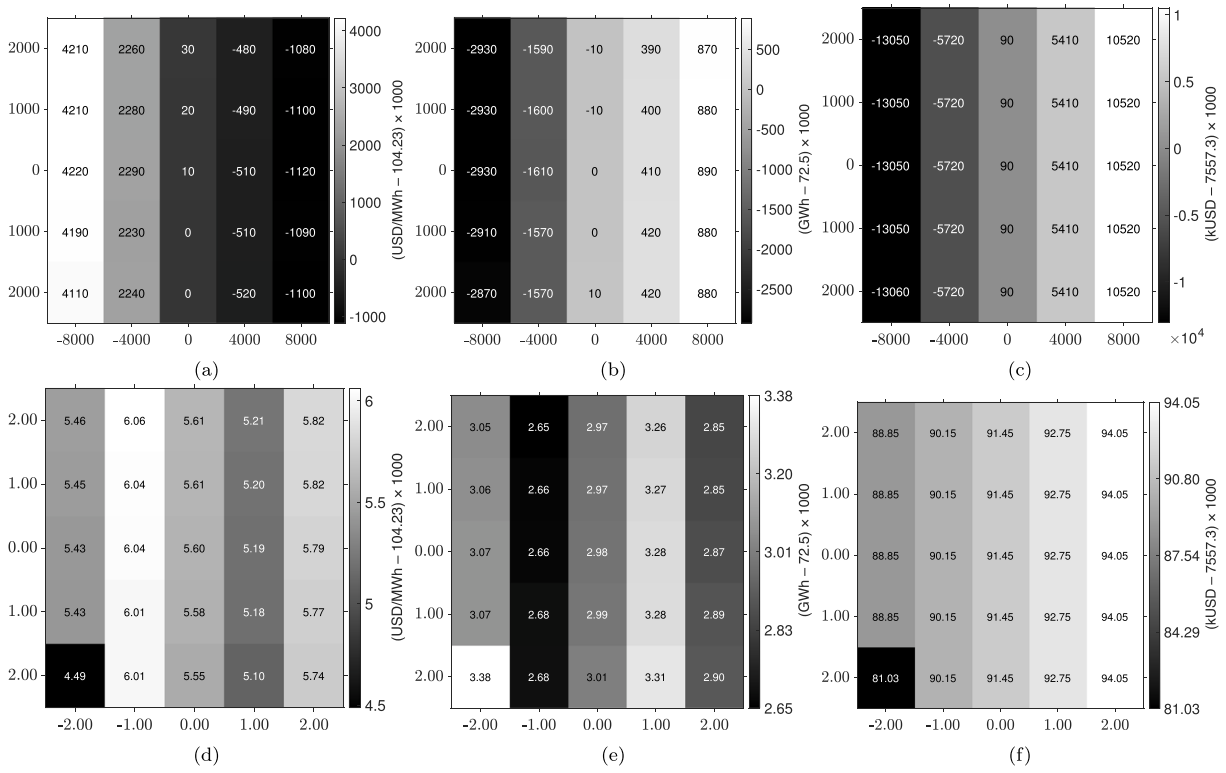

Fig. 16. Characterizing the strength of design coupling between rotor diameter (x-axis) and main column diameter (y-axis) for three objective functions: LCOE in sub-figures (a & d), AEP in (b & e), and cost in (c & f). Large design perturbations (4000 mm increments in D_{rotor} and 1000 mm increments in $D_{\text{Main-Clmn}}$) are in upper row sub-figures (a, b, & c), and small design perturbations (1 mm increments in both D_{rotor} and $D_{\text{Main-Clmn}}$) are in lower row sub-figures (d, e, & f). In all sub-figures, the vertical text adjacent to each plot denotes the corresponding color bar label, indicating the magnitude of the objective function variation.

Even when using fully coupled tools, prevalent sequential workflows with discipline-specific objectives, e.g., optimizing structure then control, diminish the core CCD advantages by fragmenting system-wide goals into decoupled or weakly coupled sub-problems. For instance, [221,222] presented sequential design approaches, although their simulation tool (i.e., OpenFAST) already equips a fully-coupled simulation capability of all associated design disciplines. Employing different disciplinary objective functions also leads the design solution toward different directions at every phase of the design sequence. They frequently compete with each other for conflicting optimization directions. While this sequential optimization process may facilitate convergence of the optimization results at each step, it may not fully represent the overarching goal of wind turbine design. Because of this, it may be beneficial to utilize CCD and consider only one unique objective.

4.5. Identifying plant and control disciplinary coupling mechanisms

CCD provides a framework to optimize plant and control disciplines, considering interactions. The primary motivation for adopting CCD is to leverage potential couplings between plant and control disciplines to enhance performance, cost efficiency, and find novel design mechanisms. These couplings (herein referred to as *disciplinary coupling*) presented in [223] highlight the effectiveness and value of CCD in achieving these goals. However, within wind turbine CCD, consensus on a precise definition of disciplinary coupling lacks clarity. This ambiguity complicates the establishment of standardized methodologies and impedes the broader adoption of CCD.

Despite the theoretical advantages of CCD, there are few studies that quantify plant-control disciplinary couplings in wind energy to date. Existing research predominantly demonstrates successful CCD applications for wind turbine design, and justifies the advantageous characteristics of CCD for particular study focuses, but often omits the effort to identify detailed design mechanisms that enable these advantages. This lack of critical analysis raises an important question: why would a specific wind turbine design problem benefit from a CCD approach? Addressing this question requires developing robust methods to quantify couplings and identify design problems where CCD is most advantageous. Without such methods, CCD remains underutilized, and innovations in the wind energy industry risk being driven by intuition rather than systematic methodology.

Some progress has been made in quantifying couplings in CCD problems. For example, Iori et al. [211] proposed a metric based on design sensitivity analysis to estimate the change in the optimal objective value for small variations in control parameters. This method uses post-optimal information from optimization problems solved with a fixed control design to predict the results of a tower CCD problem, achieving good accuracy. However, this approach is limited to gradient-based problems and has not been validated for control architectures with large parameter spaces, such as problems with OLOC or MPC. This limitation underscores the need for further research to extend the applicability of such methods.

To fully realize the potential of CCD in wind energy systems, it is imperative to develop clear methodologies for identifying and quantifying couplings. These methodologies should provide actionable insights, enabling the systematic application of CCD to relevant design problems. By bridging these gaps, CCD can become a cornerstone of innovative and cost-effective wind turbine design.

4.6. Identifying design couplings and systematic problem decomposition

While disciplinary coupling discussed in Section 4.5 quantifies influences of one discipline on another, e.g., structural response to aerodynamics, and vice versa, designing with them requires another quantification, that is, influences on design decisions made. This quantification

Table 3
Tracking the optimal solutions that arise from holding different variables constant during optimization.

min	$f(x,y,z)$	$f(y,z;\tilde{x})$	$f(x,z;\tilde{y})$	$f(x,y;\tilde{z})$
x	x^*	$\tilde{x}$	$x^*_{\tilde{y}}$	$x^*_{\tilde{z}}$
y	y^*	$y^*_{\tilde{x}}$	$\tilde{y}$	$y^*_{\tilde{z}}$
z	z^*	$z^*_{\tilde{x}}$	$z^*_{\tilde{y}}$	$\tilde{z}$
f	f^*	$f^*_{\tilde{x}}$	$f^*_{\tilde{y}}$	$f^*_{\tilde{z}}$

can be described in the following context: what if one design decision changes, how should the optimal decision change in another design decision? Answers to this question can be quantified by $\partial x^*_j/\partial x_i$ Jacobian, and referred to as *design coupling*. Design coupling has been recently analyzed in several domains, e.g., [224–228].

Although design coupling analysis provides profound information on design knowledge, one specific area where this information can be beneficial is in constructing efficient design optimization problem formulations. Design coupling analysis provides insights into uni- and bidirectional relationships [225,229] among design variables that allow an effective decomposition of a larger optimization problem into smaller sub-problems or a set of sequential sub-problems [226,227].

In Section 2, for example, we noted that the LCOE objective function can be represented as a ratio of total cost to AEP, and the cost term is frequently a noisy, discontinuous function, necessitating the use of gradient-free optimization algorithms for, at least, plant design variables. However, many gradient-free algorithms do not scale effectively beyond one or two dozen variables. In such cases, the CCD problem needs to be simplified in certain ways [227]. One possible option is to select a subset of design variables that are highly sensitive to the objective function and highly coupled to each other. Another possibility is to decompose the problem into a sequence of smaller sub-problems and solve them sequentially.

Suppose there are three design variables (x, y, z) and an objective function ($f(x,y,z)$), presented in Table 3. The column with the first optimization case represents optimal solutions in design variables (x^*, y^*, and z^*) and in the objective function (f^*), where all design variables are concurrently optimized. On the other hand, the remaining three columns represent solutions of optimizing two variables while one variable remains fixed to an approximated solution. For example, the column with the second case represents the optimization problem with respect to y and z, while x is fixed to $\tilde{x} = x^* + \delta x$, where δx represents the deviation from the optimal solution to the approximated solution. This case yields the optimal solution in objective function $f^*_{\tilde{x}} = f\left(y^*_{\tilde{x}}, z^*_{\tilde{x}}; \tilde{x}\right)$.

With these results, Table 4 can be computed. This table shows the coupling strength between design variables in the rows and the scenarios in the columns. For example, in row 1, column 2 shows the coupling between x and y when y is fixed, and element 2, 1 shows the coupling between x and y when x is fixed. The last column shows the summation of each row, and the last row shows the summation of corresponding columns. Here, F_i^{-1} indicates how much the design variable i depends on all other variables, and F_i shows how much other design variables are a function of design variable i.

Using this quantified design coupling strengths, the original optimization problem ($f^* = f(x^*, y^*, z^*)$ can be decomposed into a sequence of smaller optimization problems following the rule given in Fig. 17. The quantities F and F^{-1} represent the aggregated strengths of upstream and downstream dependencies (i.e., couplings) associated with each design variable.

Specifically, a design variable that has a small F combined with a large F^{-1} exhibits weak upstream dependence, but strong downstream dependence. This means that the optimal solution of this variable is insensitive to changes in other variables, but change in this variable exerts a strong downstream influence on the optimal solution of other design variables. In such cases, changes in other design variables have little effect on their optimum, but perturbations in this variable significantly affect the optima of other variables. Consequently, the sequential optimization process begins with variables with small F and large F^{-1}.

Table 4
A symbolic design coupling study, where each element represents the relative strength of coupling between two design variables near an optimal design.

	x	y	z	$\Sigma\|\cdot\|$
x		$\dfrac{\frac{x^*_{\tilde{y}} - x^*}{x^*}}{\frac{y_{\tilde{y}} - y^*}{y^*}}$	$\dfrac{\frac{x^*_{\tilde{z}} - x^*}{x^*}}{\frac{z_{\tilde{z}} - z^*}{z^*}}$	F_x^{-1}
y	$\dfrac{\frac{y^*_{\tilde{x}} - y^*}{y^*}}{\frac{x_{\tilde{x}} - x^*}{x^*}}$		$\dfrac{\frac{y^*_{\tilde{z}} - y^*}{y^*}}{\frac{z_{\tilde{z}} - z^*}{z^*}}$	F_y^{-1}
z	$\dfrac{\frac{z^*_{\tilde{x}} - z^*}{z^*}}{\frac{x_{\tilde{x}} - x^*}{x^*}}$	$\dfrac{\frac{z^*_{\tilde{y}} - z^*}{z^*}}{\frac{y_{\tilde{y}} - y^*}{y^*}}$		F_z^{-1}
$\Sigma\|\cdot\|$	F_x	F_y	F_z	

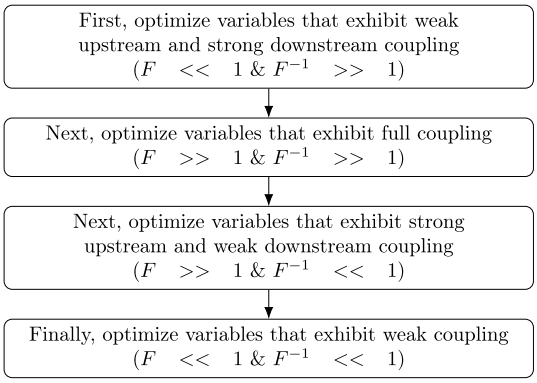

Fig. 17. Decomposing a problem based on the coupling magnitudes between pairs of design variables.

The subsequent stage in Fig. 17 addresses bidirectionally coupled design variables, which exhibit large values of both F and F^{-1}. In the third stage, variables with strong upstream dependence (i.e., large F) but weak downstream influence (i.e., small F^{-1}) are optimized. Lastly, design variables that have small values in both F and F^{-1} are optimized as decisions on these variables are relatively independent of other design variables. Design variables optimized in each stage are held fixed in all subsequent stages.

This type of coupling-informed problem decomposition is particularly useful for early-stage design studies, where simplified or reduced-order models enable tractable computation. For example, in wind turbine design, such analyses can be performed using frequency-domain models (e.g., RAFT [49]) or surrogate-based models (e.g., Fernandez Bravo et al. [227]).

4.7. Limitations in design freedom

The wind turbine design process is governed by multiple interrelated constraints. In addition to system performance targets, structural load limits, and the operational/control envelopes, designers must also consider the capabilities and restrictions of existing manufacturing processes together with other compatibility requirements. However, some constraints are inherent in conventional rule-based design practices and may not be imposed intentionally. While many constraints steer design outcomes toward a narrow set of predefined configurations or

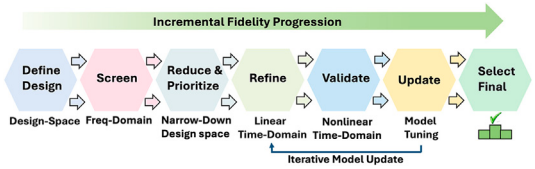

Fig. 18. Structured multi-fidelity CCD workflow illustrating progression from low-fidelity screening to high-fidelity validation and final design selection.

control strategies, identifying and deliberately relaxing unnecessarily restrictive constraints drastically expands the feasible design space and opens avenues for unprecedented innovation. For example, conventional FOWT concepts often lock floating structure geometry into simple, easily manufactured forms, such as cylinders combined with rectangular members, thereby limiting the ability to tailor hydrodynamic responses. Cain and Lee [230] demonstrated that eliminating the a priori shape constraint and treating the platform geometry as a free-form design variable significantly reduces the impact of hydrodynamic loads, allowing for substantially lighter and more cost-effective platforms.

In a CCD context, relaxing restrictive constraints can yield even greater innovation. Traditional wind turbine blades are built with a fixed twist distribution optimized for a narrow band of operating conditions. Khakpour Nejadkhaki and Hall [231] adopted a continuously reconfigurable design perspective, exploiting a compliant blade structure to enable actively controlled spanwise twist. The adaptive twist simultaneously improves aerodynamic efficiency and mitigates fatigue loads. Together, these examples illustrate the broader principle that deliberate relaxation of conventional constraints expands the design space, fostering novel design concepts and simultaneously improving multiple competing performance metrics.

4.8. Leveraging insights from multi-fidelity models

While models at different fidelity levels provide varying degrees of physical detail (Section 3.8), wind turbine CCD requires balancing computational efficiency and model accuracy. Multi-fidelity modeling addresses this need by combining low-order models for rapid design-space exploration with higher-fidelity models for detailed validation. A representative example is the WEIS framework [232], which employs frequency-domain, linear time-domain, and fully nonlinear simulations.

Despite these advances, current multi-fidelity approaches lack standardized workflows for transitioning between fidelity levels and maintaining consistency across models. Discrepancies between models and limitations in tool integration can affect convergence and reliability of optimization results, and validation across operating conditions remains challenging [233,234].

While not all limitations can be easily addressed by a single guideline, the following structured multi-fidelity CCD workflow provides a practical starting point for integrating multi-fidelity models into the design process:

1. Define design variables, objectives, and constraints, resulting in a high-dimensional design space $X_{N_{\text{all}}}$.
2. Perform low-fidelity screening (frequency-domain) to efficiently explore the design space.
3. Reduce the design space using sensitivity and coupling analysis.
4. Refine designs using linear time-domain models.
5. Validate using high-fidelity nonlinear simulations under realistic conditions.
6. Iteratively update models to ensure consistency across fidelity levels.
7. Select final designs based on performance and feasibility.

Fig. 18 illustrates this hierarchical process, where early-stage exploration is performed using low-cost models, followed by refinement and validation at higher fidelity levels. This approach enables efficient allocation of computational resources while ensuring that final designs remain accurate under realistic operating conditions. Overall, multi-fidelity CCD provides a practical pathway for managing large design spaces and improving the tractability of wind turbine design.

4.9. Uncertainties

Uncertainty plays a central role in wind turbine CCD, affecting performance, reliability, and cost. It arises from environmental, structural, operational, and modeling sources, making robust design challenging. While many studies adopt deterministic formulations for tractability, recent work has increasingly incorporated uncertainty through stochastic and robust CCD frameworks [235,236]. In these approaches, uncertainty is embedded in objective functions and constraints using statistical measures or worst-case formulations, enabling more reliable designs under realistic conditions [236–238].

Environmental uncertainty is particularly critical for offshore and floating systems, where coupled wind-wave effects strongly influence system dynamics, fatigue, and extreme loads [239–242]. Monte Carlo simulation remains widely used for uncertainty propagation due to its flexibility, but its high computational cost limits scalability [240,242,243]. To address this, more efficient methods such as polynomial chaos expansion, sparse grids, and surrogate-based approaches (e.g., Kriging, Bayesian optimization) have been developed to approximate system responses and enable scalable uncertainty-aware CCD [243–246]. Surrogate-based approaches to CCD have also been applied to wave energy converters [247,248].

Despite these advances, integrating uncertainty quantification into CCD remains challenging. Propagating uncertainty through coupled aero-hydro-servo-elastic models is computationally demanding, and seamless integration with multidisciplinary optimization frameworks is still limited (see Section 2.11). Additional uncertainties from material variability, manufacturing tolerances, and operational factors such as control errors or misalignment further complicate design and are often simplified in practice [249,250]. Modeling uncertainties, particularly in surrogate-based methods, introduce approximation errors that must be carefully managed to avoid degradation of optimization results [245,246,251,252]. More broadly, uncertainty-aware control co-design (UCCD) formulations, including stochastic, robust, and possibilistic approaches, have been systematically categorized in the general CCD literature [236]; however, their application to wind turbine systems remains limited, particularly for fully coupled aero-hydro-servo-elastic models. This gap represents an important open research direction. Moreover, current industry practices and emerging standards are only beginning to incorporate probabilistic design methodologies [253].

Validation of uncertainty-aware CCD is also limited, with most studies relying on stochastic time-domain simulations rather than full-scale deployment [240–242]. While integrating uncertainty quantification into wind turbine modeling and optimization improves decision-making [236,254–257], it also increases computational burden. Therefore, future work should focus on scalable methods that integrate uncertainty efficiently within CCD, leveraging surrogate modeling, machine learning, and reduced-order techniques. Such developments are essential for designing wind energy systems that are both high-performing and robust under real-world conditions [250,252].

4.10. The role of AI in advancing wind turbine control co-design

Recent advances in AI provide a promising pathway for accelerating wind turbine CCD and extending it to more complex formulations. Across the broader wind energy literature, AI has been increasingly adopted in design optimization, structural analysis, control, monitoring, and lifecycle management, suggesting that it is becoming an enabling computational layer rather than merely an auxiliary tool [4,258–263]. This is particularly relevant to wind turbine CCD, where major bottlenecks include high computational cost, large design spaces, strong

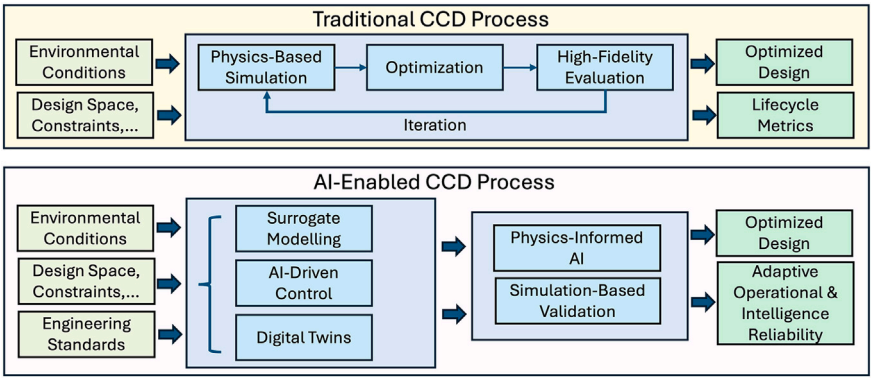

Fig. 19. Comparison of traditional and AI-enabled control co-design (CCD) for wind turbines and floating offshore systems. Traditional CCD relies on iterative high-fidelity simulations, leading to computational bottlenecks. In contrast, AI-enabled CCD integrates surrogate modeling, data-driven control, and digital twins within a physics-informed framework, enabling faster evaluation, adaptive control, and lifecycle-aware design. Key benefits include improved computational efficiency and flexibility, while challenges remain in data requirements, generalization, interpretability, and certification.

multiphysics coupling, and the need to evaluate performance across broad operating conditions.

One immediate opportunity for AI in CCD lies in surrogate modeling and data-driven reduced-order representations. Because high-fidelity aero-hydro-servo-elastic simulations are often too expensive for large-scale optimization, machine learning models can be trained to emulate selected system responses, such as loads, platform motions, fatigue metrics, and performance quantities, enabling much faster evaluation of plant-control design candidates [4,261]. Such approaches are especially attractive for offshore and floating wind turbine applications, where computational efficiency is a major limitation [260,263]. In this role, AI can support design-space screening, sensitivity studies, and multi-fidelity CCD workflows.

AI may also broaden the control-design space within CCD. Most existing wind turbine CCD studies still rely on fixed-structure controllers with only a small number of tunable gains. In contrast, AI-driven control strategies, including reinforcement learning and adaptive data-driven policies, can potentially learn control actions directly from system dynamics and environmental feedback [260,262]. These methods may be particularly valuable for systems with strong nonlinearities, changing operating regimes, or coupled wind-wave disturbances, and may also support wake-aware farm-level control and grid-connected operation [258,262].

Beyond design optimization and control, AI is also gaining relevance in structural health monitoring, fault detection, predictive maintenance, and digital twins [258,263]. For offshore and floating systems, where access is limited and uncertainty is high, these capabilities could help connect design-stage CCD decisions with long-term operation, reliability, and lifecycle management [263].

Despite these opportunities, several challenges remain. Many AI methods require large and representative datasets, which are difficult to obtain for offshore and floating systems, especially under rare or extreme conditions [4,258]. Generalization, interpretability, limited field-scale validation, and compatibility with certification and engineering standards also remain important barriers [263]. Therefore, the most promising role of AI in wind turbine CCD is not to replace physics-based modeling, but to complement it through hybrid frameworks that combine physical models with machine learning, uncertainty-aware surrogates, and safe or constrained learning-based controllers [4,260,263]. Fig. 19 summarizes this transition from traditional to AI-enabled CCD, highlighting how AI can improve computational tractability and flexibility while preserving the need for physics-based validation.

4.11. Industrial implementation, standardization, and validation challenges

Despite significant advances in CCD methodologies, their adoption in industrial wind turbine development remains limited due to several practical challenges. One of the primary barriers is the computational complexity associated with CCD frameworks, particularly when high-fidelity aero-hydro-servo-elastic models are coupled with optimization routines. Industrial design workflows typically rely on sequential and modular processes, whereas CCD requires tightly integrated, iterative simulations, making direct implementation within existing pipelines nontrivial [175].

Another key challenge lies in integration with established control architectures and industrial practices. Commercial wind turbines predominantly employ well-established control strategies, such as PI/PID-based controllers, which are robust, interpretable, and compatible with certification processes [84,264]. In contrast, CCD frameworks often introduce higher-dimensional design spaces and more complex control representations, which may not easily align with current industrial standards or real-time implementation requirements.

Standardization and certification constraints further limit the adoption of CCD. Wind turbine design must comply with rigorous industry standards and guidelines, including prescribed load cases, safety factors, and reliability requirements [265]. These standards are generally formulated around conventional design approaches, making it challenging to directly incorporate CCD methodologies without additional validation and adaptation. Ensuring that co-designed systems satisfy certification criteria across all operating conditions remains an open challenge.

In addition, there is a notable gap in full-scale validation and field deployment of CCD strategies. While advanced control approaches, such as wake steering and coordinated wind farm control, have demonstrated potential benefits in field experiments, large-scale implementation remains limited [175]. The increasing size and complexity of modern wind turbines further amplify this challenge, as scaling effects introduce additional structural, control, and reliability considerations that are difficult to fully capture in simulation environments [266].

Additionally, a broader gap between academic research and industrial deployment persists. Many CCD studies are conducted in controlled simulation settings, often with simplified assumptions, whereas real-world systems must account for uncertainties, operational constraints, and long-term reliability [267]. Bridging this gap requires the development of computationally efficient frameworks, improved integration with industrial toolchains, and systematic validation across multiple fidelity levels. Addressing these challenges is essential for transitioning

CCD from a promising research paradigm to a practical design methodology in commercial offshore wind farm development.

Beyond these technical and practical considerations, broader policy and regulatory environments play a critical role in shaping the pace of renewable energy deployment, as differences in governmental support, permitting frameworks, and market incentives across regions can either facilitate or hinder the adoption, standardization, and large-scale validation of advanced design methodologies such as CCD [268,269].

5. Conclusion

CCD has emerged as a powerful methodology for advancing the design and optimization of wind turbines, offering significant potential to address the intertwined challenges of performance enhancement, cost reduction, and sustainability. This integrative approach enables the simultaneous consideration of control strategies and physical design parameters, fostering innovations that are unattainable through traditional sequential design methods. By capturing the intricate couplings between disciplines such as aerodynamics, structural dynamics, and control systems, CCD provides a robust framework for designing next-generation wind energy systems.

This review has underscored the progress made in applying CCD to wind turbine design, detailing advancements in methodologies, optimization techniques, and practical applications. Notable successes include reducing LCOE, improving AEP, and optimizing components such as rotor blades, towers, and floating platforms. However, the field still faces substantial challenges. Among these are the lack of standardization in defining and quantifying design couplings, the computational intensity of CCD approaches, and the limited exploration of multidisciplinary interactions in current studies. Moreover, the reliance on fixed-structure controllers and the segmented optimization of sub-components limits the realization of truly optimal solutions.

To fully harness the potential of CCD, future research should prioritize the development of comprehensive, fully coupled models that integrate all relevant disciplines, including control, aerodynamics, structural dynamics, and farm-level considerations. The adoption of unified objective functions, such as LCOE, will facilitate the evaluation and comparison of design trade-offs while advancing the broader applicability of CCD methodologies. Furthermore, incorporating advanced computational tools, such as high-fidelity simulations, surrogate modeling, and machine learning, can address the computational barriers and enable more efficient optimization processes.

The inclusion of uncertainties, such as environmental variability and operational risks, in CCD frameworks will also be critical for developing resilient and adaptable wind energy systems. Expanding CCD applications to offshore and hybrid energy systems, including those combining wind and wave energy, represents another promising direction that aligns with the growing demand for sustainable and diversified energy sources.

In conclusion, CCD enables the co-optimization of wind turbine plant and controller design, reducing cost and increasing AEP. By lowering the overall LCOE, wind energy systems will become an increasingly viable source of renewable energy. Looking ahead, we see three immediate priorities: (i) establishing standard, reproducible benchmarks for wind turbine CCD; (ii) comparative analyses that establish guidelines for how to best decompose wind turbine design problems based on systematic analysis of design coupling; and (iii) extending the scope of wind turbine CCD studies toward more fully-coupled tower-platform-control studies, quantifying and mitigating effects such as negative damping. Targeted collaboration between academia, industry, and government will be essential to ensure that advances in design methodologies translate into practical impact on wind turbine deployment and energy cost.

CRediT authorship contribution statement

Saeid Bayat: Writing – review & editing, Writing – original draft, Visualization, Validation, Investigation, Formal analysis, Data curation, Conceptualization. **Chad Peterson:** Writing – review & editing, Visualization. **Yong Hoon Lee:** Writing – review & editing, Writing – original draft, Visualization, Investigation, Conceptualization. **Jenna Iori:** Writing – review & editing, Conceptualization. **James T. Allison:** Writing – review & editing, Supervision, Project administration, Funding acquisition.

Funding source

The information, data, or work presented herein was funded in part by the U.S. Department of Energy, Advanced Research Projects Agency-Energy (ARPA-E) under grant numbers DE-AR-0001182 and DE-AR-0001766.

Declaration of competing interest

The authors declare that they have no known competing financial interests or personal relationships that could have appeared to influence the work reported in this paper.

Acknowledgements

The authors gratefully acknowledge Mr. Austin Griffin for his valuable assistance during the early discussions on the wind-turbine designs presented herein. His insightful feedback was instrumental in shaping the initial concepts of this work.

Data availability

All data required to replicate the results can be generated by the MATLAB optimization code. A MATLAB optimization code for a select problem demonstrated in the manuscript is available upon request to the first or corresponding authors. Readers may need a commercial pseudospectral optimal control solver, GPOPS-II, to run the provided MATLAB codes.

References

[1] IEA. Global energy review 2025. Technical Report. URL, Paris, France: International Energy Agency; 2025. https://www.iea.org/reports/global-energy-review-2025.
[2] Wiatros-Motyka M, Fulghum N, Jones D. Global electricity review 2024. Technical Report. URL, London, UK: Ember; 2024. https://ember-energy.org/latest-insights/global-electricity-review-2024/.
[3] McCoy A, Musial W, Hammond R, Hernando DM, et al. Offshore wind market report. Technical Report NREL/TP-5000-90525, URL, Golden, CO, USA: National Renewable Energy Laboratory; 2024. https://www.nrel.gov/docs/fy24osti/90525.pdf.
[4] Ribeiro JA, Ribeiro BA, Pimenta F, Tavares SM, Zhang J, Ahmed F. Offshore wind turbine tower design and optimization: a review and AI-driven future directions. Appl Energy 2025;397:126294. https://doi.org/10.1016/j.apenergy.2025.126294
[5] Betts JT. Practical methods for optimal control and estimation using nonlinear programming. 2 ed. Philadelphia, PA, USA: Society for Industrial and Applied Mathematics; 2010. https://doi.org/10.1137/1.9780898718577
[6] Fischer B, Shan M. A survey on control methods for the mitigation of tower loads. Technical Report Project report 01/104256. URL, Kassel, Germany: Fraunhofer IWES; 2013. https://publica.fraunhofer.de/handle/publica/296582.
[7] Sørensen P, Hansen AD, Iov F, Blaabjerg F, Donovan MH. Wind farm models and control strategies. Technical Report Risø-R-1464. URL, Roskilde, Denmark: Risø National Laboratory; 2005. https://orbit.dtu.dk/en/publications/wind-farm-models-and-control-strategies/.
[8] Liu W, Liu Y. Hierarchical model predictive control of wind farm with energy storage system for frequency regulation during black-start. Int J Electr Power Energy Syst 2020;119:105893. https://doi.org/10.1016/j.ijepes.2020.105893
[9] Li B, Ge M, Li X, Liu Y. Dynamic wake steering control for maximizing wind farm power based on a physics-guided neural network dynamic wake model. Phys Fluids 2024;36:085163. https://doi.org/10.1063/5.0223631

[10] Herber DR, Allison JT. Nested and simultaneous solution strategies for general combined plant and control design problems. J Mech Des 2019;141:011402. https://doi.org/10.1115/1.4040705

[11] Bayat S, Lee YH, Allison JT. Nested control co-design of a spar buoy horizontal-axis floating offshore wind turbine. Ocean Eng 2025;328:121037. https://doi.org/10.1016/j.oceaneng.2025.121037

[12] Sundarrajan AK, Herber DR. Towards a fair comparison between the nested and simultaneous control co-design methods using an active suspension case study. In: American control conference. New Orleans, LA, USA; 2021. p. 358–65. https://doi.org/10.23919/ACC50511.2021.9482687

[13] Rao AV, A survey of numerical methods for optimal control. In: Advances in the astronautical sciences, vol. 135. Pittsburgh, PA, USA: AAS 09-334; 2009. p. 497–528. URL: https://www.univelt.com/book=1260.

[14] Nikolaou M. Model predictive controllers: a critical synthesis of theory and industrial needs. Adv Chem Eng 2001;26:131–204. https://doi.org/10.1016/S0065-2377(01)26003-7

[15] Bayat S, Allison JT. Control co-design with varying available information applied to vehicle suspensions. In: ASME international design engineering technical conferences, detc2023-114690. Boston, MA, USA; 2023. https://doi.org/10.1115/DETC2023-114690, p. V03AT03A002.

[16] Nagy ZK, Braatz RD. Open-loop and closed-loop robust optimal control of batch processes using distributional and worst-case analysis. J Process Control 2004;14:411–22. https://doi.org/10.1016/j.jprocont.2003.07.004

[17] Jonkman JM, Buhl ML, et al. FAST user's guide, software Manual NREL/TP-500-38230, Golden, CO, USA: National Renewable Energy Laboratory; 2005. URL: https://docs.nrel.gov/docs/fy06osti/38230.pdf.

[18] Beardsell A, Alexandre A, Child B, Harries R, McCowen D. Beyond oc5 – further advances in floating wind turbine modelling using bladed. J Phys Conf Ser 2018;1102:012023. https://doi.org/10.1088/1742-6596/1102/1/012023

[19] Marten D. QBlade: a modern tool for the aeroelastic simulation of wind turbines [Ph.D. thesis]. Berlin, Berlin, Germany: Technische Universität; 2020. https://doi.org/10.14279/depositonce-10646

[20] Lemmer F, Yu W, Luhmann B, Schlipf D, Cheng PW. Multibody modeling for concept-level floating offshore wind turbine design. Multibody Syst Dyn 2020;49:203–36. https://doi.org/10.1007/s11044-020-09729-x

[21] Sundarrajan AK, Lee YH, Allison JT, Zalkind DS, Herber DR. Open-loop control co-design of semisubmersible floating offshore wind turbines using linear parameter-varying models. J Mech Des 2024;146:041704. https://doi.org/10.1115/1.4063969

[22] Deshmukh AP, Allison JT. Design of dynamic systems using surrogate models of derivative functions. J Mech Des 2017;139:101402. https://doi.org/10.1115/1.4037407

[23] Sundarrajan A, Herber DR, Using high-fidelity time-domain simulation data to construct multi-fidelity state derivative function surrogate models for use in control and optimization. In: ASME international mechanical engineering congress & exposition. New Orleans, LA, USA: IMECE2023-112316; 2023. https://doi.org/10.1115/IMECE2023-112316, p. V006T07A089.

[24] Lee YH, Bayat S, Allison JT. Wind turbine control co-design using dynamic system derivative function surrogate model (DFSM) based on OpenFAST linearization. Appl Energy 2025;396:126203. https://doi.org/10.1016/j.apenergy.2025.126203

[25] Haimes YY, Lasdon LS, Wismer DA. On a bicriterion formulation of the problems of integrated system identification and system optimization. IEEE Trans Syst, Man, Cybern SMC-1 1971:296–7. https://doi.org/10.1109/TSMC.1971.4308298

[26] Ascher UM, Petzold LR. Computer methods for ordinary differential equations and Differential-Algebraic equations. Philadelphia, PA, USA: SIAM; 1998.

[27] Patterson MA, Rao AV. GPOPS-II: a MATLAB software for solving multiple-phase optimal control problems using hp-adaptive Gaussian quadrature collocation methods and sparse nonlinear programming. ACM Trans Math Softw 2014;41:1–37. https://doi.org/10.1145/2558904

[28] Wolpert DH, Macready WG. No free lunch theorems for optimization. IEEE Trans Evol Comput 1997;1:67–82. https://doi.org/10.1109/4235.585893

[29] Martins JRRA, Ning A. Engineering design optimization. Cambridge, UK: Cambridge University Press; 2022. URL: https://doi.org/10.1017/9781108980647. https://mdobook.github.io.

[30] Powell MJD, A direct search optimization method that models the objective and constraint functions by linear interpolation. In: Advances in optimization and numerical analysis: Mathematics and its applications, vol. 275. Dordrecht: Springer; 1994. p. 51–67. https://doi.org/10.1007/978-94-015-8330-5_4

[31] Hansen N, Müller SD, Koumoutsakos P. Reducing the time complexity of the derandomized evolution strategy with covariance matrix adaptation (CMA-ES). Evol Comput 2003;11:1–18. https://doi.org/10.1162/106365603321828970

[32] Fateman RJ. Macsyma's general simplifier: philosophy and operation. In: Macsyma users conference. Washington, DC, USA; 1979. p. 563–82. URL: https://maxima.sourceforge.io/misc/Fateman-Salz_Simplifier_Paper.pdf.

[33] Falck R, Gray JS, Ponnapalli K, Wright T. Dymos: a Python package for optimal control of multidisciplinary systems. J Open Source Softw 2021;6:2809. https://doi.org/10.21105/joss.02809

[34] Nie Y, Faqir O, Kerrigan EC. Iclocs2: try this optimal control problem solver before you try the rest. In: UKACC international conference on control. Sheffield, UK; 2018. p. 336. https://doi.org/10.1109/CONTROL.2018.8516795

[35] Becerra VM. Solving complex optimal control problems at no cost with PSOPT. In: IEEE international symposium on Computer-Aided control system design. Yokohama, Japan; 2010. p. 1391–6. https://doi.org/10.1109/CACSD.2010.5612676

[36] Houska B, Ferreau HJ, Diehl M. ACADO toolkit—an open-source framework for automatic control and dynamic optimization. Optim Control Appl Methods 2011;32:298–312. https://doi.org/10.1002/oca.939

[37] Ross IM. Enhancements to the DIDO optimal control toolbox; 2020. URL: https://arxiv.org/abs/2004.13112. arXiv:2004.13112.

[38] Mathworks, Inc. Model predictive control toolbox: MATLAB documentation, software manual, mathworks. Natick, MA, USA: Inc; 2025. URL:. https://www.mathworks.com/products/model-predictive-control.html [Accessed 9 October 2025].

[39] Bayat S, Allison JT. SS-MPC: a user-friendly software based on single shooting optimization to solve model predictive control problems. Softw Impacts 2023;17:100566. https://doi.org/10.1016/j.simpa.2023.100566

[40] Bayat S, Allison JT. A practical open-source approach to model predictive control using the Legendre-Gauss-Radau pseudospectral method. Softw Impacts 2025;25:100769. https://doi.org/10.1016/j.simpa.2025.100769

[41] Fiedler F, Karg B, Lüken L, et al. Do-mpc: towards FAIR nonlinear and robust model predictive control. Control Eng Pract 2023;140:105676. https://doi.org/10.1016/j.conengprac.2023.105676

[42] Gagnon F, Thivierge A, Desbiens FBC. ModelPredictiveControl.jl: advanced process control made easy in julia; 2024. URL: https://arxiv.org/abs/2411.09764. arXiv:2411.09764.

[43] Abbas NJ, Zalkind DS, Pao L, Wright A. A reference open-source controller for fixed and floating offshore wind turbines. Wind Energy Sci Discuss 2022;7:53–73. https://doi.org/10.5194/wes-7-53-2022

[44] Hansen MH, Henriksen LC. Basic DTU wind energy controller, technical report DTU wind energy e-0028. URL, Roskilde, Denmark: Technical University of Denmark; 2013. https://orbit.dtu.dk/en/publications/basic-dtu-wind-energy-controller/.

[45] Mulders S, van Wingerden J. Delft research controller: an open-source and community-driven wind turbine baseline controller. J Phys Conf Ser 2018;1037:032009. https://doi.org/10.1088/1742-6596/1037/3/032009

[46] Perez-Becker S, Marten D, Nayeri CN, Paschereit CO. Implementation and validation of an advanced wind energy controller in aero-servo-elastic simulations using the lifting line free vortex wake model. Energies 2021;14:783. https://doi.org/10.3390/en14030783

[47] Larsen TJ, Hansen AM. How 2 hawc2, the user's manual, software manual risø national laboratory, risø-r-1597(ver. 13.0)(EN). Roskilde, Denmark: Technical University of Denmark; 2023.

[48] Chabaud VB. Real-time hybrid model testing of floating wind turbines [Ph.D. thesis, URL]. Trondheim, Norway: Norwegian University of Science and Technology; 2016. https://hdl.handle.net/11250/2433010.

[49] Hall M, Housner S, Zalkind D, Bortolotti P, Ogden D, Barter G. An open-source frequency-domain model for floating wind turbine design optimization. J Phys Conf Ser 2022;2265:042020. https://doi.org/10.1088/1742-6596/2265/4/042020

[50] Hansen MH, Henriksen LC, Tibaldi C, Bergami L, Verelst D, Pirrung G, Riva R, Meng F, Rinker J. Hawcstab2 2.16: user manual. Roskilde, Denmark: Software Manual DTU Wind Energy, Technical University of Denmark; 2024.

[51] Pegalajar-Jurado A, Borg M, Bredmose H. An efficient frequency-domain model for quick load analysis of floating offshore wind turbines. Wind Energy Sci 2018;3:693–712. https://doi.org/10.5194/wes-3-693-2018

[52] Jonkman J, Shaler K. FAST.farm user's guide and theory manual, software Manual NREL/TP-5000-78485, Golden, CO, USA: National Renewable Energy Laboratory; 2021. URL: https://www.nrel.gov/docs/fy21osti/78485.pdf.

[53] Pedersen MM, Forsting AM, van der Laan P, et al. PyWake 2.5.0: an open-source wind farm simulation tool. Roskilde, Denmark: Software Manual DTU Wind Energy, Technical University of Denmark; 2023.

[54] National Renewable Energy Laboratory. FLORIS wake modeling & wind farm controls; 2023. URL:. https://nrel.github.io/floris [Accessed 9 October 2025].

[55] Churchfield MJ, Lee S, Michalakes J, Moriarty PJ. A numerical study of the effects of atmospheric and wake turbulence on wind turbine dynamics. J Turbul 2012;13:1–32. https://doi.org/10.1080/14685248.2012.668191

[56] Camarena E, Anderson E, Bonney KL, Clarke RJ, Paquette J. pyNuMAD 1.1.0, zenodo archive. Albuquerque, NM, USA: Sandia National Laboratory; 2024. URL: https://doi.org/10.5281/zenodo.13952158. https://github.com/sandialabs/pyNuMAD.

[57] Yu W. VABS manual for users. AnalySwift, LLC, West Lafayette, IN, USA: Software Manual; 2024. URL: www.analyswift.com.

[58] WAMIT I. WAMIT user manual version 7.5, software manual, WAMIT. Chestnut Hill, MA, USA: Inc; 2023. URL: https://www.wamit.com/manual7.x/v75_manual.pdf.

[59] Liu Y, Yoshida S, Hu C, et al. A reliable open-source package for performance evaluation of floating renewable energy systems in coastal and offshore regions. Energy Convers Manag 2018;174:516–36. https://doi.org/10.1016/j.enconman.2018.08.012

[60] Ancellin M, Dias F. Capytaine: a python-based linear potential flow solver. J Open Source Softw 2019;4:1341. https://doi.org/10.21105/joss.01341

[61] Kurnia R, Ducrozet G. NEMOH: open-source boundary element solver for computation of first- and second-order hydrodynamic loads in the frequency domain. Comput Phys Commun 2023;292:108885. https://doi.org/10.1016/j.cpc.2023.108885

[62] Hall M. MoorDyn v2: new capabilities in mooring system components and load cases. In: ASME international conference on offshore mechanics and Arctic engineering, omae2020-19341. Virtual, Online; 2020. https://doi.org/10.1115/OMAE2020-19341, p. V009T09A078.

[63] Foundation C-O. COIN-OR: computational infrastructure for operations research, software manual. COIN-OR Foundation; 2025. URL:. https://www.coin-or.org/ [Accessed 9 October 2025].

[64] Wächter A, Biegler L. On the implementation of an interior-point filter line-search algorithm for large-scale nonlinear programming. Math Program 2006;106:25–57. https://doi.org/10.1007/s10107-004-0559-y
[65] Gill PE, Murray W, Saunders MA. SNOPT: an SQP algorithm for large-scale constrained optimization. SIAM Rev 2005;47:99–131. https://doi.org/10.1137/S1052623499350013
[66] Wu E, Kenway G, Mader CA, Jasa J, Martins JRRA. pyOptSparse: a Python framework for large-scale constrained nonlinear optimization of sparse systems. J Open Source Softw 2020;5:2564. https://doi.org/10.21105/joss.02564
[67] Hart WE, Watson J-P, Woodruff DL. Pyomo: modeling and solving mathematical programs in Python. Math Program Comput 2011;3:219–60. https://doi.org/10.1007/s12532-011-0026-8
[68] The SciPy community. Optimization (scipy.optimize), SciPy user guide, software manual, the SciPy community; 2008. URL:. https://docs.scipy.org/doc/scipy/tutorial/optimize.html [Accessed 9 October 2025].
[69] Mathworks, Inc. Fmincon: find minimum of constrained nonlinear multivariable function, MATLAB documentation, software manual, mathworks. Natick, MA, USA: Inc; 2025. URL:. https://www.mathworks.com/help/optim/ug/fmincon.html [Accessed 9 October 2025].
[70] Gray JS, Hwang JT, Martins JR, Moore KT, Naylor BA. OpenMDAO: an open-source framework for multidisciplinary design, analysis, and optimization. Struct Multidiscip Optim 2019;59:1075–104. https://doi.org/10.1007/s00158-019-02211-z
[71] Adams BM, Bohnhoff WJ, Dalbey KR, et al. Dakota 6.21.0 documentation, software manual sand2025-05563o. Albuquerque, NM, USA: Sandia National Laboratories; 2025. URL: http://snl-dakota.github.io.
[72] Gen M, Cheng R. Genetic algorithms and engineering design. New York: John Wiley & Sons; 1996. https://doi.org/10.1002/9780470172254
[73] Wang D, Tan D, Liu L. Particle swarm optimization algorithm: an overview. Soft Comput 2018;22:387–408. https://doi.org/10.1007/s00500-016-2474-6
[74] Kirkpatrick S, Gelatt CD, Vecchi MP. Optimization by simulated annealing. Science 1983;220:671–80. https://doi.org/10.1126/science.220.4598.671
[75] Kraft D. A software package for sequential quadratic programming, software manual DFVLR-FB 88-28, deutsches zentrum für luft- und raumfahrt. Köln, Germany: Institut Für Dynamik der Flugsysteme Oberpfaffenhofen; 1988.
[76] Bertsekas DP. Constrained optimization and lagrange multiplier methods. New York: Academic Press; 1982. https://doi.org/10.1016/C2013-0-10366-2
[77] Boyd S, Vandenberghe L. Convex optimization. Cambridge, UK: Cambridge University Press; 2004.
[78] Weinstein MJ, Rao AV. Algorithm 984: ADiGator, a toolbox for the algorithmic differentiation of mathematical functions in MATLAB using source transformation via operator overloading. ACM Trans Math Softw 2017;44:1–25. https://doi.org/10.1145/3104990
[79] Andersson JAE, Gillis J, Horn G, Rawlings JB, Diehl M. CasADi – a software framework for nonlinear optimization and optimal control. Math Program Comput 2019;11:1–36. https://doi.org/10.1007/s12532-018-0139-4
[80] Bradbury J, Frostig R, Hawkins P, et al. JAX: composable transformations of python+NumPy programs; 2018. URL:. http://github.com/jax-ml/jax [Accessed 9 October 2025].
[81] Forth SA, Edvall M. User guide for MAD - a matlab automatic differentiation toolbox, TOMLAB/MAD, version 1.4 the forward mode, software manual. San Diego, CA, USA: TOMLAB Optimization; 2007. URL: https://tomopt.com/docs/TOMLAB_MAD.pdf.
[82] Saves P, Lafage R, Bartoli N, Diouane Y, Bussemaker J, Lefebvre T, Hwang JT, Morlier J, Martins JRRA. SMT 2.0: a surrogate modeling toolbox with a focus on hierarchical and mixed variables Gaussian processes. Adv Eng Softw 2024;188:103571. https://doi.org/10.1016/j.advengsoft.2023.103571
[83] Mathworks, Inc. Surrogateopt: surrogate optimization for global minimization of time-consuming objective functions, MATLAB documentation, software manual, mathworks. Natick, MA, USA: Inc; 2025. URL:. https://www.mathworks.com/help/gads/surrogateopt.html [Accessed 9 October 2025].
[84] Menezes EJN, Araújo AM, Silva NSBD. A review on wind turbine control and its associated methods. J Clean Prod 2018;174:945–53. https://doi.org/10.1016/j.jclepro.2017.10.297
[85] Caselitz P, Kleinkauf W, Krüger T, Petschenka J, Reichardt M, Störzel K. Reduction of fatigue loads on wind energy converters by advanced control methods. In: Proceedings of the european wind energy conference. Dublin, Ireland; 1997. p. 555–8.
[86] Bossanyi EA. Individual blade pitch control for load reduction. Wind Energy 2002;6:119–28. https://doi.org/10.1002/we.76
[87] Stol KA, Zhao W, Wright AD. Individual blade pitch control for the controls advanced research turbine (CART). J Sol Energy Eng 2006;128:498–505. https://doi.org/10.1115/1.2349542
[88] Lackner MA, van Kuik G. A comparison of smart rotor control approaches using trailing edge flaps and individual pitch control. Wind Energy 2010;13:117–34. https://doi.org/10.1002/we.353
[89] Jelavić M, Petrović V, Perić N. Estimation based individual pitch control of wind turbine. Automatika 2010;51:181–92. https://doi.org/10.1080/00051144.2010.11828370
[90] Pao LY, Pusch M, Zalkind DS. Control co-design of wind turbines, annual review of control. Robot Auton Syst 2024;7:201–26. https://doi.org/10.1146/annurev-control-061423-101708
[91] Santoni C, Khosronejad A, Seiler P, Sotiropoulos F. Toward control co-design of utility-scale wind turbines: collective VS. Individual blade pitch control. Energy Rep 2023;9:793–806. https://doi.org/10.1016/j.egyr.2022.12.041
[92] Andersen PB. Advanced load alleviation for wind turbines using adaptive trailing edge flaps: sensoring and control [Ph.D. thesis, URL]. Technical University of Denmark; 2010. https://orbit.dtu.dk/en/publications/advanced-load-alleviation-for-wind-turbines-using-adaptive-traili/.
[93] Dahlberg JA, Medici D. Potential improvement of wind turbine array efficiency by active wake control (AWC). In: Proceedings of the european wind energy conference. Madrid, Spain; 2003. p. 65–84.
[94] Li S, Haskew TA, Xu L. Conventional and novel control designs for direct driven PMSG wind turbines. Electr Power Syst Res 2010;80:328–38. https://doi.org/10.1016/j.epsr.2009.09.016
[95] Zuo H, Bi K, Hao H. A state-of-the-art review on the vibration mitigation of wind turbines. Renew Sustain Energy Rev 2020;121:109710. https://doi.org/10.1016/j.rser.2020.109710
[96] Krenk S, Svendsen MN, Høgsberg J. Resonant vibration control of three-bladed wind turbine rotors. AIAA J 2012;50:148–61. https://doi.org/10.2514/1.J051164
[97] Long T, Yang Q, Wang Q, Huang G, Zhou X, Yang Y. Active vibration control of wind turbine using virtual TMD algorithm based on aerodynamic-structure-servo coupling model. Struct Control Health Monit 2023;2023:6618783. https://doi.org/10.1155/2023/6618783
[98] Yang J, He EM, Hu YQ. Dynamic modeling and vibration suppression for an offshore wind turbine with a tuned mass damper in floating platform. Appl Ocean Res 2019;83:21–9. https://doi.org/10.1016/j.apor.2018.08.021
[99] Zhang H, Wen B, Tian X, Li X, Dong Y, Wang M, Peng Z. Experimental study on mitigating vibration of floating offshore wind turbine using tuned mass damper. Ocean Eng 2023;288:115974. https://doi.org/10.1016/j.oceaneng.2023.115974
[100] Sarkar S, Fitzgerald B. Vibration control of spar-type floating offshore wind turbine towers using a tuned mass-damper-inerter. Struct Control Health Monit 2020;27:e2471. https://doi.org/10.1002/stc.2471
[101] Schaarup J. Guidelines for design of wind turbines. Technical Report, URL, Roskilde, Denmark: Det Norske Veritas (DNV) and Risø National Laboratory; 2002. https://orbit.dtu.dk/en/publications/guidelines-for-design-of-wind-turbines-2-ed/.
[102] Adhikari S, Bhattacharya S. Dynamic analysis of wind turbine towers on flexible foundations. Shock Vib 2012;19:408493. https://doi.org/10.3233/SAV-2012-0615
[103] van der Tempel J, Molenaar DP. Soft-soft not hard enough? In: Proceedings of the world wind energy conference. Berlin, Germany; 2002. p. 1–6.
[104] Veljkovic M, Feldmann M, Naumes J, Pak D, Simões L, Rebelo C, et al. Wind turbine tower design, erection and maintenance. In: Sørensen JD, Sørensen JN, editors. Wind energy systems. Elsevier; 2011. p. 274–300. https://doi.org/10.1533/9780857090638.2.274
[105] Hernandez-Estrada E, Lastres-Danguillecourt O, Robles-Ocampo JB, Lopez-Lopez A, et al. Considerations for the structural analysis and design of wind turbine towers: a review. Renew Sustain Energy Rev 2021;137:110447. https://doi.org/10.1016/j.rser.2020.110447
[106] Lantz EJ, Roberts JO, Nunemaker J, DeMeo E, Dykes KL, Scott GN. Increasing wind turbine tower heights: opportunities and challenges. Technical Report NREL/TP-5000-73629. URL, Golden, CO, USA: National Renewable Energy Laboratory; 2019. https://www.nrel.gov/docs/fy19osti/73629.pdf.
[107] Allen C, Viselli A, Dagher H, et al. Definition of the UMaine VolturnUS-S reference platform developed for the IEA wind 15-megawatt offshore reference wind turbine. Technical Report NREL/TP-5000-76773. URL, Golden, CO, USA: National Renewable Energy Laboratory; 2020. https://www.nrel.gov/docs/fy20osti/76773.pdf.
[108] Papi F, Bianchini A, Ferri G, Bruschi N, Marino E. Influence of tower design on floating offshore wind turbine dynamics. In: ASME international conference on offshore mechanics and Arctic engineering, omae2023-104864. Melbourne, Australia; 2023. https://doi.org/10.1115/OMAE2023-104864, p. V008T09A053.
[109] Sergiienko NY, Silva LSPD, Bachynski-Polić EE, Cazzolato BS, Arjomandi M, Ding B. Review of scaling laws applied to floating offshore wind turbines. Renew Sustain Energy Rev 2022;162:112477. https://doi.org/10.1016/j.rser.2022.112477
[110] Baldock N, Sevilla F, Redfern R, Storey A, Kempenaar A, Elkinton C. Optimization of installation, operation and maintenance at offshore wind projects in the u.s.: review and modeling of existing and emerging approaches, Technical Report 701216-UKBR-R-01, San Diego, CA, USA: Garrad Hassan America, Inc; 2014. https://doi.org/10.2172/1333103
[111] Stanley APJ, Ning A, Dykes K. Optimization of turbine design in wind farms with multiple HUB heights, using exact analytic gradients and structural constraints. Wind Energy 2019;22:605–19. https://doi.org/10.1002/we.2310
[112] Hermansen SM, Lund E. Multi-material and thickness optimization of a wind turbine blade root section. Struct Multidiscip Optim 2024;67:107. https://doi.org/10.1007/s00158-024-03811-0
[113] Schubel PJ, Crossley RJ. Wind turbine blade design. Energies 2012;5:3425–49. https://doi.org/10.3390/en5093425
[114] Cao Z, Li S, Li C, Li P, Ko TJ. Formation mechanism and detection and evaluation methods as well as repair technology of crack damage in fiber-reinforced composite wind turbine blade: a review. Int J Adv Manuf Technol 2022;120:5649–72. https://doi.org/10.1007/s00170-022-09230-z
[115] Tangler JL, The evolution of rotor and blade design. In: American wind energy association WindPower 2000. Palm Springs, CA, USA: NREL/CP-500-28410; 2000. p. 1–9. URL: https://docs.nrel.gov/docs/fy00osti/28410.pdf.
[116] Firoozi AA, Hejazi F, Firoozi AA. Advancing wind energy efficiency: a systematic review of aerodynamic optimization in wind turbine blade design. Energies 2024;17:2919. https://doi.org/10.3390/en17122919

[117] Timmer WA, Bak C, Aerodynamic characteristics of wind turbine blade airfoils. In: Advances in wind turbine blade design and materials. Elsevier; 2023. p. 129–67. https://doi.org/10.1016/B978-0-08-103007-3.00011-2
[118] Okulov V, van Kuik GAM. The Betz-Joukowsky limit for the maximum power coefficient of wind turbines. Int Sci J Altern Energy Ecol 2009;9:106–11. URL: https://orbit.dtu.dk/en/publications/the-betz-joukowsky-limit-for-the-maximum-power-coefficient-of-win/.
[119] Boudis A, Hamane D, Guerri O, Bayeul-Lainé AC. Airfoil shape optimization of a horizontal axis wind turbine blade using a discrete adjoint solver. J Appl Fluid Mech 2023;16:724–38. https://doi.org/10.47176/jafm.16.04.1493
[120] Loenbaek K, Bak C, Madsen JI, Dam B. Optimal relationship between power and design-driving loads for wind turbine rotors using 1-d models. Wind Energy Sci 2020;5:155–70. https://doi.org/10.5194/wes-5-155-2020
[121] Oerlemans S, Fisher M, Maeder T, Kögler K. Reduction of wind turbine noise using optimized airfoils and trailing-edge serrations. AIAA J 2009;47:1470–81. https://doi.org/10.2514/1.38888
[122] Bottasso CL, Campagnolo F, Croce A. Multi-disciplinary constrained optimization of wind turbines. Multibody Syst Dyn 2012;27:21–53. https://doi.org/10.1007/s11044-011-9271-x
[123] Chen J, Wang Q, Shen WZ, Pang X, Li S, Guo X. Structural optimization study of composite wind turbine blade. Mater Des 2013;46:247–55. https://doi.org/10.1016/j.matdes.2012.10.036
[124] Camarena E, Anderson E, Paquette J, Bortolotti P, Feil R, Johnson N. Land-based wind turbines with flexible rail-transportable blades – part 2: 3d finite element design optimization of the rotor blades. Wind Energy Sci 2022;7:19–35. https://doi.org/10.5194/wes-7-19-2022
[125] Marzec Ł, Buliński Z, Krysiński T, Tumidajski J. Structural optimisation of h-rotor wind turbine blade based on one-way fluid structure interaction approach. Renew Energy 2023;216:118957. https://doi.org/10.1016/j.renene.2023.118957
[126] Sessarego M, Dixon KR, Rival DE, Wood DH. A hybrid multi-objective evolutionary algorithm for wind-turbine blade optimization. Eng Optim 2015;47:1043–62. https://doi.org/10.1080/0305215X.2014.941532
[127] Monte AD, Castelli MR, Benini E. Multi-objective structural optimization of a HAWT composite blade. Compos Struct 2013;106:362–73. https://doi.org/10.1016/j.compstruct.2013.05.038
[128] Couto LDL, Moreira NE, Saito JYD, Hallak PH, Lemonge ACD. Multi-objective structural optimization of a composite wind turbine blade considering natural frequencies of vibration and global stability. Energies 2023;16:3363. https://doi.org/10.3390/en16083363
[129] Alkhoury P, Soubra A-H, Rey V, Aït-Ahmed M. A full three-dimensional model for the estimation of the natural frequencies of an offshore wind turbine in sand. Wind Energy 2021;24:699–719. https://doi.org/10.1002/we.2598
[130] Yao S, Chetan M, Griffith DT, et al. Aero-structural design and optimization of 50 MW wind turbine with over 250-m blades. Wind Eng 2022;46:273–95. https://doi.org/10.1177/0309524X211027355
[131] Agbayani NA, A technical overview of ASCE/AWEA rp2011: recommended practice for compliance of large land-based wind turbine support structures. In: Structures Congress 2014. Boston, MA, USA: ASCE; 2014. p. 1759–1770. https://doi.org/10.1061/9780784413357.155
[132] Byrne BW, Houlsby GT. Foundations for offshore wind turbines, philosophical transactions of the royal society of London. Ser A Math Phys Eng Sci 2003;361:2909–30. https://doi.org/10.1098/rsta.2003.1286
[133] Wu X, Hu Y, Li Y, et al. Foundations of offshore wind turbines: a review. Renew Sustain Energy Rev 2019;104:379–93. https://doi.org/10.1016/j.rser.2019.01.012
[134] Wang L, Kolios A, Liu X, Venetsanos D, Cai R. Reliability of offshore wind turbine support structures: a state-of-the-art review. Renew Sustain Energy Rev 2022;161:112250. https://doi.org/10.1016/j.rser.2022.112250
[135] Stehly T, Duffy P, Hernando DM. 2022 cost of wind energy review. Technical Report NREL/PR-5000-88335. URL, Golden, CO, USA: National Renewable Energy Laboratory; 2023. https://docs.nrel.gov/docs/fy24osti/88335.pdf.
[136] Lago BD, Flessati L, Marveggio P, Martinelli P, Fraraccio G, di Prisco C, di Prisco M. Experimental tests on shallow foundations of onshore wind turbine towers. Struct Concr 2022;23:2986–3006. https://doi.org/10.1002/suco.202100655
[137] Svensson H. Design of foundations for wind turbines [Master's thesis, URL]. Lund, Sweden: Lunds Tekniska Högskola; 2010. https://www.lunduniversity.lu.se/lup/publication/3566985.
[138] Jones KES, Li M. Life cycle assessment of additively manufactured foundations for ultratall wind turbine towers. Wind Energy 2024;27:1427–49. https://doi.org/10.1002/we.2947
[139] Jiménez Toña R, Rojo JC, Rojí Chandro E. Foundations of onshore wind turbines: current situation and trends. Inf Constr 2024;76:6443. https://doi.org/10.3989/ic.6443
[140] Shrestha S, Ravichandran N, Rahbari P. Geotechnical design and design optimization of a pile-raft foundation for tall onshore wind turbines in multilayered clay. Int J Geomech 2018;18:04017143. https://doi.org/10.1061/(ASCE)GM.1943-5622.0001061
[141] Gazetas G, Foundation vibrations. In: Fang HY, editor. Foundation engineering handbook. Boston, MA, USA: Springer; 1991. p. 553–93. https://doi.org/10.1007/978-1-4615-3928-5_15
[142] Horwath S, Hassrick J, Grismala R, Diller E. Comparison of environmental effects from different offshore wind turbine. Technical Report OCS Study BOEM 2020-041. URL, LLC, Fairfax, VA, USA: ICF International; 2020. https://tethys.pnnl.gov/publications/comparison-environmental-effects-different-offshore-wind-turbine-foundations.
[143] Seidel M, Hendrikse H. Analytical assessment of sea ice-induced frequency lock-in for offshore wind turbine monopiles. Mar Struct 2018;60:87–100. https://doi.org/10.1016/j.marstruc.2018.02.003
[144] Empire Engineering Limited. The empire engineering guide to offshore wind foundations. Technical Report. URL, Bristol, UK: Empire Engineering Limited; 2023. https://www.empireengineering.co.uk/guide-to-offshore-wind-foundations/.
[145] Nikitas G, Bhattacharya S, Vimalan N, Wind energy. In: Letcher TM, editor. Future energy, 3 ed. Elsevier; 2020. p. 331–55. https://doi.org/10.1016/B978-0-08-102886-5.00016-5
[146] Scharff R, Siems M. Monopile foundations for offshore wind turbines – solutions for greater water depths. Steel Constr 2013;6:47–53. https://doi.org/10.1002/stco.201300010
[147] Sánchez S, López-Gutiérrez J-S, Negro V, Esteban MD. Foundations in offshore wind farms: evolution, characteristics and range of use. Analysis of main dimensional parameters in monopile foundations. J Mar Sci Eng 2019;7. https://doi.org/10.3390/jmse7120441
[148] Kallehave D, Byrne BW, Thilsted CL, Mikkelsen KK. Optimization of monopiles for offshore wind turbines. Philos Trans R Soc a Math Phys Eng Sci 2015;373:20140100. https://doi.org/10.1098/rsta.2014.0100
[149] Smilden E, Bachynski EE, Sørensen AJ, Amdahl J. Site-specific controller design for monopile offshore wind turbines. Mar Struct 2018;61:503–23. https://doi.org/10.1016/j.marstruc.2018.03.002
[150] Damgaard M, Zania V, Andersen LV, Ibsen LB. Effects of soil–structure interaction on real time dynamic response of offshore wind turbines on monopiles. Eng Struct 2014;75:388–401. https://doi.org/10.1016/j.engstruct.2014.06.006
[151] Arany L, Bhattacharya S, Macdonald JHG, Hogan SJ. Closed form solution of eigen frequency of monopile supported offshore wind turbines in deeper waters incorporating stiffness of substructure and ssi. Soil Dyn Earthq Eng 2016;83:18–32. https://doi.org/10.1016/j.soildyn.2015.12.011
[152] McWilliam MK, Natarajan A, Pollini N, Dykes K, Barter GE. Conceptual monopile and tower sizing for the IEA wind task 37 borssele reference wind farm. J Phys Conf Ser 2021;2018:012025. https://doi.org/10.1088/1742-6596/2018/1/012025
[153] Oh K-Y, Nam W, Ryu MS, Kim J-Y, Epureanu BI. A review of foundations of offshore wind energy convertors: current status and future perspectives. Renew Sustain Energy Rev 2018;88:16–36. https://doi.org/10.1016/j.rser.2018.02.005
[154] Abdullahi A, Wang Y, Bhattacharya S. Comparative modal analysis of monopile and jacket supported offshore wind turbines including soil-structure interaction. Int J Struct Stab Dyn 2020;20:2042016. https://doi.org/10.1142/S021945542042016X
[155] Jalbi S, Bhattacharya S. Concept design of jacket foundations for offshore wind turbines in 10 steps. Soil Dyn Earthq Eng 2020;139:106357. https://doi.org/10.1016/j.soildyn.2020.106357
[156] Lopez A, Green R, Williams T, Lantz E, Buster G, Roberts B. Offshore wind energy technical potential for the contiguous united states. Technical Report NREL/PR-6A20-83650. URL, Golden, CO, USA: National Renewable Energy Laboratory; 2022. https://www.nrel.gov/docs/fy22osti/83650.pdf.
[157] Faraggiana E, Giorgi G, Sirigu M, Ghigo A, Bracco G, Mattiazzo G. A review of numerical modelling and optimisation of the floating support structure for offshore wind turbines. J Ocean Eng Mar Energy 2022;8:433–56. https://doi.org/10.1007/s40722-022-00241-2
[158] Karimi M, Hall M, Buckham B, Crawford C. A multi-objective design optimization approach for floating offshore wind turbine support structures. J Ocean Eng Mar Energy 2017;3:69–87. https://doi.org/10.1007/s40722-016-0072-4
[159] Collu M, Borg M, Design of floating offshore wind turbines. In: Ng C, Ran L, editors. Offshore wind farms: technologies, design and operation. Sawston, UK: Woodhead Publishing; 2016. p. 359–85. https://doi.org/10.1016/B978-0-08-100779-2.00011-8
[160] Zhou BZ, Wu GX. Resonance of a tension leg platform exited by third-harmonic force in nonlinear regular waves. Philos Trans R Soc a Math Phys Eng Sci 2015;373:20140105. https://doi.org/10.1098/rsta.2014.0105
[161] Adrezin R, Benaroya H. Response of a tension leg platform to stochastic wave forces. Probabilistic Eng Mech 1999;14:3–17. https://doi.org/10.1016/S0266-8920(98)00012-5
[162] Jia Z, Wu H, Chen H, Li W, Li X, Lian J, He S, Zhang X, Zhao Q. Hydrodynamic response and tension leg failure performance analysis of floating offshore wind turbine with inclined tension legs. Energies 2022;15:8584. https://doi.org/10.3390/en15228584
[163] Lee YH, Bayat S, Allison JT, Hossain MS, Griffith DT. Multidisciplinary modeling and control co-design of a floating offshore vertical-axis wind turbine system. J Mech Des 2025;147:061702. https://doi.org/10.1115/1.4068072
[164] Jonkman JM. Dynamics modeling and loads analysis of an offshore floating wind turbine. Technical Report NREL/TP-500-41958. URL, Golden, CO, USA: National Renewable Energy Laboratory; 2007. https://docs.nrel.gov/docs/fy08osti/41958.pdf.
[165] Prowell I, Robertson A, Jonkman J, Stewart GM, Goupee AJ. Numerical prediction of experimentally observed behavior of a scale model of an offshore wind turbine supported by a tension-leg platform. In: Offshore technology conference, OTC 24233. Houston, TX, USA; 2013. p. 3246–69. URL: https://docs.nrel.gov/docs/fy13osti/57615.pdf.
[166] Larsen TJ, Hanson TD. A method to avoid negative damped low frequent tower vibrations for a floating, pitch controlled wind turbine. J Phys Conf Ser 2007;75:012073. https://doi.org/10.1088/1742-6596/75/1/012073
[167] López-Queija J, Robles E, Jugo J, Alonso-Quesada S. Review of control technologies for floating offshore wind turbines. Renew Sustain Energy Rev 2022;167:112787. https://doi.org/10.1016/j.rser.2022.112787

[168] Fowler ML, Lenfest E, Viselli A, Goupee AJ, et al. 1:70-scale model testing of the reference opensource controller (ROSCO) on the IEA-wind 15mw reference wind turbine including floating feedback. In: ISOEP international ocean and polar engineering conference, ISOPE-i-23-074. Ottawa, Canada; 2023. p. 1–7. URL: https://onepetro.org/ISOPEIOPEC/proceedings-abstract/ISOPE23/ISOPE23/ISOPE-I-23-074/524502.
[169] Subbulakshmi A, Verma M, Keerthana M, Sasmal S, Harikrishna P, Kapuria S. Recent advances in experimental and numerical methods for dynamic analysis of floating offshore wind turbines—an integrated review. Renew Sustain Energy Rev 2022;164:112525. https://doi.org/10.1016/j.rser.2022.112525
[170] Pedersen MM, Larsen GC. Integrated wind farm layout and control optimization. Wind Energy Sci 2020;5:1551–66. https://doi.org/10.5194/wes-5-1551-2020
[171] Thomas JJ, Baker NF, Malisani P, Quaeghebeur E, Perez-Moreno SS, Jasa J, Bay C, Tilli F, Bieniek D, Robinson N, Stanley APJ, Holt W, Ning A. A comparison of eight optimization methods applied to a wind farm layout optimization problem. Wind Energy Sci 2023;8:865–91. https://doi.org/10.5194/wes-8-865-2023
[172] Howland MF, Lele SK, Dabiri JO. Wind farm power optimization through wake steering. In: Proceedings of the national academy of sciences, vol. 116. 2019. p. 14495–500. https://doi.org/10.1073/pnas.1903680116
[173] Simley E, Fleming P, King J. Design and analysis of a wake steering controller with wind direction variability. Wind Energy Sci 2020;5:451–68. https://doi.org/10.5194/wes-5-451-2020
[174] Simley E, Fleming P, King J, Sinner M. Wake steering wind farm control with preview wind direction information. In: American control conference. New Orleans, LA, USA; 2021. p. 1783–9. https://doi.org/10.23919/ACC50511.2021.9483008
[175] Stanley AP, Bay CJ, Fleming P. Enabling control co-design of the next generation of wind plants. Wind Energy Sci 2023;8:1341–50. https://doi.org/10.5194/wes-8-1341-2023
[176] Baricchio M, Gebraad PMO, van Wingerden J-W. Evaluating the potential of a wake steering co-design for wind farm layout optimization through a tailored genetic algorithm. Wind Energy Sci 2024;9:2113–32. https://doi.org/10.5194/wes-9-2113-2024
[177] Houck DR. Review of wake management techniques for wind turbines. Wind Energy 2022;25:195–220. https://doi.org/10.1002/we.2668
[178] Nash R, Nouri R, Vasel-Be-Hagh A. Wind turbine wake control strategies: a review and concept proposal. Energy Convers Manag 2021;245:114581. https://doi.org/10.1016/j.enconman.2021.114581
[179] Fleming P, Annoni J, Shah JJ, Wang L, Ananthan S, Zhang Z, Hutchings K, Wang P, Chen W, Chen L. Field test of wake steering at an offshore wind farm. Wind Energy Sci 2017;2:229–39. https://doi.org/10.5194/wes-2-229-2017
[180] Fleming P, Annoni J, Scholbrock A, Quon E, Dana S, Schreck S, Raach S, Haizmann F, Schlipf D. Full-scale field test of wake steering. J Phys Conf Ser 2017;854:012013. https://doi.org/10.1088/1742-6596/854/1/012013
[181] Doekemeijer BM, Kern S, Maturu S, Kanev S, Salbert B, Schreiber J, Campagnolo F, Bottasso CL, Schuler S, Wilts F, et al. Field experiment for open-loop yaw-based wake steering at a commercial onshore wind farm in Italy. Wind Energy Sci 2021;6:159–76. https://doi.org/10.5194/wes-6-159-2021
[182] Fleming P, King J, Dykes K, Simley E, Roadman J, Scholbrock A, Murphy P, Lundquist JK, Moriarty P, Fleming K, et al. Initial results from a field campaign of wake steering applied at a commercial wind farm – part 1. Wind Energy Sci 2019;4:273–85. https://doi.org/10.5194/wes-4-273-2019
[183] Kanev S. Dynamic wake steering and its impact on wind farm power production and yaw actuator duty. Renew Energy 2020;146:9–15. https://doi.org/10.1016/j.renene.2019.06.122
[184] Howland MF, Johlas HM, Quesada JB, Martínez JJP, Zhong W, Larrañaga FP. On the impact of the yaw update frequency and wind direction forecasting on open-loop wake steering control. In: American control conference. Atlanta, GA, USA; 2022. p. 4218–23. https://doi.org/10.23919/ACC53348.2022.9867443
[185] Shapiro CR, Starke GM, Meneveau C, Gayme DF. A wake modeling paradigm for wind farm design and control. Energies 2019;12:2956. https://doi.org/10.3390/en12152956
[186] Meyers J, Bottasso C, Dykes K, Fleming P, Gebraad P, Giebel G, Göçmen T, Van Wingerden J-W. Wind farm flow control: prospects and challenges. Wind Energy Sci 2022;7:2271–306. https://doi.org/10.5194/wes-7-2271-2022
[187] Goit JP, Meyers J. Optimal control of energy extraction in wind-farm boundary layers. J Fluid Mech 2015;768:5–50. https://doi.org/10.1017/jfm.2015.70
[188] Frederik JA, Weber R, Cacciola S, Campagnolo F, Croce A, Bottasso C, van Wingerden J-W. Periodic dynamic induction control of wind farms: proving the potential in simulations and wind tunnel experiments. Wind Energy Sci 2020;5:245–57. https://doi.org/10.5194/wes-5-245-2020
[189] Frederik JA, Doekemeijer BM, Mulders SP, van Wingerden J-W. The helix approach: using dynamic individual pitch control to enhance wake mixing in wind farms. Wind Energy 2020;23:1739–51. https://doi.org/10.1002/we.2513
[190] Pahus ML, Nishino T, Kirby A, Vogel CR. Control co-design of a large offshore wind farm considering the effect of wind extractability. J Phys Conf Ser 2024;2767:092026. https://doi.org/10.1088/1742-6596/2767/9/092026
[191] Wayman EN, Sclavounos P, Butterfield S, Jonkman J, Musial W. Coupled dynamic modeling of floating wind turbine systems. In: Offshore technology conference, OTC-18287-MS. Houston, TX, USA; 2006. p. 1–22. https://doi.org/10.4043/18287-MS
[192] Otter A, Murphy J, Pakrashi V, Robertson A, Desmond C. A review of modelling techniques for floating offshore wind turbines. Wind Energy 2022;25:831–57. https://doi.org/10.1002/we.2701
[193] Hegseth JM, Bachynski EE. A semi-analytical frequency domain model for efficient design evaluation of spar floating wind turbines. Mar Struct 2019;64:186–210. https://doi.org/10.1016/j.marstruc.2018.10.015
[194] Pan Q, Yu W, Cheng PW. Simplified modeling of floating offshore wind farms with shared mooring line configurations. Ocean Eng 2025;327:121018. https://doi.org/10.1016/j.oceaneng.2025.121018
[195] Ltd O. OrcaFlex user manual, version 11.4e, software manual. Ulverston, Cumbria, UK: Orcina Ltd; 2023. URL: https://www.orcina.com.
[196] ANSYS, Inc. AQWA user's manual, release 2024 r2, software manual, ANSYS. Canonsburg, PA, USA: Inc; 2024. URL: https://www.ansys.com.
[197] Jasak H. OpenFOAM: open source CFD in research and industry. Int J Nav Archit Ocean Eng 2009;1:89–94. https://doi.org/10.2478/IJNAOE-2013-0011
[198] Siemens SS-C. User guide, software manual. Plano, TX, USA: Siemens Industry Software Inc; 2023. URL: p. 2310. https://www.siemens.com/en-us/products/simcenter/fluids-thermal-simulation/star-ccm/.
[199] ANSYS I. ANSYS fluent theory guide, software manual, ANSYS. Canonsburg, PA, USA: Inc; 2025. URL: https://www.ansys.com.
[200] Kohnke PC, ANSYS. In: Brebbia CA, editor. Finite element systems: a handbook. Berlin, Heidelberg: Springer; 1982. p. 19–25. https://doi.org/10.1007/978-3-662-07229-5_2
[201] Ning SA, Damiani R, Moriarty PJ. Objectives and constraints for wind turbine optimization. J Sol Energy Eng 2014;136:041010. https://doi.org/10.1115/1.4027693
[202] Chehouri A, Younes R, Ilinca A, Perron J. Review of performance optimization techniques applied to wind turbines. Appl Energy 2015;142:361–88. https://doi.org/10.1016/j.apenergy.2014.12.043
[203] De Kooning JD, Samani AE, De Zutter S, De Maeyer J, Vandevelde L. Techno-economic optimisation of small wind turbines using co-design on a parametrised model. Sustain Energy Technol Assess 2021;45:101165. https://doi.org/10.1016/j.seta.2021.101165
[204] Bayat S, Allison JT. Impact of control strategies on the control co-design of spar floating offshore wind turbines. Ocean Eng 2025;336:121763. https://doi.org/10.1016/j.oceaneng.2025.121763
[205] Pusch M, Stockhouse D, Abbas N, Phadnis M, Pao L. Optimal operating points for wind turbine control and co-design. Wind Energy 2024;27:1286–301. https://doi.org/10.1002/we.2879
[206] Pao LY, Zalkind DS, Griffith DT, Chetan M, et al. Control co-design of 13 MW downwind two-bladed rotors to achieve 25% reduction in levelized cost of wind energy. Annual Reviews in Control 2021;51:331–343. https://doi.org/10.1016/j.arcontrol.2021.02.001
[207] Abbas NJ, Bortolotti P, Kelley C, Paquette J, Pao L, Johnson N. Aero-servo-elastic co-optimization of large wind turbine blades with distributed aerodynamic control devices. Wind Energy 2023;26:763–85. https://doi.org/10.1002/we.2840
[208] Abbas NJ, Jasa J, Zalkind DS, Wright A, Pao L. Control co-design of a floating offshore wind turbine. Appl Energy 2024;353:122036. https://doi.org/10.1016/j.apenergy.2023.122036
[209] Yu W, Zhou ST, Lemmer F, Cheng PW. Control co-design optimization of floating offshore wind turbines with tuned liquid multi-column dampers. Wind Energy Sci 2024;9:1053–68. https://doi.org/10.5194/wes-9-1053-2024
[210] Zalkind D, Bortolotti P. Control co-design studies for a 22 MW semisubmersible floating wind turbine platform. J Phys Conf Ser 2024;2767:082020. https://doi.org/10.1088/1742-6596/2767/8/082020
[211] Iori J, Bottasso CL, McWilliam MK. A sensitivity-based estimation method for investigating control co-design relevance. Wind Energy Sci 2024;9:1289–304. https://doi.org/10.5194/wes-9-1289-2024
[212] Ashuri T, Zaaijer MB, Martins JR, Zhang J. Multidisciplinary design optimization of large wind turbines—technical, economic, and design challenges. Energy Convers Manag 2016;123:56–70. https://doi.org/10.1016/j.enconman.2016.06.004
[213] Hegseth JM, Bachynski EE, Martins JRRA. Integrated design optimization of spar floating wind turbines. Mar Struct 2020;72:102771. https://doi.org/10.1016/j.marstruc.2020.102771
[214] López Muro J, Du X, Condomines J-P, Bilgen O, Burlion L, Wind turbine tower thickness and blade pitch control co-design optimization. In: AIAA SciTech forum and exposition. San Diego, CA, USA: AIAA 2022-1150; 2022. p. 1–10. https://doi.org/10.2514/6.2022-1150
[215] Deshmukh AP, Allison JT. Multidisciplinary dynamic optimization of horizontal axis wind turbine design. Struct Multidiscip Optim 2016;53:15–27. https://doi.org/10.1007/s00158-015-1308-y
[216] Deshmukh AP, Allison JT. Unrestricted wind farm layout design with optimal control considerations. In: ASME international design engineering technical conference, detc2017-67480. Cleveland, OH, USA; 2017. https://doi.org/10.1115/DETC2017-67480, p. V02AT03A021.
[217] Lao Y, Rotea MA, Koeln JP, Sakib MS, Griffith DT. Economic nonlinear model predictive control of offshore vertical-axis wind turbines. In: American control conference. Atlanta, GA, USA; 2022. p. 3518–25. https://doi.org/10.23919/ACC53348.2022.9867846
[218] Ashuri T, Zaaijer MB, Martins JRRA, Van Bussel GJW, Van Kuik GAM. Multidisciplinary design optimization of offshore wind turbines for minimum levelized cost of energy. Renew Energy 2014;68:893–905. https://doi.org/10.1016/j.renene.2014.02.045
[219] Du X, Liang J, Muro JL, Qian G, Burlion L, Bilgen O. Development of a control co-design optimization framework with aeroelastic-control coupling for floating offshore wind turbines. Appl Energy 2024;372:123728. https://doi.org/10.1016/j.apenergy.2024.123728
[220] Lemmer F, Müller K, Yu W, Schlipf D, Cheng PW. Optimization of floating offshore wind turbine platforms with a self-tuning controller. In: ASME international conference on offshore mechanics and Arctic engineering, omae2017-62038. Trondheim, Norway; 2017. https://doi.org/10.1115/OMAE2017-62038, p. V010T09A080.

[221] Jasa J, Bortolotti P, Zalkind D, Barter G. Effectively using multifidelity optimization for wind turbine design. Wind Energy Sci 2022;7:991–1006. https://doi.org/10.5194/wes-7-991-2022
[222] Bortolotti P, Bottasso CL, Croce A. Combined preliminary-detailed design of wind turbines. Wind Energy Sci 2016;1:71–88. https://doi.org/10.5194/wes-1-71-2016
[223] Alyaqout SF, Peters DL, Papalambros PY, Ulsoy AG. Generalized coupling management in complex engineering systems optimization. J Mech Des 2011;133:091005. https://doi.org/10.1115/1.4004541
[224] Chinthoju P, Lee YH, Das GK, James KA, Allison JT, Optimal design of eVTOLs for urban mobility using analytical target cascading (ATC). In: AIAA SciTech forum and exposition. Orlando, FL, USA: AIAA 2024-2235; 2024. p. 1–13. https://doi.org/10.2514/6.2024-2235
[225] Fernández Bravo E, Ornik M, Allison JT. Numerical estimation of bidirectional plant-control design coupling in control co-design. In: ASME international design engineering technical conference, detc2024-142636. Washington, DC, USA; 2024. p. 1–10. https://doi.org/10.1115/DETC2024-142636
[226] Tamang S, Lee YH, Formulating a sequence of compact optimization problems for floating offshore wind turbine based on design coupling information. In: ASME international mechanical engineering congress & exposition. Memphis, TN, USA: IMECE2025-173460; 2025. p. 1–5.
[227] Fernández Bravo E, Tamang S, Lee YH, Allison JT. Surrogate-based co-design coupling analysis for floating offshore wind turbines; 2026. http://arxiv.org/abs/2604.22969. arXiv:2604.22969.
[228] Fernández Bravo E, Allison J. Satellite MDO problem formulation using design coupling information. In: IAF space systems symposium. Milan, Italy; 2024. p. 1225–33. https://doi.org/10.52202/078372-0123
[229] Fernández Bravo E, Ornik M, Dierks B, Allison JT. Numerical estimation of the sensitivity of optimal plant design to control perturbations. In: ASME international design engineering technical conference, detc2025-164458. Anaheim, CA, USA; 2025. https://doi.org/10.1115/DETC2025-164458, p. V03AT03A004.
[230] Cain CS, Lee YH, Hydro-structural design exploration of floating platform for offshore energy systems. In: ASME international mechanical engineering congress & exposition. New Orleans, LA, USA: IMECE2023-112479; 2023. https://doi.org/10.1115/IMECE2023-112479, p. V006T07A035.
[231] Nejadkhaki HK, Hall JF. Control framework and integrative design method for an adaptive wind turbine blade. J Dyn Syst Meas Control 2020;142:101001. https://doi.org/10.1115/1.4047098
[232] Jonkman J, Wright A, Barter G, Hall M, Allison J, Herber DR. Functional requirements for the WEIS toolset to enable controls co-design of floating offshore wind turbines. In: ASME international offshore wind technical conference, iowtc2021-3533. Virtual, Online; 2021. https://doi.org/10.1115/IOWTC2021-3533, p. V001T01A007.
[233] de Luna RB, Papi F, Marten D, Paschereit CO. Analyzing the impact of aeroelastic model fidelity on control co-design optimization of floating offshore wind turbines. Wind Energy Sci 2025;10:3045–68. https://doi.org/10.5194/wes-10-3045-2025
[234] Mikkola P, Martinelli J, Filstroff L, Kaski S. Multi-fidelity Bayesian optimization with unreliable information sources. In: Ruiz F, Dy J, van de Meent J-W, editors. Proceedings of the 26th international conference on artificial intelligence and statistics, vol. 206. Valencia, Spain: Palau de Congressos; 2023. p. 7425–54. URL: https://proceedings.mlr.press/v206/mikkola23a.html.
[235] Behtash M, Alexander-Ramos MJ. A reliability-based formulation for simulation-based control co-design using generalized polynomial chaos expansion. J Mech Des 2021;144:051705. https://doi.org/10.1115/1.4052906
[236] Azad S, Herber DR. An overview of uncertain control co-design formulations. J Mech Des 2023;145:091709. https://doi.org/10.1115/1.4062753
[237] Azad S, Herber DR. A case study comparing both stochastic and worst-case robust control co-design under different control structures. J Dyn Syst Meas Control 2025;147:054501. https://doi.org/10.1115/1.4068144
[238] Azad S, Herber DR, Investigations into uncertain control co-design implementations for stochastic in expectation and worst-case robust. In: ASME international mechanical engineering congress & exposition. Columbus, OH, USA: IMECE2022-95229; 2022. https://doi.org/10.1115/IMECE2022-95229, p. V005T07A103.
[239] Ditlevsen O. Stochastic model for joint wave and wind loads on offshore structures. Struct Saf 2002;24:139–63. https://doi.org/10.1016/S0167-4730(02)00022-X
[240] Nispel A, Ekwaro-Osire S, Dias JP, Cunha Jr A. Uncertainty quantification for fatigue life of offshore wind turbine structure. ASCE-ASME J Risk Uncertainty Eng Syst, Part B: Mech Eng 2021;7:040901. https://doi.org/10.1115/1.4051162
[241] Dao CD, Kazemtabrizi B, Crabtree CJ. Offshore wind turbine reliability and operational simulation under uncertainties. Wind Energy 2020;23:1919–38. https://doi.org/10.1002/we.2526
[242] Müller K, Cheng PW. Application of a monte carlo procedure for probabilistic fatigue design of floating offshore wind turbines. Wind Energy Sci 2018;3:149–62. https://doi.org/10.5194/wes-3-149-2018
[243] Richter P, Wolters J, Frank M. Uncertainty quantification of offshore wind farms using monte carlo and sparse grid, energy sources, part b: economics. Planning, and Policy 2022;17:2000520. https://doi.org/10.1080/15567249.2021.2000520
[244] Shao Y, Liu J. Uncertainty quantification for dynamic responses of offshore wind turbine based on manifold learning. Renew Energy 2024;222:119798. https://doi.org/10.1016/j.renene.2023.119798
[245] Thapa M, Missoum S. Surrogate-based stochastic optimization of horizontal-axis wind turbine composite blades. Struct Multidiscip Optim 2022;65:41. https://doi.org/10.1007/s00158-021-03114-8
[246] Aristondo A, Nava V, Penalba M, Esteras M. Uncertainty-aware Bayesian optimisation framework for the design of floating offshore wind turbines. Ocean Eng 2025;342:123080. https://doi.org/10.1016/j.oceaneng.2025.123080
[247] Azad S, Herber DR. Concurrent probabilistic control co-design and layout optimization of wave energy converter farms using surrogate modeling. In: ASME international design engineering technical conferences, detc2023-116896. Boston, MA, USA; 2023. https://doi.org/10.1115/DETC2023-116896, p. V03BT03A035.
[248] Azad S, Herber DR, Khanal S, Jia G. Concurrent geometry, control, and layout optimization of wave energy converter farms in probabilistic irregular waves using surrogate modeling. Ocean Eng 2025;320:120183. https://doi.org/10.1016/j.oceaneng.2024.120183
[249] Campobasso MS, Minisci E, Caboni M. Aerodynamic design optimization of wind turbine rotors under geometric uncertainty. Wind Energy 2016;19:51–65. https://doi.org/10.1002/we.1820
[250] Negro V, López-Gutiérrez J-S, Esteban MD, Matutano C. Uncertainties in the design of support structures and foundations for offshore wind turbines. Renew Energy 2014;63:125–32. https://doi.org/10.1016/j.renene.2013.08.041
[251] Damiani RR. Uncertainty and risk assessment in the design process for wind. Technical Report NREL/TP-5000-67499. URL, Golden, CO, USA: National Renewable Energy Laboratory; 2018. https://www.nrel.gov/docs/fy18osti/67499.pdf.
[252] Ramezani M, Choe D-E, Heydarpour K, Koo B. Uncertainty models for the structural design of floating offshore wind turbines: a review. Renew Sustain Energy Rev 2023;185:113610. https://doi.org/10.1016/j.rser.2023.113610
[253] Dimitrov NK, Kelly M, McWilliam M, Guiton M, et al. End-to-end wind turbine design under uncertainties: a practical example. J Phys Conf Ser 2024;2767:082017. https://doi.org/10.1088/1742-6596/2767/8/082017
[254] Marepally K, Jung YS, Baeder J, Vijayakumar G. Uncertainty quantification of wind turbine airfoil aerodynamics with geometric uncertainty. J Phys Conf Ser 2022;2265:042041. https://doi.org/10.1088/1742-6596/2265/4/042041
[255] Sharma H, Wang W, Huang B, She B, Ramachandaran T. Control co-design under uncertainty for offshore wind farms: optimizing grid integration, energy storage, and market participation. Renew Energy Focus 2026;57:100806. https://doi.org/10.1016/j.ref.2025.100806
[256] Chen P, Siano P, Bak-Jensen B, Chen Z. Stochastic optimization of wind turbine power factor using stochastic model of wind power. IEEE Trans Sustain Energy 2010;1:19–29. https://doi.org/10.1109/TSTE.2010.2044900
[257] Caboni M, Campobasso MS, Minisci E. Wind turbine design optimization under environmental uncertainty. J Eng Gas Turbines Power 2016;138:082601. https://doi.org/10.1115/1.4032665
[258] Bošnjaković M, Martinović M, Đokić K. Application of artificial intelligence in wind power systems. Appl Sci 2025;15:2443. https://doi.org/10.3390/app15052443
[259] De Anda J, Ruiz SE, Bojórquez E, Inzunza-Aragon I. Towards optimal reliability-based design of wind turbines towers using artificial intelligence. Eng Struct 2023;294:116778. https://doi.org/10.1016/j.engstruct.2023.116778
[260] Song D, Shen G, Huang C, Huang Q, Yang J, Dong M, Joo YH, Duić N. Review on the application of artificial intelligence methods in the control and design of offshore wind power systems. J Mar Sci Eng 2024;12:424. https://doi.org/10.3390/jmse12030424
[261] Jiang Z, Li H, Yang H, Wu H, Liu W, Chen Z. Review of artificial intelligence-based design optimization of wind power systems. Wind 2025;5:18. https://doi.org/10.3390/wind5030018
[262] Farrar NO, Ali MH, Dasgupta D. Artificial intelligence and machine learning in grid connected wind turbine control systems: a comprehensive review. Energies 2023;16:1530. https://doi.org/10.3390/en16031530
[263] Kostecka E, Miller T, Durlik I, Nerć A. Artificial intelligence in floating offshore wind turbines: a critical review of applications in design, monitoring, control, and digital twins. Energies 2025;18:5937. https://doi.org/10.3390/en18225937
[264] Njiri JG, Söffker D. State-of-the-art in wind turbine control: trends and challenges. Renew Sustain Energy Rev 2016;60:377–93. https://doi.org/10.1016/j.rser.2016.01.110
[265] Sirnivas S, Musial W, Bailey B, Filippelli M. Assessment of offshore wind system design, safety, and operation standards. Technical Report NREL/TP-5000-60573. URL, Golden, CO, USA: National Renewable Energy Laboratory; 2014. https://www.nrel.gov/docs/fy14osti/60573.pdf.
[266] McKenna R, vd Leye PO, Fichtner W. Key challenges and prospects for large wind turbines. Renew Sustain Energy Rev 2016;53:1212–21. https://doi.org/10.1016/j.rser.2015.09.080
[267] Sørensen JD, Toft HS. Probabilistic design of wind turbines. Energies 2010;3:241–57. https://doi.org/10.3390/en3020241
[268] Kunskaja S, Pažėraitė A. Determinants of renewable energy technology deployment: a systematic review. Sustainability 2025;17:10538. https://doi.org/10.3390/su172310538
[269] Agupugo CP, Ajayi AO, Nwanevu C, Oladipo SS. Policy and regulatory framework supporting renewable energy microgrids and energy storage systems. Eng Sci Technol Int J 2022;5:2589–615. https://doi.org/10.51594/estj.v5i8.1460